



HAL
open science

Path reconstruction in diffusion tensor magnetic resonance imaging

Xin Song

► **To cite this version:**

Xin Song. Path reconstruction in diffusion tensor magnetic resonance imaging. Other. INSA de Lyon, 2011. English. NNT : 2011ISAL0066 . tel-00694403

HAL Id: tel-00694403

<https://theses.hal.science/tel-00694403>

Submitted on 4 May 2012

HAL is a multi-disciplinary open access archive for the deposit and dissemination of scientific research documents, whether they are published or not. The documents may come from teaching and research institutions in France or abroad, or from public or private research centers.

L'archive ouverte pluridisciplinaire **HAL**, est destinée au dépôt et à la diffusion de documents scientifiques de niveau recherche, publiés ou non, émanant des établissements d'enseignement et de recherche français ou étrangers, des laboratoires publics ou privés.

THÈSE

présentée devant

L'Institut National des Sciences Appliquées de Lyon

pour obtenir

LE GRADE DE DOCTEUR

ÉCOLE DOCTORALE: ÉLECTRONIQUE, ÉLECTROTECHNIQUE, AUTOMATIQUE
FORMATION DOCTORALE : SCIENCES DE L'INFORMATION, DES DISPOSITIFS ET
DES SYSTÈMES

par

Xin Song

Path Reconstruction in Diffusion Tensor Magnetic Resonance Imaging

Soutenue le 13 juillet 2011

Jury :

Carlos Canudas de Wit	Directeur de recherche CNRS	Examineur
Guo-Liang Huang	Professeur	Rapporteur
Isabelle Magnin	Directeur de recherche Inserm	Examineur
Jean-Claude Vivalda	Directeur de Recherches INRIA	Rapporteur
Cheng-Zhong Xu	Professeur	Examineur
Jia-Wei Ye	Professeur	Co-directeur de thèse
Yue-Min Zhu	Directeur de recherche CNRS	Co-directeur de thèse
Zao-Jian Zou	Professeur	Rapporteur

SIGLE	ECOLE DOCTORALE	NOM ET COORDONNEES DU RESPONSABLE
CHIMIE	<u>CHIMIE DE LYON</u> http://sakura.cpe.fr/ED206 M. Jean Marc LANCELIN Insa : R. GOURDON	M. Jean Marc LANCELIN Université Claude Bernard Lyon 1 Bât CPE 43 bd du 11 novembre 1918 69622 VILLEURBANNE Cedex Tél : 04.72.43 13 95 Fax : lancelin@hikari.cpe.fr
E.E.A.	<u>ELECTRONIQUE, ELECTROTECHNIQUE, AUTOMATIQUE</u> http://www.insa-lyon.fr/eea M. Alain NICOLAS Insa : C. PLOSSU ede2a@insa-lyon.fr Secrétariat : M. LABOUNE AM. 64.43 – Fax : 64.54	M. Alain NICOLAS Ecole Centrale de Lyon Bâtiment H9 36 avenue Guy de Collongue 69134 ECULLY Tél : 04.72.18 60 97 Fax : 04 78 43 37 17 eea@ec-lyon.fr Secrétariat : M.C. HAVGOUDOUKIAN
E2M2	<u>EVOLUTION, ECOSYSTEME, MICROBIOLOGIE, MODELISATION</u> http://biomserv.univ-lyon1.fr/E2M2 M. Jean-Pierre FLANDROIS Insa : H. CHARLES	M. Jean-Pierre FLANDROIS CNRS UMR 5558 Université Claude Bernard Lyon 1 Bât G. Mendel 43 bd du 11 novembre 1918 69622 VILLEURBANNE Cédex Tél : 04.26 23 59 50 Fax 04 26 23 59 49 06 07 53 89 13 e2m2@biomserv.univ-lyon1.fr
EDISS	<u>INTERDISCIPLINAIRE SCIENCES- SANTÉ</u> Sec : Safia Boudjema M. Didier REVEL Insa : M. LAGARDE	M. Didier REVEL Hôpital Cardiologique de Lyon Bâtiment Central 28 Avenue Doyen Lépine 69500 BRON Tél : 04.72.68 49 09 Fax :04 72 35 49 16 Didier.revel@creatis.uni-lyon1.fr
INFOMATHS	<u>INFORMATIQUE ET MATHÉMATIQUES</u> http://infomaths.univ-lyon1.fr M. Alain MILLE	M. Alain MILLE Université Claude Bernard Lyon 1 LIRIS - INFOMATHS Bâtiment Nautibus 43 bd du 11 novembre 1918 69622 VILLEURBANNE Cedex Tél : 04.72. 44 82 94 Fax 04 72 43 13 10 infomaths@bat710.univ-lyon1.fr - alain.mille@liris.cnrs.fr
Matériaux	<u>MATERIAUX DE LYON</u> M. Jean Marc PELLETIER Secrétariat : C. BERNAVON 83.85	M. Jean Marc PELLETIER INSA de Lyon MATEIS Bâtiment Blaise Pascal 7 avenue Jean Capelle 69621 VILLEURBANNE Cédex Tél : 04.72.43 83 18 Fax 04 72 43 85 28 Jean-marc.Pelletier@insa-lyon.fr
MEGA	<u>MECANIQUE, ENERGETIQUE, GENIE CIVIL, ACOUSTIQUE</u> M. Jean Louis GUYADER Secrétariat : M. LABOUNE PM : 71.70 –Fax : 87.12	M. Jean Louis GUYADER INSA de Lyon Laboratoire de Vibrations et Acoustique Bâtiment Antoine de Saint Exupéry 25 bis avenue Jean Capelle 69621 VILLEURBANNE Cedex Tél :04.72.18.71.70 Fax : 04 72 43 72 37 mega@lva.insa-lyon.fr
ScSo	<u>ScSo*</u> M. OBADIA Lionel Insa : J.Y. TOUSSAINT	M. OBADIA Lionel Université Lyon 2 86 rue Pasteur 69365 LYON Cedex 07 Tél : 04.78.77.23.88 Fax : 04.37.28.04.48 Lionel.Obadia@univ-lyon2.fr

Path Reconstruction in Diffusion Tensor Magnetic Resonance Imaging

Abstract

The present thesis aims to investigate the similarities between the heart fiber tracking algorithm and the underwater robot path tracking algorithm, and propose some new ideas and methods to solve the problem of choosing the coming back paths of underwater robot and construct the fiber structure of the human heart. Nowadays super-mini underwater cable robots are playing more and more important parts in the application of oceans, rivers, lakes and shallow water. However, the complicated underwater environment and the poor underwater vision make super-mini underwater cable robot hardly to be controlled. Traditionally, the manual control method by operators is adopted by this kind of robots. Unfortunately, the robots can hardly work normally in these practical circumstances. Therefore, to overcome these shortcomings and improve the abilities of these underwater cable robots, this thesis proposes several improvements, including the system design, the motion controller design, three dimensional obstacle recognition and three dimensional path reconstruction techniques, etc.

The following details are given: (1) Super-mini underwater robot system design by developing a much more powerful and intelligent control platform for underwater robot; (2) Super-mini robot motion controller design by proposing a new adaptive neural network sliding mode controller with balanced parameter controller (ANNSMB); (3) Research of three dimensional underwater environment reconstruction by investigating the theory of data collection and several new adaptive online processing techniques, and in particular by adopting diffusion tensor magnetic resonance imaging (DT-MRI) algorithm and the theory of three dimensional obstacle reconstruction for the application of the underwater robot; (4) Three dimensional path planning and its reconstruction by proposing a new random three dimensional path tracking algorithm based on Bayesian theory; (5) Algorithms and application of DT-MRI by proposing a new maximum energy fiber tracking algorithm to construct the fiber structure of the heart.

Table of contents

Table of contents	iii
Table of tables	v
Table of figures.....	vi
NOTATION.....	viii
Chapter 1 INTRODUCTION.....	1
1.1. Introduction.....	1
1.2. The development of underwater robot.....	2
1.3. Underwater robot motion control algorithm development	4
1.4. DT-MRI Fiber tracking and underwater robot path tracking reconstruction technologies, characters and significance	6
1.4.1. DT-MRI technology.....	6
1.4.2. Modeling algorithm of three dimensional objects reconstruction for DT-MRI and underwater robot	7
1.4.3. Algorithms of Robot Path tracking and DT-MRI tracking.....	10
1.4.4. Analysis, discussion and significance of path algorithms for underwater robot	13
1.5. Thesis work.....	13
1.6. Summary.....	14
Part I System and Control Technologies	15
Chapter 2 RESEARCH ON IMPROVED SUPER-MINI UNDERWATER ROBOT SYSTEM AND MONTION CONTROL.....	17
2.1. Introduction.....	17
2.2. System of super-mini underwater robot.....	18
2.2.1. Mechanical design of super-mini underwater robots.....	18
2.2.2. Design of the super-mini underwater robots and external equipment	22
2.2.3. Super-mini underwater robot software design	27
2.2.4. Super-mini underwater robot system framework summary.....	30
2.3. Theory of underwater robot dynamics	30
2.4. Theory, simulation and experimental of underwater robot motion control	34
2.4.1. Theory of control algorithms and control algorithm design for underwater robots.....	35
2.4.2. Simulations, experiments and discussions of underwater robot motion control algorithms	46
2.5. Summary	56
Part II Recognition and Path Reconstruction.....	57
Chapter 3 ALGORITHMS OF THREE-DIMENSIONAL PATH TRACKING 59	
3.1. Introduction.....	59

3.2. Streamline Algorithm Theory	60
3.3. Theory of maximum energy tracking approach.....	61
3.4. Stochastic tracking algorithm based on Bayesian theory	66
3.5. Summary	66
Chapter 4 APPLICATION OF THREE DIMENSIONAL MYOCARDIAL FIBER RECONSTRUCTION AND ITS REFERENCE VALUE FOR UNDERWATER ROBOT	67
4.1. Introduction.....	67
4.2. DT-MRI images and derived data types, characteristics	68
4.3. Application of tracking algorithms and their results comparison.....	75
4.4. Myocardial fiber structures study and the parameters	91
4.5. Reference value of myocardial tracking algorithms to the underwater robot path tracking methods	97
4.6. Summary	99
Partie III Conclusion	101
Chapter 5 CONCLUSION AND FUTURE WORK	103
5.1. Review of the contribution of this research	103
5.2. Future work.....	104
5.3. Publication of the author	105
Bibliographies.....	109

Table of tables

Table 2.1 Moment of inertia	53
Table 2.2 Thruster coefficients	53
Table 2.3 Coefficients	54
Table 4.1 Variation of Fiber Lengths as a function of FA, RA, MD, c_l , c_p , c_s	92
Table 4.2 Variation of the Number of Fibers as a function of	93

Table of figures

Fig.2-1 Forwarding Mode of Super-mini Underwater Robot.....	21
Fig.2-2 Whole Plant Frame of the Super-mini Underwater Robot.....	22
Fig.2-3 Electrical Circuit Model of the super-mini robot Control Box	23
Fig.2-4 System Frame of the Core Processing Unit	24
Fig.2-5 Whole Frame of the Super-mini Robot Electrical Design	25
Fig.2-6 Detailed Electrical System of Super-mini Underwater Robot	26
Fig.2-7 Control Software Design Frame of the Upper Computer	28
Fig.2-8 Software System of Underwater Robot Control Box.....	29
Fig.2-9 Software Design of Underwater Robot	30
Fig.2-10 PID control theory diagram.....	35
Fig.2-11 Membership function of S and U_{fuzzy}	40
Fig.2-12 ANNSMB Controller Diagram	44
Fig.2-13 Results of PID controller.....	49
Fig.2-14 Results of SMC controller.....	50
Fig.2-15 Results of SMSFC controller	50
Fig.2-16 Membership function	51
Fig.2-17 Results of AFSMC controller	52
Fig.2-18 Results of ANNSMB controller	52
Fig.2-19 Experiment of the Super-mini Underwater robot	54
Fig.2-20 Experimental record of the yaw angle	55
Fig.2-21 Standard deviation of yaw angle	56
Fig.3-1 Voxel direction energy	64
Fig.3-2 Angle between two near vector direction	65
Fig.3-3 Homogeneity level of the Energy field	65
Fig.4-1 DT-MRI Image Processing Basic Process	68
Fig.4-2 Heart Coordinate system description	74
Fig.4-3 Angle Definition	74
Fig.4-4 DWI image preprocess procedure.....	76
Fig.4-5 Construct Energy Distribution Field and Tensor Data Calculation	77
Fig.4-6 Flow Chart of Maximum Energy Tracking Approach.....	78
Fig.4-7 Flow Chart of Traditional Tracking Approach	79
Fig.4-8 Energy Value of heart images (Top view)	81
Fig.4-9 Energy Value of heart images (Lateral view)	81
Fig.4-10 Fiber Length Distribution in Z-Axis Region.....	85

Fig.4-11 Normalized Fiber Length Distribution in Z-Axis Region.....	85
Fig.4-12 Value of Smoothness Type	86
Fig.4-13 Normalized Value of Smoothness Type I.....	86
Fig.4-14 Value of Smoothness Type II.....	87
Fig.4-15 Normalized Value of Smoothness Type II.....	87
Fig.4-16 Fiber tracking result of the Maximum Energy Tracking Approach.....	88
Fig.4-17 Fiber tracking result of the advanced Streamline Approach.....	89
Fig.4-18 Fiber tracking result of the traditional Streamline Approach	90
Fig.4-19 Fiber tracking results comparison (The left two images are calculated by energy maximum method, the right two images are calculated by advanced streamline method).....	91
Fig.4-20 Normalized fiber length distribution along the apex-base axis.....	94
Fig.4-21 Normalized fiber length distributions	94
Fig.4-22 Five longest fibers of the heart.....	95
Fig.4-23 Fiber structures of helix angles between -22.50 and 22.50.....	96
Fig.4-24 Fiber structures of helix angles between 67.5° and 90°, and between -67.5° and -90°	97

NOTATION

η	Position and attitude vector in earth coordinates
$M(\eta)$	Inertial matrix
$C(\eta, \dot{\eta})$	Centripetal and coriolis terms
$D(\eta, \dot{\eta})$	Damping terms
x, y, z	Position of underwater robot in earth coordinates
ϕ, θ, ψ	Attitude of roll, pitch and yaw
p, q, r	Angle velocity of roll, pitch and yaw
δ	Disturbance
S	Sliding surface
e	Error
U_{eq}	Equivalent control
V	Weight matrix from input layer to hidden layer
n, s	Parameters of radial basis functions
U_s	Balanced parameter robust controller
ε	Energy field
v	Direction vector
P	Possibility value
ω	Weight
$H(x)$	Heaviside Function

Chapter 1 INTRODUCTION

Summary

1.1. Introduction.....	1
1.2. The development of underwater robot.....	2
1.3. Underwater robot motion control algorithm development	4
1.4. DT-MRI Fiber tracking and underwater robot path tracking reconstruction technologies, characters and significance	6
1.4.1. DT-MRI technology.....	6
1.4.2. Modeling algorithm of three dimensional objects reconstruction for DT-MRI and underwater robot	7
1.4.3. Algorithms of Robot Path tracking and DT-MRI tracking.....	10
1.4.4. Analysis, discussion and significance of path algorithms for underwater robot	13
1.5. Thesis work.....	13
1.6. Summary.....	14

1.1. Introduction

Nowadays, most earth areas are covered by the water. To explore the resource of the water, people work frequently in the sea, lake, river etc. Through the accumulation of experience and the technology development, more and more equipments etc. for exploiting resources, such as the offshore platform, the warship and other assisted working foundations, have been developed from the traditional working ways, such as the previous fish ship or diving. Through the improvement of the industry, the available land resources are largely reduced. However, the ocean resource is rich and unexploited, for example, biological resources, oil, natural gas, rare metals, and other various important resources required for industrial development. Therefore, people have an obvious and urgent demand for the exploitation and utilization of the resources in the oceans etc. Otherwise, in marine technology, the emergence of the underwater robot instead of the traditional diving is a leap in science. The underwater robot has now become a hot research topic, which has been applied in the observation of marine biology, environmental detection, deep-sea salvage, rescue etc. Thus, the research of underwater robots are significant and necessary [Chance, 2003]

1.2. The development of underwater robot

The underwater robot can be categorized into three groups based on control mode [Zhu, 1992][Song, 2004], including manned underwater vehicle, unmanned remotely operated underwater vehicle (ROV), unmanned underwater vehicle (UUV) or automatic unmanned underwater vehicle (AUV). The remotely operated underwater robot (ROV) is mainly operated by the manual control. This type of underwater robot is developed early in the 20th century and the first remote sensing underwater robot has been developed in the 50th century. However, the whole marine technology is not paid enough attention in the later 20 years. Thus, the development is relatively slow. After 70th century, due to the oil development and production of marine platforms, remote operated underwater robot has been developed rapidly and many products have been created and devoted into application. Unmanned underwater vehicle are mainly adopting the semi-automatic or pre-programmed control mode. Operator need download the exact command program to the control computer of underwater robot, before the implementation of the work in the water. This type of underwater robot can be used for stress mapping, temperature mapping mission. It can work well in the predicted space with little changes in the environment. This type of underwater robot is used little in industrial application. The underwater robot 'otter' which is developed by Stanford University is one of the famous UUV products. The control method of automatic underwater robot is totally self-automatic and self-adapted. It is a new type of intelligent robot with the rapid development of the computer, the wireless communication and the artificial intelligence technology etc. Operators just need to download the commands to these robots. They are not required to receive the details of working procedures. These robots can automatically design a strategy and detailed working plans. Then they follow the strategies, accomplish the tasks and safely move back to the destinations. However, this type of underwater robot is very complicated and is a beginning research in latest years.

According to the need of this research, we move our attention to the development of the super-mini underwater robot. The size of this super-mini underwater robot is usually between 0.4 m and 1.6 m, which is bigger than tiny biological robot (the size is below 30 cm). Compared with the small type of underwater robot, it is smaller. The size of the small underwater robot is mostly between 2 m and 3 m and the weight is between several dozens and two hundred kilograms. Though they can carry enough payload and they can sail a long time with stable and good performance, they can hardly play well and the action is not convenient when they work in the narrow circumstances. With the development of MEMS, researchers develop underwater micro-robot, such as the united states of "micro-hunter", the weight is only 70 g. However, it is a puzzle that how to install sensors at the robot. These sensors designs are related to the higher technology. For the basic researches, this type of micro robot is mainly considered in experimental models and theory. The size is too small. The quality is too small, lower capacity and it is now far from normal application in current time. The super-mini robot is between small and micro robot, which is very suitable for shallow water (less than 40m), observation of the cruise, the narrow regional security detection, surveillance etc. It is also easy to be carried, operated and relatively inexpensive.

At present, the development of super-mini intelligent underwater robots is paid by a large attention. At every year, the United States of America holds an AUV competition, which

assembles a lot of competitors and relevant famous experts who can give the on-site assessment. There are many AUV products that are shown in this international marine and maritime scientific meeting. Woods oceanographic institution in USA developed AUV, which is now applied in Navy's special branch of forces. The quality of SAHRV in the air is 36.5 kg, the width is 19 cm and the length is 160 cm. Sensors can detect 3 to 60 meter water depth. The United States researchers also develop several REMUS AUV products. There are three types REMUS-100, REMUS-600 and REMUS-6000. REMUS-100 is the super-mini underwater robot. REMUS-600 and REMUS-6000, respectively, are small and medium-sized underwater robot. REMUS-100 is currently the most famous and successful super-mini unmanned underwater robot. Its maximum diameter is 19 cm. The maximum length is 160 cm and the quality in the air is 37 kg. The largest submarine depth is 100 meters. It equips DC brushless motors and its maximum speed can reach 2.6 m/s (5 knot). A doppler speedometer, a side-scan sonar, a long baseline, a short baseline, temperature sensors, pressure sensors, acoustic imaging systems, camera, inertial navigation equipment, GPS etc. are equipped for the underwater robot to improve the working abilities. Some other communication equipment includes internet gateway buoys, which allows the corporation of four or more REMUS. REMUS-100, because of its excellent performance has been reported a lot and used in the Navy or some other applications of many countries. University of Tokyo developed a miniature AUV underwater test platform "Tam-egg", with a 1.22 m length, 0.58 m width, 0.5 m height, the weight is about 131 kilograms, 100 m submersible depth, three hours sustainable working time, four 100 w forward propellers. It is equipped with a magnetic (TCM2), stress (depth) sensors, the optic gyroscope, two cameras, four acoustic search sensors, two sets of LED lighting etc. This type of detector is usually used for the detection of complex structure of the seabed.

The upper examples shows that in the application of super-mini AUV, the main job is at the coast, the port for inspection, monitoring, underwater search of fish, underwater environmental detection, coastal search, reconnaissance, surveillance, mine-clearing missions etc. They are small, high automatic and unmanned underwater robots.

From the development time of ROV underwater robot, we can know that ROV is a pioneer in the history of the underwater robot. At the mid-16th century, the utilization of the first diving bell "helmet" is the first attempt to improve the efficiency of diving. It is a very simple device. The leather bag was soaked in oil and added with a pass to the surface of the ventilation tube. The beginning technology was very rough, till the 60 century, the U.S. Navy's underwater cable of the robot CURV has successfully been applied for the salvage of the lost hydrogen bomb and this won a popular reputation. At the beginning of 70's century, a number of commercial companies are beginning to apply ROV at the prospect of offshore oil industry, and develop new type of ROV. At present, with the development of the petroleum industry to deep-sea, ROV has become an indispensable part of the industry and towards the development of higher reliability.

Super-mini ROV is also an important research with great values. Taking into account of the working environment such as offshore, shallow water, rivers or lakes, the size of deep sea underwater robot is large and expensive, which is not suitable and adaptive for the narrow and shallow space. Compared with super-mini AUV, super-mini ROV has its own advantages. It owns recycling convenience through the communication cable. You do not need to buy

expensive sensors for wireless underwater communications and these can reduce the costs largely. Taking into account of the complexities of the unknown environment, through super-mini ROV operators collaborative control, can relatively reduce errors and risks compared with the self control to hold long period of exploration by individual automatic algorithm. The protection of power cable is the insurance for the underwater robot. However, there are different requirements and different kinds of working environment that make many researchers need to develop many different types of underwater robot.

Here, we introduce the development history of the underwater ROV. Ocean Marine Systems UK developed super-min C-cat ROV which are used to detect the security of the ship bottom. Its working depth is 50 m, length is 700 mm, width is 150 mm and height is 150 mm. It adopts a color camera and one fixed image scan sonar. The SEABOTIX Company of the USA has developed the observation ROV LBV 150, the quality in the air is 10.4 kg. Maximum diving depth is 150 m, with 270 degrees scanning sonar, two cameras, depth sensors, and working depth is 50 m. One similar ROV is LBV300, the quality in the air is 13.6 kg, and water depth is 100 m. It is mainly used in shallow water as the Harbor Police, surveillance. Dams can also be carried out on quality and safety tests.

Canada's ultra-Inuktun developed underwater robots small VideoRayPro, standard diving depth is 75 m, length is 35 cm, width is 22.5 cm, height is 21 cm and weight is 4 kg. These products are equipped with cameras and sensors such as sonar images. U.S. ROV-1000: length 61cm, width 35.6cm, height 25.4cm, weight 17 kg and maximum dive depth of 150 m. The top part of its body is loaded with color camera, black-and-white camera, salinity meter, the flow meter and so on.

1.3. Underwater robot motion control algorithm development

Underwater robot motion control has been a hot research for a long time, mainly due to a variety of underwater robots, the unknown environment. Due the demands of application of underwater robots are increasing gradually, their autonomy, motion control precision and stability of the requirements are also increased. Thus, how to improve the performance of the motion control research has become a hard nut to crack.

Compared with land robot or aerial robot, the motion control of underwater robot is necessary to take into account non-linear fluid dynamic and complex changes in the fluid environment. The velocity of underwater robot is slow and we can not design the motion control simply by its shape. Underwater robots have additional weights, large inertia forces. These can not lead to a quick reaction in motion. Changes and interfere of water flow is disordered. The underwater robot control system is necessary to have good robustness and adaptability. At present, there are many control algorithms that have been applied to control the motion of underwater robots, such as expert system, neural network control system, self - adaptive control, sliding mode control, fuzzy control, genetic algorithms and other methods.

[Yoerger 1986] proposed the use of expert control algorithm for the movement of ROV. [Yoerger 1985] proposed a sliding mode controller to control the trajectory of underwater robots. They studied the uncertainties of water coefficient and neglected the impact of

coupling. In [Healey 1993], the equations of complex system are divided into several independent equations, including heading control equations, deep control equations, speed control equations etc. [Nakamura 1992] proposed a tracking algorithm in four degrees of freedom including surge, roll, pitch, yaw. This paper discussed non-holonomic system characteristics, but it did not consider the dynamic characters of the system. [Goheen 1990] proposed multi-variable adaptive control of underwater robots and automatic positioning algorithm was proposed to strengthen the reliability of the model. [Yuh 1996][Choi 2004] proposed multi-input multi-output adaptive controller. [Tabaï 1994] proposed hybrid adaptive controller, and implement a simulation experiment. [Yuh 1990] put forward the neural network controller for the control of underwater robots. There was no precise model in the experiment and the online self-tuning controller was to learn the motion model of the underwater robots. [Ishii, etc., 1998] proposed a self-organized neural network control system that was applied to yaw movement and verified the effectiveness of the algorithm.

[Kato 1993], [Smith 1994] used the fuzzy logic controllers for different types of underwater robots of motion control and experimental simulation. [Debitetto 1994] studied the control of the UUV depth and they proposed 14 rules fuzzy logic controller.

In Underwater robot motion control methods, there are also a variety of control algorithms considering the combination of different algorithms, such as fuzzy neural network, neural network and sliding mode control, genetic fuzzy controller, and the neural network prediction movement etc.

In this research, the motion control of super-mini underwater robots is to discuss the sliding mode control theory and the combination with fuzzy logic, neural network controller etc. for the study of the underwater robots application. Underwater robot is a highly nonlinear system, and taking into account the time-varying, complexity, and uncertainties of the environment and. It is difficult to establish a precise model of underwater robot. In reference to the previous research studies, sliding mode controller is not highly sensitive and has anti-uncertainties characters to the parameters and the un-modeled parts of the system. Since the last century 80's, in most studies of underwater robots, one popular control algorithm is the sliding mode control algorithm. However, there are some defects of ideal switch process in sliding mode control algorithm and the practical system can hardly provide this ideal switch due to the system's inertia, time-delay, and disturbance etc. These make the sliding mode control hardly realize the high switch frequency. Meanwhile, the system lags, vibration and chattering can also disturb the effects of sliding mode control and they can also make serious damage for the performance of sliding mode controller.

To solve the above problems, more and more researchers begin to use bilateral sliding mode controller, or other improved ways to solve the defects of the traditional sliding mode control algorithm, such as fuzzy logic and sliding mode algorithm, neural network sliding mode controller. They are proposed to overcome the defects of the independence of the system models, reduce the number of systematic control parameters and the chattering phenomena.

1.4. DT-MRI Fiber tracking and underwater robot path tracking reconstruction technologies, characters and significance

1.4.1. DT-MRI technology

DT-MRI (Diffusion tensor magnetic resonance imaging) ([Filler 1991], [Richards 1992], [Minati 2006], [Carano 2003], [Mori 1999], [Koyama 2006], [Denis 2001], [Basser 1994])) is a study on the effects of molecular diffusion characteristics developed from the diffusion magnetic resonance imaging in recent years, providing the clinical micro-structure and a large amount of information in micro dynamics. It is the only non-invasive method to describe the white matter fibers or other fibers in the organ. It is an effective method that can be used for early diagnosis of many diseases through minor pathological changes, such as the white matter lesions and so on.

[Hahn 1950] proposed the first water molecule diffusion through MRI signal and they observed anisotropy diffusion in muscle. Subsequently, many scholars also observed the anisotropy diffusion effects in the gray matter of rat brain and axons of human brain. Diffusion is the random molecular movement, namely Brownian motion. This word is often used to describe the micro-movement of particles from high concentration area to low concentration area. In fact, the diffusion magnetic resonance imaging measures the water molecules movement from cell-to-cell. In the period of 50ms, water molecules in the cells can leap in a range of 10 micrometer, as well as the mutual roles among the biological organizations, such as the cell membranes, fibers and macromolecular tissues. DWI (Diffusion weighted imaging) is a real three-dimensional process. Like the white matters of brain, the actions of water molecular in the organs are also anisotropic. They are similar to a special organization order, or limit the movement of water molecules in some directions. During the pulsed MR signal coding process of magnetic field gradient, only the molecular diffusion along the gradient direction can be obtained. For the anisotropy effect of the diffusion, it can be observed from the diffusion differences, which are the different characteristics between the diffusion tensor imaging and the conventional MR imaging.

The normal diffusion MRI can be described by a single parameter, called diffusion coefficient D . The diffusion effects of MR signal depend on the factor D and the factor b . These two factors can be used to describe the gradient pulse $A = \exp(-bD)$. However, due to the existence of the anisotropy, the diffusion can not be described by a single parameter, and it need a tensor D to give a full description of the molecular motion in all directions and the relevance in these directions. The parameters are symmetric, D_{xx}, D_{yy}, D_{zz} representing the molecular movement along the X, Y, Z axis ([Denis 2001], [Basser 1994]).

Diffusion gradient pulse is always attenuated in one direction along one direction such as X axis. However, it is not only dependent on this direction of diffusion effects, but also on the role of other directions, such as the Y axis and Z axis. Thus, in order to determine the

diffusion tensor data, diffusion weighted imaging (DWI) should firstly be collected on a number of different directions by using the diffusion sensitive MR pulse sequences, such as EPI. Since the diffusion tensor is symmetrical, it can be measured with only 6 directions instead of 9 directions. When the signal to noise ratio (SNR) is low, imaging numbers should be increased for better results.

In the case of the anisotropy, each voxel value of D will be changed according to the different directions. Thus, it is very useful to express the scanning sequence of this linear changing b values, and the corresponding MRI hardware features (stability and anti-vortex).

Here, a simple description about DT-MRI of the image processing is introduced. First of all, it is estimated by the diffusion-weighted D values from multiple linear regressions. The diffusion tensor can be calculated and the corresponding parameter is not only a reflection of an average degree of diffusion, but also the diffusion degrees of each voxel. The diffusion tensor also determines the main direction of each voxel and the diffusion value in this direction. Reference to the tensor D , the vector v and the eigenvalues according to different direction can be calculated. Therefore, the best diffusion direction and the relevant diffusion coefficient can be obtained.

The imaging principle of DT-MRI is to consider the weighted values of the three-dimensional diffusion images. Therefore, the data that are analyzed from a variety of images include not only a variety of location information, but also the tensor information in different positions.

1.4.2. Modeling algorithm of three dimensional objects reconstruction for DT-MRI and underwater robot

In general ways of three-dimensional imaging, there are many problems have to be solved, such as:

- (1). Image processing algorithms of image data extraction, data noise reduction, segmentation, registration;
- (2). How to use image data for three-dimensional reconstruction;
- (3). How to quickly render a three-dimensional scene;

These issues are also parts of the problems in underwater robot objects reconstruction, and for the preliminary studies, these are very complex problems. For the three-dimensional environment reconstruction algorithm of underwater robot, only a few papers have been presented. [Castellani 2005], used the three-dimensional underwater sonar equipment to scan the space, and proposed grid remodeling ideas based on the triangulation of the 3D mosaic. At

present, most of the research is more concerned about the use of sonar sensors to image path planning and study the shape of the seabed.

As the operators can not view the objects with the naked eye under the water, the visual environment of three-dimensional object reconstruction by underwater robots for the tasks in the water, plays a significant role. Although the underwater robots can be equipped with cameras, the visibility of the camera is very low because of the muddy water conditions. By the adoption of a single camera observing the objects, it is difficult to construct the whole perception of three dimensional spaces. For operators, the underwater robot is still more difficult to be operated. Through the computer-aided three-dimensional space to achieve the external environment, it can be greatly enhanced to operate on the intuitive sense of the unknown space, to make up for the shortcomings of low visibility in the water environment. Meanwhile, three-dimensional reconstruction that compares with the only two-dimensional data reconstruction is a big raise. According to the current image sonar equipment, the corresponding imaging software only contains 2D image and depth information. Taking into account the algorithm complexity of the three-dimensional imaging, that is one reason that current research do not concern too much about 3D reconstruction.

Since the 90's 20th century, the technologies of combining computer image processing and analysis, realistic computer image science technology, virtual reality such as three-dimensional image reconstruction has been a hot research and reported in many studies (Tian, 2003). The most critical part of three-dimensional image reconstruction is the three-dimensional modeling, then restore three-dimensional images objects (revisualization). The three-dimensional reconstruction of DT-MRI medical images is through a series of two dimensional images. Firstly, identify the images, then partition. According to the some imaging processing algorithms, we can restore the detected objects into three-dimensional image. After the reconstruction of three-dimensional model, the real tissues or organs of the surface profile can be produced to improve the quality of visualization. The reconstruction model is sliced to conveniently observe the internal organization or body shape changes, size and location. These can be better used for clinical diagnosis purposes. At present, three-dimensional medical image reconstruction methods can be categorized into three types: (1) Fitting the surface contour through the line between faults. (2) Generate isosurface directly from the three-dimensional volume data. (3) Do not construct the surface and give color and light resistance values to each voxel for direct volume rendering. The front types are the surface reconstruction and the last type is the volume reconstruction. The surface reconstruction is characterized by the use of surface modeling techniques with the isosurface generation, then use the surface illumination model to render the image. Compared with the surface rendering, volume rendering is a key feature and is to give up the traditional graphics side of the body structure by the concept of direct analysis of the light through the three-dimensional data field changes and achieve the final drawing results. Therefore, volume rendering is also sometimes referred as direct volume rendering.

The surface of the first reconstruction method is based on [Keppel 1975] contour description of the surface reconstruction method, that is, in the sectional image through manual or automated means to achieve the objectives of the uncertainty contour partition. Based on the volume data characteristics that they consist of many equality slices, the closed contours of objects in each slice can be derived and the object surface can be jointed by the

outlines of near slices. This method is simple with small amount of data, but it is more difficult to determine the multi-branch contour, judge the topology relationship between the near slices and the relationship between the connection points of branches. The display quality of pictures is rough.

In three dimensional surface reconstructions of medical images, the data are generated directly from the three-dimensional isosurface by a number of different methods. The first way was put forward in [Fucks 1977]. Polygon-based technology is an outline of the triangular plane algorithm. It uses a triangular piece to fit the set of surface contours. Lin used the contours of the B spline interpolation algorithm to get the whole smooth surface. The most popular cube algorithm is (Marching Cubes, MC), as well as dividing cube algorithm. [Lorenesen 1987] proposed a three-dimensional reconstruction algorithm. This algorithm has been implemented by a large number of applications in the field of medical images. As it has been applied for a patent, it is now recognized as the most popular method of surface display.

Based on three-dimensional reconstruction, the volume rendering method is to define each individual voxel a non-transparency value and consider each individual light transmission, emission and reflection effects. The transmission of light depends on the opacity of the voxel. Light emission depends on the voxel material, when the material is greater and the degree of its reflection is stronger. The reflection of light depends on the voxel according to the angle between the surface of voxel and the incoming light. Volume rendering method can be divided into four steps, including the projection, blanking, rendering and compositing. Volume rendering algorithms that deal with the objects in the corresponding three-dimensional space can be categorized into two types. One is regular data field of the volume rendering and the other is three-dimensional irregular data field of volume rendering. Irregular data field refers to the structured data of the irregular field data and unstructured data. However, the research and development of three-dimensional irregular volume data visualization algorithm is still a problem and need to be further addressed. The volume rendering field data studies are growing mature. There are four algorithms including [Zhang 2002]: projection ray (Ray Casting) [Levoy 1988], throwing a snowball method (Splatting), shear – surface reform [Iacroule 1994] and hardware 3D texture mapping method.

Volume rendering indeed can better reflects the true structure of the object structure. But due to the computation of volume rendering algorithm is too much, even if the use of high-performance computers, it is still unable to meet the practical application of the demand for interoperability. Therefore, surface rendering algorithm is still the mainstream.

Each algorithm has its own advantages and disadvantages. The choice of these algorithms is decided by the scope of engineering applications. For relatively simple, regular objects, a lot of algorithms may be satisfied for rebuilding. For highly complex, irregular and non-linear objects, there will be a great challenge for these three-dimensional reconstruction algorithms, and the problems should be further discussed. However, at the current application of underwater robots, these algorithms are able to meet the preliminary attempt.

The important contributions of this study are to improve the inadequacy of the current research of underwater robots. Taking advantages of advanced medical imaging processing methods to realize underwater three-dimensional reconstruction of objects and the path reconstruction, these technologies are firstly applied to improve the effectiveness and performance of the research in underwater robot.

The final chapter will show the use of known technology to the initial surface reconstruction by the online experiments. We adopt the image sonar in the experiment, which is used to collect images of objects distribution. Finally, we discuss the technical problems.

1.4.3. Algorithms of Robot Path tracking and DT-MRI tracking

1. The development of robot path planning algorithm

Generally compared with the autonomous mobile robot navigation problems, it is mainly to resolve the problems which are raised by Durrant-Whyte. These three problems: (1) 'Where am I?'; (2) 'Where should I go?'; (3) 'How can I go?'. Mobile robot path planning is to solve the second problem.

[Nilsson 1968] described the general movement of mobile robot path planning problem. He proposed visibility graph method for a robot to find the shortest path without collision. After nearly 40 years of research, a lot of algorithms have been proposed, these algorithms can hardly be perfect. They have their own advantages and disadvantages. As a result of a variety of methods in environmental modeling and different search strategy, although these algorithms are path algorithm, it is difficult to do further specific division. Reference to a large number of relevant path planning literature, drawing on the classification of the most common path planning algorithm, the algorithms above are categorized as a low-dimensional space path algorithm that has a complete planning approach. There are some new researches in recent years that solve high-dimensional space, including random sampling planning methods, the intelligent planning algorithms based on neural network etc. and some map theory algorithms.

Low-dimensional space planning approach can be categorized in detail as follows: (1) Visibility graph method [Nilsson 1969]. (2) Voronoi diagram [Canny 1985]. this algorithm is used in a wide range of fields including computational geometry study of the classic problem. The real-time character of Voronoi-based path planning is better and this algorithm generates relatively safe paths away from obstacles. These paths are smoother, reasonable, but can not guarantee the optimal paths. [Choset A 1995][Choset B 1995] proposed an improved research of generalized Voronoi sensor-based path planning. (3) The tangent map method. This algorithm is based on polygon obstacles and these arbitrary shape obstacles can be instead of similar polygon. To compare the results of building environment, [Liu 1994] shows that the tangent map view path planning can be more efficient than visibility graph method. (4) Grid based decomposition method. Grid based decomposition method [Kambhampati 1986] is the most extensive study of path planning methods. The robot work space is divided into a number of simple regions, commonly referred to the cell. As the grid constitutes a connected graph, the algorithm is in search of a map grid from the start of the path grid to the target. The path is presented with a serial number of grids. This type of algorithms is divided into an exact grid algorithm and an uncertain grid decomposition method. The first algorithm is the most commonly used as trapezoidal decomposition grids [Parsons1990][Latombe 1991]. The second algorithm sets the grids to be predetermined shapes, usually rectangular. The whole environment is cut into many larger rectangles, and these rectangles are consecutive [Chen 1997][Khatib 1986]. If the larger rectangle contains a barrier or border, it is divided into small

rectangles that continue to repeat till the boundaries of implementation. This algorithm is also known as the "Quad-tree." (5) Artificial potential field method; [Khabit 1985] proposed this method. The basic idea is to introduce a value called the potential field function to describe the geometry of space robots. The movement is tracked by searching the descending direction of potential. By continuously calculating the negative potential field gradient from the cooperation of the positive attraction potential field (between target and robot) and negative rejection potential field (between obstacles and robot), a virtual force can be achieved for the robot. The main advantage of this algorithm is less computation. However, this method has the following shortcomings (1) trap region; (2) hard to find the path between near obstacles; (3) an easy oscillation before the barrier; (4) swing in the middle of the narrow channel.

Though low dimensional space path planning algorithms above have nice completeness, these algorithms have the dimension problems when make path planning in high dimensional space. High dimensional space of the path planning is mainly based on random sampling methods to achieve the planning, but they have to improve efficiency in the condition of losing completeness. These high dimensional path methods can be categorized as follows: (1) Probability record method (PRM) [Lydia 1994] etc. Then a series of papers refer to road PRM application were published. PRM algorithm is to deal with the main problem that is the existing defects of the narrow passages. Many researchers proposed the solutions, such as [Wilmarth A 1999][Wilmarth B -1999] MAPRM, OBPRM etc. (2) Rapid random tree method [Lavalle 1998]. Its efficient search algorithm is concerned with high dimensional non-convex space. The random tree of rapid expansion adopts a special kind of incremental approach for construction. This method can rapidly reduce the expected distance between a random status and the tree. This random search tree can be considered as a Monte-Carlo method that tends to search maximum Voronoi regions. [Lavalle 2000] put forth an improvement algorithm Bi-RRT of bilateral tree method. This type of algorithm is now growing to be paid attention by more and more people.

Genetic algorithm [Jianping 2003][Nearchou 1998][Sun 2000], neural network algorithm [Janglova 2004][Kassim 1992][Yu 2001], fuzzy algorithm [Juidette 2000][Xin 2005]and many other intelligent path algorithms also have considerable prospects. Many scholars begin to add bionics theory such as the ant colony optimization algorithm [Fan 2004][Zhu 2005] and Particle Swarm Optimization [Sun 2005][Qin 2004] into the path planning algorithms. These algorithms are advantaged in finding the global optimum. However, due to too many parameters, a large amount of the calculation and the refractory degree of evolution, these also bring many defects.

Map search algorithms can be categorized as follows: (1) depth first search algorithm and breadth first search algorithm. These two methods are most popular graph search algorithms. In depth-first algorithm, the larger depths of nodes are expanded primarily. If the smaller depth of the node is expanded firstly, that is breadth-first search algorithm. (2) Dijkstra algorithm. The classic shortest path algorithm is Dijkstra search algorithm. This algorithm can be found from the source node to any node of the map through the shortest path. (3) A* algorithm [Huyn 1980]. This algorithm is a heuristic search algorithm that is applied a lot and its definition of the distance function is heuristic. However, an important condition for the polynomial in this algorithm is that the distance function must have a log derivate precision. However, in the actual applications, this requirement is very difficult to be achieved. Though

it is proved that the problem of plane obstacle avoidance A^* is a polynomial time algorithm, this algorithm is inefficient when the environment condition becomes complex and large. Therefore, to solve this defect, some of the ideas are proposed to improve them such as parallel algorithm, hierarchical planning algorithm. (4) D^* algorithm [Stentz 1994]. This algorithm is a dynamic algorithm. Here, it is called D^* algorithm, as reported in some other references. The main characteristics of this search are working with the dynamics of perception during the path of environment.

2. Development of DT-MRI path algorithm

The DT-MRI images tracking algorithm is different from the above algorithms. The main goals of this algorithm are built on a series of possible three-dimensional direction field, which may provide the most possible paths. However, the directions of the information are not reliable. They consist of a series of uncertain vectors. In DT-MRI path tracking algorithms, they can be categorized into three types. One type is based on the streamline tracking algorithms, which are proposed and developed to a series of algorithms [Basser 2000][Batchelon 2001][Parker 2001][Poupon 2000][Westin 1997][Westin 2002][Parker 2003][Gilbert 2007][Gössl 2002][Helm 2005][Hsu 1998][Lazar 2003][Lenoid 2003][Mori 1999][Pierpaoli 1996][Tuch 1999][Westin 2002]. The principle of this type of algorithms is relatively simple, mainly based on the direction integration of a number of spatial information for the final path. They are fast algorithms, but the algorithm does not take into account the direction of the unreliability of information. This defect makes them easy to get the wrong path information. Although subsequent work, many scholars put forward a number of improvement ideas, such as increasing the number of initial directions, considering joint of multi-directional information. Due to the inner defects of this algorithm, these improved methods remain a lot of wrong paths. The other type of algorithm is based on the random probability for high dimensional path [Behrens 2003][Björnemo 2002][Friman 2005][Friman 2006][Jones 2005][Lazar 2005][Lu 2006]. The advantages of this type of algorithm are paid attentions to the uncertainty factors of the path location. The direction is modified based on the theory of magnetic resonance imaging and the reliability is also improved. However, because a large number of random factors bring a large amount of calculation, this type of algorithm becomes slow. [Ola Friman 2006] proposed an improved method of the initial random path algorithm and the speed of calculation is also speeded up. [Fillard 2007][Fillard 2003][Fletcher 2004][Arsigny 2005][Pennec1999][Pennec 2006] proposed a new type of algorithm based on the Riemann space and the Log-Euclidean geodesic space that can provide strong mathematical characteristics for the point-to-point path tracking. However, the calculation time is long and the normalization of the direction may cause the distortion of original images and bring out the uncertain information.

Therefore, all the three algorithms has their own advantages and disadvantages, these algorithms need to be further enhanced and strengthened, and these are the main contributions in this research.

1.4.4. Analysis, discussion and significance of path algorithms for underwater robot

Underwater robots compare to land mobile robot, which is to solve the second question "I want to go where?" Design of AUV path is completely autonomous, therefore it is much more complicated to realize. For ROV control, the traditional way of method is to set the movement path by the operator. Compared with the AUV, the path design of ROV is relatively simple.

Although this research is mainly based on the ROV motion control, the traditional human manipulation is often difficult to achieve the desired results. It is also difficult to control the robot to well approximate the targets or do target tracking movement, especially for this type of ROV. Therefore, it is necessary to develop an intelligent control platform to bring the self-control and the operators' aided control together to realize effective dual-control.

The path theoretical study is needed to be explored in this research. Here, the definition of the task is that in the environment with obstacles, the underwater robot need to find a suitable path from the starting point domain to the target point domain without collisions, and then safely return to the starting point domain.

According to this task, we can see the movement of underwater robots can be divided into two parts: one part is to go; the other part is to return. Based on path planning algorithm development of mobile robot, it can be seen that these series of algorithms in solving the first part of path planning have certain advantages. Meanwhile, the tracking algorithms of DT-MRI show obvious advantages in solving the second part of the robot path planning. This is also a key technical problem that the thesis is going to solve.

1.5. Thesis work

The premise of this paper is that our research group develops a new type of super-mini underwater robot platform. The research group starts a series of related research works. Reference to a lot of documents of underwater robots, the improvement of the super-mini underwater robots is proposed to solve the design deficiencies of previous open-loop control algorithm. Based on the underwater robot motion control system design, this study puts forward new ideas and control algorithms, and get the results of experiments that verify the performance.

For the idea of three-dimensional reconstruction, we develop a preliminary applicable platform for underwater scene of three-dimensional reconstruction and its path tracking algorithms. This paper consists of following six major parts:

The first chapter describes the current underwater robots development in the world. A brief introduction to the underwater robot motion control algorithm development. DT-MRI three dimensional reconstruction algorithms are described. Their application for underwater robots and the significance are proposed. Then we introduce the development of robot path planning algorithm and DT-MRI path algorithm. We point out the significance of joining these two algorithms. Finally, a brief account of the research's content and its framework are described.

The second chapter describes in detail the framework of a new type of super-mini underwater robot including the system design, software and hardware design etc. A new adaptive neural network sliding mode controller with the balanced controller (ANNSMB) is proposed. An adaptive fuzzy sliding mode controller (AFSMC) is applied to underwater robot. Considering the PID controller, sliding mode controller, simple fuzzy sliding mode controller, AFSMC controller and ANNSMB controller, all the results are compared and analyzed through the simulation experiments. The experimental results of the comparison and analysis verify the effectiveness of the algorithm.

Chapter 3 describes the theory of the streamline algorithm. We propose a new maximum energy tracking algorithm theory. We put forward a new random path algorithm for three-dimensional tracking based on the Bayesian theory.

Chapter 4 presents the basic theory of DT-MRI image processing and the general ideas of spatial orientation. Then we describe the algorithm steps and interpretation of the new proposed maximum energy tracking algorithm. Based on the myocardial research background of human hearts, we accomplish the three-dimensional reconstruction experiments. Comparing the new algorithm with the traditional streamline algorithm and its improved algorithms, the results from these different algorithms prove that the new algorithm is effectiveness and has good performance. Finally, we discuss the reference value and the significance to the underwater robots path tracking from the results and algorithms of myocardial tracking.

Chapter 5 shows detailed analysis of DT-MRI from the three-dimensional space reconstruction algorithm and a number of cases are proposed to describe the steps of this algorithm. The experimental analysis and presentation have been done. The corresponding multi-sensors theory and several adaptive algorithms concerning how to acquire and cluster the spatial distribution of objects are proposed and the results are compared. Using these three-dimensional space reconstruction technologies, experiments were carried out and achieved a direct description of the distribution of space objects. The results satisfy our requirement.

Secondly, we propose a random three dimensional path algorithm based on the Bayesian theory. Using this new three-dimensional path tracking theory, the simulations are carried out for the underwater robot return path tracking and the results of the path reconstruction are discussed in detail. Finally, the ideas concerning how to use the streamline algorithm and the maximum energy tracking algorithm are proposed to implement the underwater robots tracking path reconstruction and the experiments.

Chapter 6 is to summarize this research and point out future works.

1.6. Summary

This chapter describes the development of underwater robots, underwater robots control algorithm. It discusses the development, relationship, significance through the study of three-dimensional objects reconstruction and path tracking algorithms between DT-MRI and the underwater robots.

PART I

SYSTEM AND CONTROL TECHNOLOGIES



Chapter 2 RESEARCH ON IMPROVED SUPER-MINI UNDERWATER ROBOT SYSTEM AND MONTION CONTROL

Summary

2.1. Introduction.....	17
2.2. System of super-mini underwater robot.....	18
2.2.1. Mechanical design of super-mini underwater robots.....	18
2.2.2. Design of the super-mini underwater robots and external equipment .	22
2.2.3. Super-mini underwater robot software design.....	27
2.2.4. Super-mini underwater robot system framework summary.....	30
2.3. Theory of underwater robot dynamics.....	30
2.4. Theory, simulation and experimental of underwater robot motion control	34
2.4.1. Theory of control algorithms and control algorithm design for underwater robots.....	35
2.4.2. Simulations, experiments and discussions of underwater robot motion control algorithms	46
2.5. Summary	56

2.1. Introduction

Research in the field of underwater robots, a large number of researchers has done a large number of research trials and developed many underwater robots. Due to wide range and complex applications, many different types of underwater robots are invented. As the development of no cable automatic underwater robot is very difficult and the expense as well as the experimental risk is relatively high, this type of underwater robot is not suitable for our preliminary developing work. Take into account of power provided by the cable, the cable underwater robots can continue to work for a long time and are easy to carry out experiments. The signal transmission is also simple, stable, secure and conducive to the recovery jobs etc. In the absence of prior experience on the adequate designs and development of underwater robots, our research team chooses the cable underwater robot to carry out research, which is beneficial to the accumulation of relevant knowledge and experience.

Research on this paper, there are obvious differences between super-mini underwater robots and other deep sea underwater robots, such as light weight, relatively small load, low anti-interference ability, low force of propellers. In different working environment, there are also great differences between these two types of robots. For deep-sea underwater robots, the current is not disorder. But the super-mini underwater robots as its main work is in shallow water, rivers and lakes, especially near the bridge environment, the water flow is very complex and this work is a very difficult and challenging. Therefore, how to design a robust and strong adaptive motion controller is a hard nut to crack. Although the super-mini underwater robots have many problems that need to be resolved, it is gradually applied to many works as it is cheap, portable, flexible for operation etc.

Super-mini underwater robot system platform is very complicated, which combines mechanical, hydraulic, electronic, computer science and mechanics etc. Thus, it is a complex research and development process. For the purposes of this research, how to construct simple, practical, efficient and reliable super-mini underwater robots are the most interested.

Generally, based on the previous designs, we move our attention to the advanced products of the underwater robots. We propose the methods to solve their problems under the condition of the actual experiments and strength their abilities by adding intelligent control platform instead of the idea of simple manual operation. Our Research starts from zero based point and step by step to build the super-mini underwater robot's mechanical equipment, electronic hardware circuit equipment, intelligent control, display platform, software platform etc. For the algorithm design of motion control, with references to the well-known experts [Fossen.T 1994][Morrison 1993][Newman 1977][Shi 1995][Shang 1988] etc., we carry out a wide range of theoretical and simulation studies and propose a new algorithm design based on the adaptive neural sliding mode controller combining with a new balanced controller. Considering the self-developed experimental platform, combined with a variety of motion control algorithms, many experimental tests are implemented. Although the theoretical simulation results are good, there remain some problems in experiments. The experimental results are effective to verify the algorithms for the improvement of system design, and provide many valuable experiences. We believe that the future research experiments will certainly provide better results. The main contents are listed as follows: 2.2 System of super-mini underwater robot; 2.3 Theory of underwater robot dynamics; 2.4 Theory, simulation and experimental of underwater robot motion control; 2.5 Summary.

2.2. System of super-mini underwater robot

The manufacturing design of Super-mini underwater robot is a highly integrated combination of mechanical and electrical knowledge. Reference to previous experience in the design of many designers, we suppose to implement an initial intelligent control platform and a display system. For the design framework of super-mini underwater robots, the design steps are divided into three parts, including the mechanical design, the electronic design and the software design. Here, this section will describe the design framework of these three parts. Due to too much work of system design, the contents are not described in detail. We present only the major emphasis of the design framework of the system, the key technical issues to facilitate the super-mini underwater and its practical applications in the experimental environment.

2.2.1. Mechanical design of super-mini underwater robots

The mechanical design research of the super-mini underwater robots, is drawn on the improvement of previous design ideas, including some mechanical designs and partial improvements [song 2007]. Mechanical design can be categorized into the following contents:

(1) Underwater robot body shape design

Underwater robots usually consist of pressure shell (body) and external structure. The pressure shell of underwater robots takes use of the ball and the cylindrical shape, or some combinations (the ball and the ball, the ball and the cylinder). There is also ellipsoid shape, ball - cylinder – conic type. Pressure vessel requires very good water resistant ability, and the general use is O-ring seal. The O-ring seals are attached to the back wall because of the press, and play important roles in sealing. When the gap is too large under high pressure, O-ring is squeezed out easily from the gap. Thus, the destruction of seals happens and the robot leaks. The gap is the small while anti-pressure ability is the high.

Generally, the shape of underwater robots is focused on the streamline design. Underwater robot body takes use of long ellipsoid shape and consists of the anti-pressure shell. This kind of shell is sealed to withstand the pressure of deep water. Long ellipsoid model is designed to reduce the water resistance, increase the flexibility, reduce the entanglement risk of underwater obstacles and improve the speed of obstacle avoidance.

Taking into account the working environment in shallow water, the requirement of the anti-pressure capabilities of the watertight shell is relatively lower than deep sea underwater robots. This study pays the attention to the use of full closure design model, to better resolve the watertight underwater robots problem. However, some cable underwater robots used in deep sea put emphasis on open-frame design and their watertight demands are higher.

Taking into account the expense and simple way of design work for fast mechanical design, we use a full-sealed shell. The underwater robot system core circuit boards, driver circuit board of external device, propulsion device, energy back-up devices etc. are all laid in the main body of underwater robots. This design is mainly on account of the simplicity of a whole package that can be relatively simple to deal with the issue of water, rather than taking into account many various watertight problems. However, it can also cause large problems. The risk of this design is larger than the open-frame underwater robots. If there are pressure shell problems, the entire underwater robots can lead to water seepage and the inner devices meet terrible disaster. This type of packaging design and electronic hardware design requirements are high, because the multi circuit boards interfere with each other by the large magnetic field. It is required for the use of a magnetic isolation shield to improve the reliability of underwater robots. For the mechanical enclosure design, we propose the supporting frames and anti-crash frames to prevent accidental collisions in the experiment.

In the mechanical design of underwater robots, it is important to pay attention to the weight in the water and the buoyancy, which is to ensure the balance. For the experiment, the design is necessary to revise the load of robot due to the mechanical handling equipment, some external equipment, materials etc. Thus, at the beginning of the experiment, the balanced tests are needed for super-mini underwater robot to keep good working condition and satisfy the needs of the experimental environment. We increase or reduce fiber foam or other weight-bearing and choose an appropriate location to satisfy conditions as the following:

$$\begin{aligned} G_R + G_A &= F_R + F_X, \text{ if } V_{\text{Water}} = 0, \\ \theta &= 0 \text{ and } \varphi = 0, \text{ if } V_{\text{Water}} = 0, \end{aligned}$$

where G_R , F_R respectively stand for the original weight and buoyancy, G_A , F_X are respectively the added weight and the buoyancy that consists of the terms from the added objects and the hydrodynamic effect, θ is roll angle, φ is the yaw angle, V_{Water} is the velocity of water flow.

Thus, if the super-mini underwater robots are not working normally due to the circuit or propeller malfunction, it dose not sink to the water unlike the ships because of the balance. However, if the sinking is caused by the broken shell, the added weights can be thrown away to make the robot float up. Therefore, security methods in the design are considered as following:

- a. Improve the reliability of commonly used devices;
- b. Focus on important systems. Enhance their anti-interference abilities and sealing or if possible, add one more backup and support system;
- c. Energy and capacity of the design have enough allowance;
- d. The structure and shape of underwater robots consider the risk of entanglement by cable, rope etc.

The body design of underwater robots is a very complex process, which remains in the continual exploration. Because the outer body of underwater robots will directly affect the shape of the reliability and flexibility. In order to take use of the theoretical knowledge of the underwater vehicle control motion equation [Fossen, 1994], our robot use the Ellipsoid strip design. We also do many experiments to accumulate more experience.

(2) The propulsion system of underwater robot design

The propulsion system design is a key part of the whole design. The functions of propulsion components are divided into three parts, propulsion generated components, power components, power transmission components. Components of propulsion are the core source of force and it shows the characteristics of propulsion from not only the shape but also the performance. Power transmission components, are composed by the propeller shaft and reduction gear. Sliding gap is the difference between screw pitch p and progress h_p . The ratio between sliding gap and screw pitch is known as sliding gap ratio S_a . Due to the existence of slippage, it can generate thrust propeller power. Propeller thrust power can occur as a momentum changes caused by the fluid passes from the front parts of the propeller to the end parts.

The general devices of underwater are powered by two methods. One is AC and the other is DC. DC motors have the characters of low price, better speed control performance, and can directly take use of battery power. However, due to DC motor commutator and brush of copper, they do not allow to contact with water and are often in the need of maintenance every 40 ~ 50h. AC motors are made relatively simple and require less maintenance. There are three types of motors that are placed in seawater: open-type, pressure compensation type and closed type. Open-type design lays all electrical motor exposed to sea water. This motor must be brushless and the stator must have excellent water-proof insulation wire, or water-proof rubber. Pressure compensation type includes pressure sealed or pressure balanced compensation film. Filling a non-conducting liquid to the motor system is used to prevent corrosion, realize cooling, lubrication and carry out the transmission of pressure to balance the external pressure. Pressure compensator or pressure balance film is playing the role of delivering the external pressure to the internal motor and making its own pressure equal to the pressure of the environment or slightly higher to prevent water intrusion. Closed type electric motor system is completely isolated from sea water and the environment. It is packaged in a corrosion-resistant metal box, and there is seal ring in the motor shaft. This design can use an ordinary motor and the closed metal box covers. Seal design must be capable of sustaining the environmental pressure. The improper seal equipment may cause water infiltration and give rise to short-circuit fault. Another type of protection for the motor is to put the motors inside the pressure-resistant shell. Similarly, in the cross part of the shaft, it is necessary to ensure the rotation of the axis besides the watertight and pressure-resistance. Therefore, we need to take into account the seal to prevent leakage and reduce the amount of the wear loss in sealed parts [Jiang 2000][Zhu 1992][SongB 2004]. In this design, DC motor is used mainly because of its better economic performance and speed control abilities, which is convenient for the design and motion control.

Generally speaking, in order to control the yaw movement, the ships are using the airfoil rudder. When flow speed is relatively large, the rudder can get good performance, otherwise, the rudder can hardly work well. Due to the low speed of underwater robot, it takes almost no effect to control the yaw angle by the rudder airfoil. Therefore, the rudder is abandoned and we suppose to apply multiple thruster devices for the movement control in this design. Meanwhile, taking into account the whole design and sealed simplicity, we use the close type motor design. Thrusters are divided into three types including the horizontal propellers, lateral and vertical thrusters, as shown in Fig.2-1.

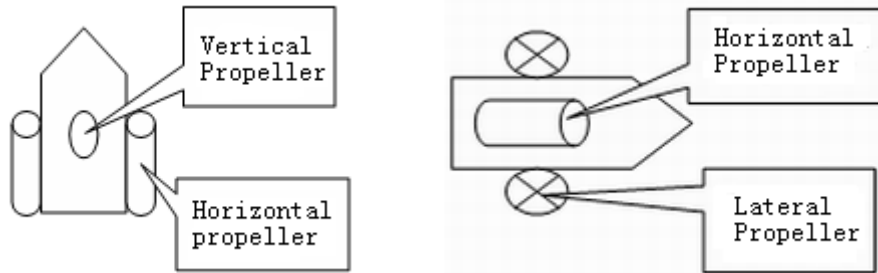


Fig.2-1 Forwarding Mode of Super-mini Underwater Robot

1) Surge and yaw

Generally, the super-mini underwater robot uses two horizontal reversed propellers to realize the forward and backward movement. These two propellers can promote positive and reversed rotation. To change yaw angle, we can change different speed of the individual thruster. We also propose two lateral thrusters to enhance the flexibility of underwater robots.

2) Sway

Sway movement is controlled by installing the central, bow or stern horizontal propeller, such as "DSRV" and "mermaid" etc. In order to increase the underwater robot's activation ability in complex environment and the flexibility of motion movement, the middle body is individually equipped with a horizontal propulsion in the upside and downside of the underwater robot. The main purposes are in twofold:

Firstly, we take into account the complexity of shallow water. For example, along the two sides' wall or closer to the bottom of the hull etc., it is unable to get the stable observation only by controlling the left and right side propellers. Though the camera can have a wide range of angle rotation, it is found that these simple two propellers are not enough for the observation of the target. The disturbance of the flow along both sides to the underwater robots is seriously interfered with the stability of underwater robots. Therefore, the proposed lateral thrusters are to enhance the flexibility and controllability.

Secondly, for the wide range of linear motion, the lateral thrusters keep fast and convenient characters. However, for small area movement, there are serious deficiencies. Thus, the lateral thrusters can improve the flexibility of underwater robot in shallow water and the robot has much stronger motion abilities and motion ways when it moves forward the target in a small area.

3) Heave

Heave refers to the depth control of underwater robots. The general underwater robot installs 360-degree rotation propellers in the vertical plane. When the two propellers transform from the horizontal position to the vertical position, the underwater robot movement is changed from surge to heave. 'Alvin' and 'sea cliff' adopt this heave movement. Another approach is the installation of vertical propellers in central or bow and stern part of robot, such as 'ALUMI' 'DSRV' and so on.

In this design of underwater robot, one vertical control propeller is installed in the central part. It can do the positive or reversal rotation to realize the heave movement.

4) Pitch

To realize pitch movement, one effective way is to use the sleeve propeller which can rotate in the vertical plane. The vertical channel propeller takes use of this propeller to realize pitch movement. However in the energy view point, it is not economic.

In this design, the pitch ability is failed to be paid enough attention, which will be improved in future work.

5) Roll

Generally it is not necessary to continuously adjust roll angle. In the navigation, the rolling balance is predetermined. For the majority of underwater robots, they do not have the significant abilities to adjust roll angle. However, for some special mission types such as the deep submergence rescue vehicle DSRV, due to the needs of docking with the accidental boat, the roll movement is realized by transferring the mercury from one side to the other. ‘The Franklin’ has a pair of thrusters on both boards. When they make opposite movement in the vertical plane, roll motion is created. In our design, roll is not fully taken into account. In our future work, this motion will be further explored.

Above all, the thruster configuration of the super-mini underwater robot is used to promote hybrid vertical and horizontal motions, which can satisfy current requirement of this research. Although there remain many inadequacies, it will be further improved and become better in future works.

(3) Energy devices of underwater robots

In this design, considering a backup power supply and external equipment control box, power supply control box transmit the energy to the underwater robot through the cables. In the condition of normal power input, the standby power of underwater robots does not work and the external power supply is used. However, when the input cable does not work correctly resulting in inadequate power supply, the system returns a warning signal. Meanwhile, the back-up power is adopted to enhance the normal operation.

2.2.2. Design of the super-mini underwater robots and external equipment

The detailed section on the key technologies of super-mini underwater robot mechanical design is described above. Because the contents are too much, we only discuss a few important points in detail. This section, we will continue to describe the electronic framework in detail, taking into account the specific design of electronic circuits, such as some complex technical problems. Here, we do not focus on the introduction of electrical chips, circuit design theory as they are the details of the normal technical problems. Thus, the overall framework for the design of electronic equipment is to be explored. The whole electronic design of our research is categorized into the following areas, shown in Fig.2-2.

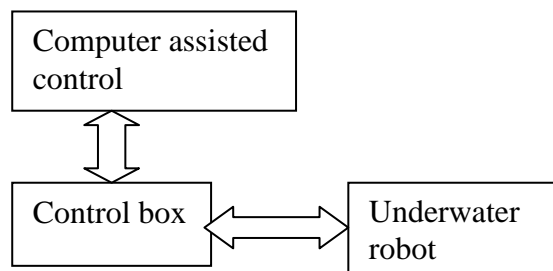


Fig.2-2 Whole Plant Frame of the Super-mini Underwater Robot

(1). Super-mini underwater robot platform surface electronic circuits

The design of the surface electronic circuits of the underwater robots is divided into three parts including the computer-assisted high performance platform, independent control box, power devices.

1). Connection equipment between the computer and the control box

In the hardware design of electronic equipment, we take into account the distribution problems about a variety of control signals, send or receive bulk data signals etc. For the design of the central control box, the multi-functional integrated computer chips are used to realize the high-performance embedded systems for a transmission terminal. Considering the

optimization of system performance, we apply many ways of high-speed transmission to avoid the data block problems brought by a single serial port that send and receive data and reduce the time delay errors. Therefore, the high-performance computer system is the highest level core to deal with the data transceiver, receiver and processing etc. These core components, which separate signals into different types of data sets and transfer them through the serial port, USB interface, Ethernet interface based on different speed rate. The priorities of different data set are determined by control box to make accurate transmission of data or control commands transfer.

Taking into account the future design process of underwater robots, more than one robot join the tasks. Thus, Ethernet communications are necessary and proper high performance communications.

2). Electronic control box design platform

Underwater robot control box is a core part of the whole design. Based on the development experience from several well-known small underwater robot design company, this circuit design of this control box can be broadly divided into power conversion circuit, switch components, joystick, LCD, integrated embedded core chip circuit, auxiliary integrated single micro process chip circuit and protection circuit, as shown in Fig.2-3. This design of the power circuit is installed with 48 volt DC power supply which is inverted from the 220 volt AC. This 48V power supply is the driving power for the entire underwater robot, including the propulsion system, microprocessor module, and camera etc. Therefore, the power circuit is a very important and necessary part, which needs strict attention to these power problems such as anti-jamming, anti-magnetic, stable power output, and many other issues. Here, more appropriate design and circuit improvement are essentially to prevent the problems of analog electronic circuits, and digital electronic circuit signal such as interoperability and mutual interference and other problems of voltage or current.

Switch circuit of the underwater robots is to deal with the power switch, light switch of the body, backup power switch, camera switch and camera motion control switch etc. These switches are mainly for the control switch of underwater robots' inner equipment.

In previous products, Joystick and associated circuit are used for the manual control of underwater robot without the computer. It is directly controlled by the console joystick for the implementation of an underwater robot open-loop control motion mode. It is mainly used to carry out easy and quick underwater robot tasks.

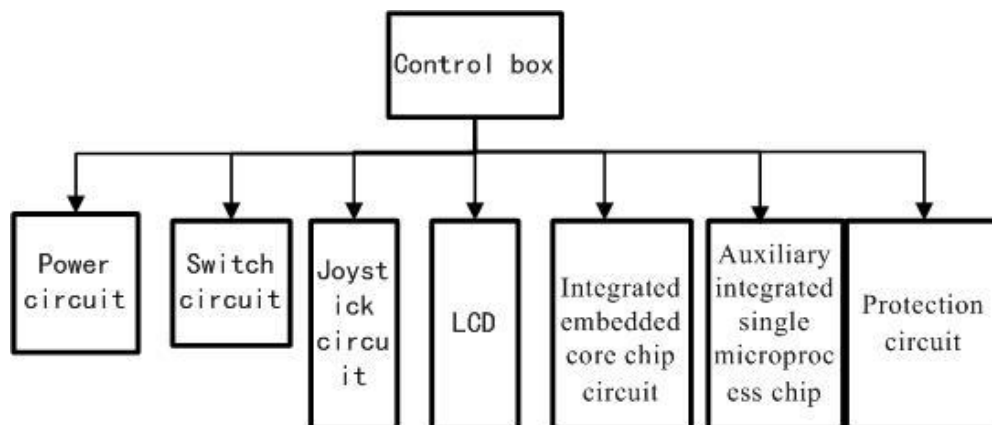


Fig.2-3 Electrical Circuit Model of the super-mini robot Control Box

This traditional joystick control method does not consider a combination of a computer. When the underwater robot wants to track targets in small areas or keep stabilities in complex environment, it is always difficult to master this robot well.

Liquid crystal displayer shows the observed image data when the underwater robot in the water. This image data are stored in hard disks. Meanwhile, when using the joystick to

operate this underwater robot, it is very convenient to control the conduct of motion through the image data shown in the liquid crystal display.

The embedded integrated chip circuit is the core of control box. It focuses not only on the operation of the whole box, but also the communications operation between the computer and the underwater robot body.

For the cores embedded chip in underwater robot which provides the communication process to the computer, it can give many ports such as USB port, network port, serial port etc. These convenient ports for communication are much more advanced than the previous single serial transmission mode. There is an obvious improvement if we take use of them. The USB port and the network port can provide a quick transmission speed for a large amount of data. They are able to adequately assure the capacity of data transmission of the underwater robot. Otherwise, the ports of the embedded chips have been greatly increased and we can fully ensure the interface for the external simple switch control circuit, the protective control circuit and display control chip etc. These advantages of chips also show potential for improvement.

Taking into account the multi-task processing performance of the core embedded chip, we use embedded chips to reduce the excessive computational burden of data pre-processing, and several Single Chip Micyoco (SCM) systems are combined for the various types of data pre-processing, such as the inclination sensors, depth sensors, position sonar data, image sonar data, electronic compass data etc. These data have different data types and formats. Therefore, we need different data pre-processing methods. The assisted SCM systems and the core embedded chip system are passing the data through the bus model. In the last few years, bus transfer mode is a popular and mature communication method for multi-level microprocessor. It is not only an effective way to realize a number of microprocessors communications, but also not be an excessive consumption of energy.

After experimental proofs, these means of communication can satisfy the various port signals for different data sources and ensure their effective transmission of data signals.

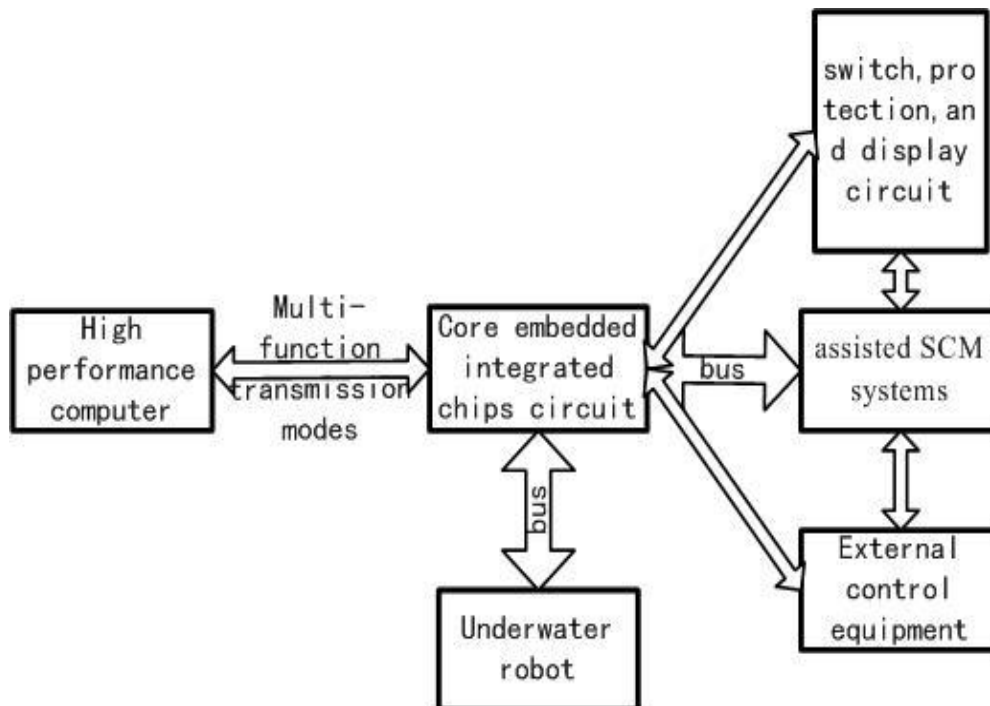


Fig.2-4 System Frame of the Core Processing Unit

Bus-based communication has the following characteristics: Strong surveillance and monitoring capability, reliability and high fault tolerance, good real-time responsiveness, small message length, low cost, architecture complexity, simple protocols, medium communication ability, medium communication speed, and low-environmental requirements. However, it has poor compatibility working with other Internet, because the bus has not

considered the connection technology with other network. Thus, this method can be applied to the core design of underwater robots, and a multi-level SCM bus technology are used to deal with multi-channel signal data, as shown in Fig.2-4.

(2). Super-mini underwater robot electronic circuits platform

Super-mini underwater robot's own platform electronic circuit is mainly responsible for dealing with communications with the control box. It receives the control information that is sent to the propulsion of underwater robotic devices. Meanwhile, all the sensors in underwater robot collect the data when the robot is working in the water. Then the robot connect with the control box by the electronic circuit platform, and sends the information back to control box to complete a cycle process of transmission, as shown in Fig.2-5.

Taking into account the embedded chips of underwater robots need to deal with a large amount of data and commands, we pass the data from position sonar equipment, image sonar directly the control box of the multi-processor systems through the cable. This main reason is to minimize the burden on the controller and to speed up its processing in control box to send the command. However, this way may lead to data errors and instability. Thus, for positioning and imaging sonar, the data cable of high quality is necessary during the process of data transfer, as shown in Figure 2-6.

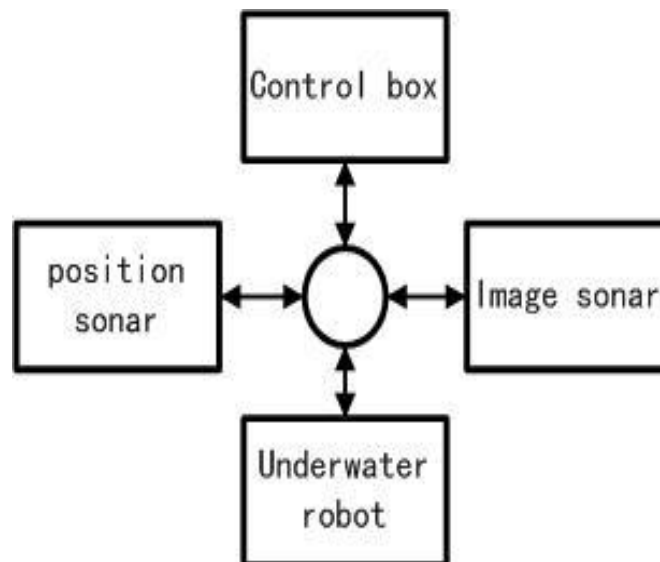


Fig.2-5 Whole Frame of the Super-mini Robot Electrical Design

In the actual testing process, position sonar and image sonar are continually collecting the data signals, once they are working for the underwater robot. They take up the time of the main motion control of underwater robot. Therefore, in order to ensure the movement characteristics of underwater robots, we adopt a multi-level processing system to deal with these two groups of large amounts of data, respectively. For the own system of underwater robots, the allocation of resources are reduced and the real-time, reliability are assured. Therefore, we like to use this hardware design methods.

The choice of core processors for super-mini underwater robot electronic circuit design consists of a number of embedded processors and microprocessors. The electronic design system is mainly involved in the following areas:

1) Power Equipment:

Underwater robot power equipment includes two parts. One is the total power imported from the control box. The other is the backup power supply. In this research, the use of backup power is battery. We use the AC-DC inverter circuit of control box to create the total power and transfer data to the underwater robot by high-quality cables.

2) Water depth pressure sensor:

Pressure sensor is to measure pressure data that is corresponding to the water depth. It can convert the pressure data to underwater depth. The following characteristics should be noted for the type selection of sensor: a nice seal for the pressure sensor; corrosion resistance and impact resistance; large range.

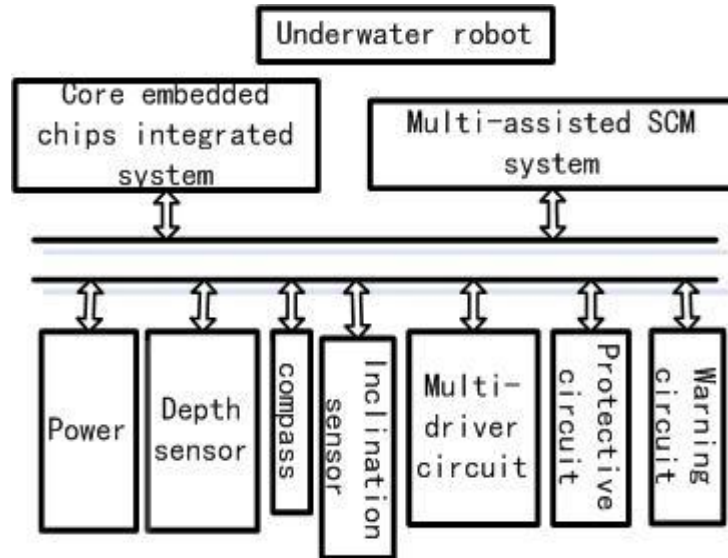


Fig.2-6 Detailed Electrical System of Super-mini Underwater Robot

3) Electronic compass:

The common magnetic flux sensor, which deals with the data acquisition and processing through specialized chips, is to overcome all kinds of hard and soft iron (magnetic) influence through the characteristics of high resolution and good repeatability. In this study, the electronic compass is located in body of underwater robot and it sends back the processed data to the control box through the embedded circuit board.

4) Inclination angle Sensor:

This work uses high-precision dual-axis digital angle module. The sensor is a high integrated posture measurement product and used to measure the inclination angles of the objects such as pitch and roll angle. This sensor takes use of simple communication protocol for attitude measurement. Through the practical testing, the work of this sensor is stable.

5) Multi-driver circuit:

Propulsion uses DC motor. DC motor drive and control circuit adopts the H-bridge driver circuit, high-power chipset. Motor Control takes use of the PWM pulse control and the entire motor circuit has nice protection such as optic coupler isolated circuit.

6) Protective Circuit:

Protective circuit is mainly used for the analog-to-digital circuit such as the power circuit isolation and protection measures. In the power circuit, the protection of the main circuit board is to monitor the status of the work. If the power supply is lower than normal one, it uses the backup power to maintain stability in the work and notify the poor status to the control box by alarm circuit. If the power supply is higher than normal one, control circuit will cut off the power circuit and open the backup power. This status also will be passed to the control box through alarm circuit.

7) Alarm Circuit:

For statistical and tracking the status of underwater robot, the alarm circuit uses hardware design and do the transmission to control box through a special cable.

Taking into account multiple thruster control circuit design, underwater robot circuit design includes the drive circuit, the analog-digital isolation circuit and protection circuit of the main circuit board. In this design, we use several high power driver circuits and are very necessary to pay attention to a steady supply of power. The test time of original main power supply circuit board is also very necessary to ensure that each thruster can work normally. In the complex flow field, this measure can ensure that the work of underwater robot and the control algorithms can show better performance.

2.2.3. Super-mini underwater robot software design

The software diagram of the super-mini underwater robot system consists of three parts: the PC software platform, the control box software design, underwater robot own software design.

<1>. PC software platform

In this design, we use Labview visualization programming software to implement software platform. Combined with C++ program language that is to carry out the algorithm and data processing procedures, we can realize a hybrid programming control platform of underwater robot. This control software program consists of front platform and back platform. These two core ideas of the specific software architecture are shown in Fig.2-7.

Labview programme idea is convenient, efficient. The Labview interface controls are very simple and easy for implementation. Taking into account the realization of the rapid process intelligent algorithms, Labview can call DLL (dynamic Link Library) and many special software modules to upgrade the programme. This way of design can improve the real-time software and to reduce the consumption of computer run-time resource. For the current research of our control algorithms, it is a nice choice for fast dynamic control development.

Computer controlled platform includes a front control interface and a background control system. Front control interface includes switch control visualization and graphical interface such as input and output buttons, as shown in Fig.2-7. The figure is the design of the front and simplified interface to implement a simple platform for an interactive interface, including the control of the propeller that is a simple box operation in the upper right corner of the figure to deal with convenient and automatic processing. Meanwhile, the background algorithm receives the command from the front interface and implements propeller's cooperative motion control commands. The left parts like clock shape in the figure displays the heading angle, respectively. One is the actual yaw angle and the other is the command angle. When heading angle is commanded, the algorithm automatically calculates the output parameters for the optimal propeller control. For yaw angle control and depth control, this platform takes use of the algorithm of the PID control algorithm etc. and set the input buttons for the initial parameters.

The main purpose of this design is to strengthen the movement abilities of underwater robots in the practical tasks through strong control systems and can reasonably satisfy the track of the fixed obstacles in the flow or the relatively stable observations etc.

For front control interface, it includes the status working buttons, the motion control buttons, communication status components, algorithm and data selection buttons etc. This front control interface also has light control buttons etc. to deal with the outer devices. For background control system, it contains the communication driver program of control box, the intelligent control algorithm, data processing algorithm, status selection and database setup program etc.

For background algorithms, the communication process of the host computer and control box includes the programme of a variety of communication protocols. There are serial ports, USB ports, and network ports etc. Different types of data pass different ports to realize the communication to the control box. In order to enhance data reliability and system stability, we pay enough consideration to the time schedule and multi-level resources distribution of

embedded systems. According to the length of the data transceiver and the size of channel occupancy time, we rationally allocate the priority of the entire transfer signals. The initial state setting is to determine the whole initial control system parameters, including the control system parameters, protocol parameters, and initial states of external devices. This process is a key point to ensure the normal communication.

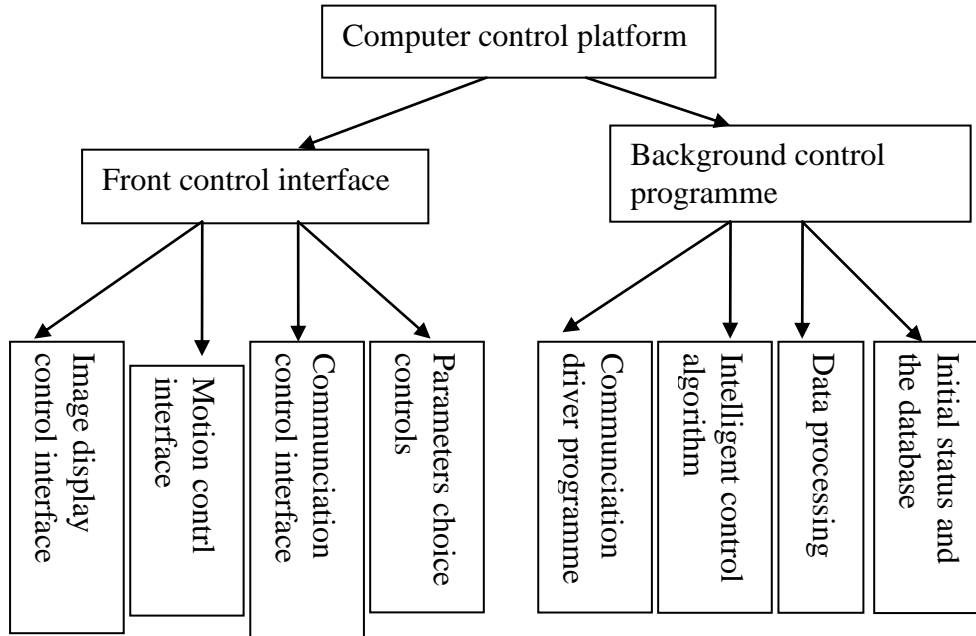


Fig.2- 7 Control Software Design Frame of the Upper Computer

Database setup program records all the transfer sensor data of various sizes and formats and the control data of underwater robot. This data can be used for simulation or testing control algorithms. Thus, we can easily carry out a combination of theoretical and experimental analysis.

Data processing algorithms includes how to resolve a variety of feedback sensor data such as the spatial location of sonar analysis, sonar images, and the inclination sensor data. Due to the different formats of these data, they need separate treatment.

Intelligent control algorithm is realize the different control algorithms for propulsion equipment or other adjustments based on the processing of feedback sensor data and the initial parameters. The obvious advantage of the algorithm is the performance of automatically locking the depth and heading angle. Control algorithm is programmed by c++ and embedded to the whole software system. This convenient program shows big advantages.

<2>. Control box software design

Super-mini underwater robot control box is mainly to deal with the embedded systems and the multi-level assisted SCM supporting system. Multi-level assisted SCM system is mainly responsible for dealing with the separate data from different sensors, through the multi-level analysis. In single-chip system, each unit is added with the data-processing algorithms, calibration and filtering algorithms. Meanwhile, in order to ensure the reliability of data, we add a number of signs to determine data and do reasonable priorities sort during the communication process of the single-chip systems and embedded processing systems. Thus, the bus bandwidth transmission of processor can be fully utilized when communications among a number of microprocessor. These microprocessors can play better data communication capabilities, in Fig.2-8.

Embedded processing system using the latest embedded system Linux, this system is an open-source code and the external device drivers are simple and very easy to be loaded for the development. They can also realize the multiple level transport protocol ports. The embedded operating system can improve the function of multi-level process scheduling. Through the

arrangement of all programs' priorities and appropriate correction and error-correcting communications protocol, we can basically realize the correctness of data transmission between the embedded operating systems and other multi-level chip-assisted systems. Meanwhile, embedded processing systems can also give a reasonable arrangement for other devices' control and protection procedures and transfer status information to underwater robot on time.

<3>. Super-mini underwater robot software design

In the super-mini underwater robot software, the image sonar systems and positioning sonar system pass directly from the communication protocol to the control box through the multi-stage process. Underwater robot embedded processing systems can not only deal with a number of sensor data, but also support the independence of various types of sensor data processing by the multi microprocessor system. It can also handle the work of multi-propulsion and driver circuit, as shown in Fig.2-9.

Multi-propulsion system of the control movement algorithm is completed in the host computer. Host computer can accept the data from underwater robot sensors. After processing algorithm, the computer returns the feedbacks to the underwater robot. The embedded system confirms the feedbacks and sends the commands to the assisted SCM systems to control the multi-propeller systems. Meanwhile, SCM system can communicate with every working propeller, and accept real-time status information etc. Then the information is sent back to the embedded system that makes reports to the control box about the working conditions. This procedure can implement the joint working abilities of underwater robots.

Embedded processing system is mainly responsible for the program deployment, information gathering process, and instructions delivery etc. Thus, the body of underwater robots can be considered as a hub and other assisted micro-processing system is to monitor and convey the information to all the units. Here, they can be divided into propulsion, sensors, power systems, protection and alarm circuit.

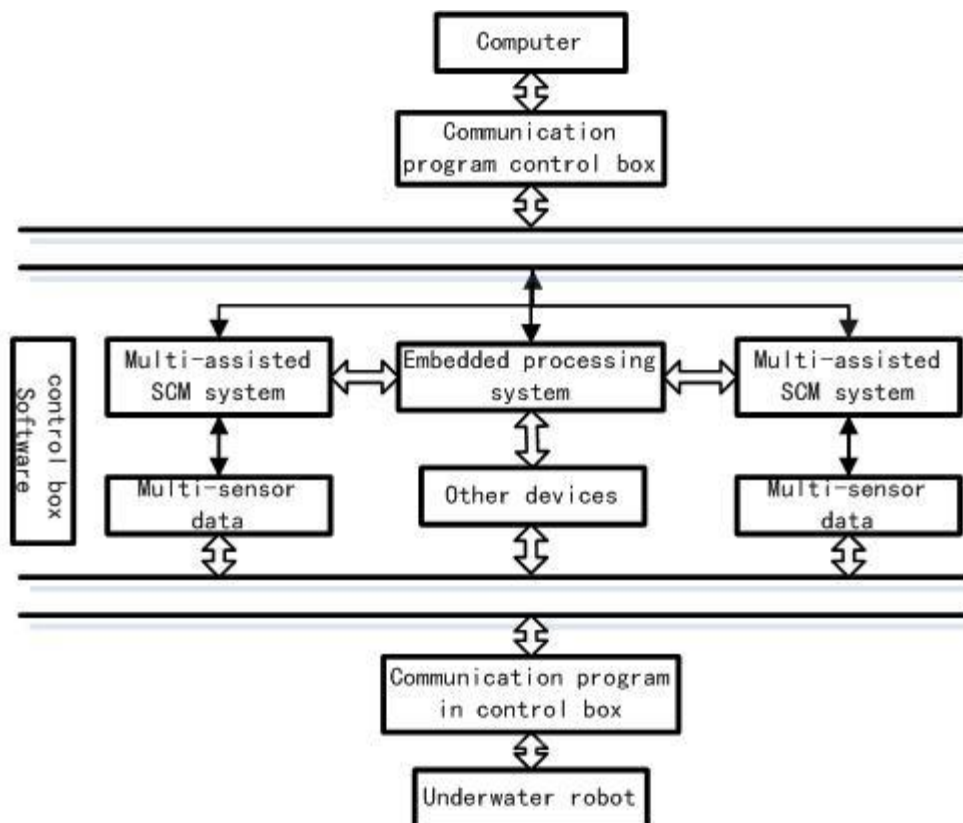


Fig.2-8 Software System of Underwater Robot Control Box

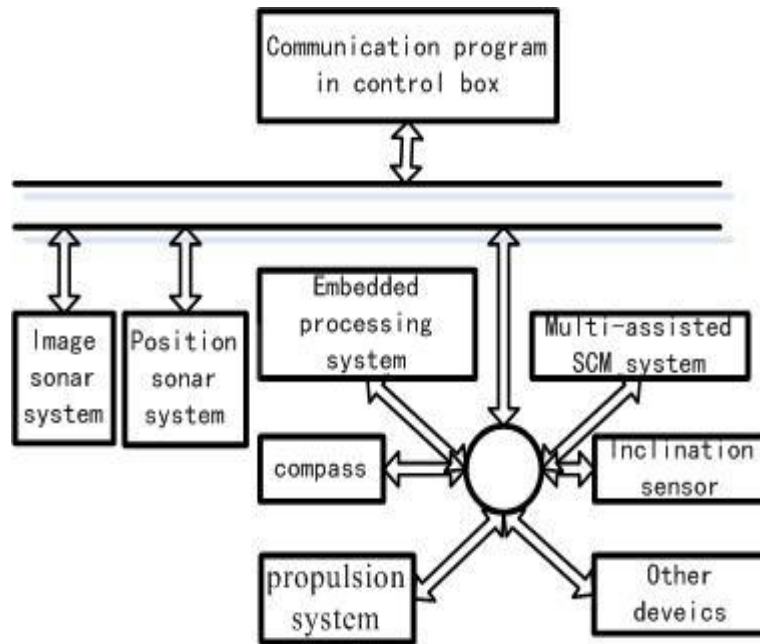


Fig.2-9 Software Design of Underwater Robot

2.2.4. Super-mini underwater robot system framework summary

Above all, a detailed description of the three main modules of the experimental design is presented. It includes improvement of underwater robot mechanics, circuit and software design. These three sections focus on the key technologies and the whole design frameworks without detailed description of engineering works.

Super-mini underwater robot system design and development are complex crossed major research and development works. We have done many works and great efforts. In the design of this new type of super-mini underwater robots, the process needs a lot of exploration, and take a lot of detours. Through the previous experience, there remain a lot of problems and they are in the need of many future works to improve the design.

2.3. Theory of underwater robot dynamics

This section describes theoretical knowledge of the dynamics of underwater robot, which includes the underwater robot kinematics, water dynamics, the additional inertia force, hydrodynamic damping, etc.[Fossen 1994][Morrison 1993][Newman 1977][Shi 1995] [Shang 1988]. This section provides a theoretical modeling basis for the control algorithms and experiment works of super-mini underwater robot research in the following sections.

1. Underwater robot kinematics

Two main reference frames are used for underwater robot. One is the earth coordinate frame, also called globe inertial coordinate frame. The other is the body-fixed coordinate frame. Body-fixed coordinate frame (X_B, Y_B, Z_B) coincide with the principle axes of inertia and the origin is generally defined at the center of gravity. The location of underwater robots $\eta_p = [x, y, z]^T$ and the direction $\eta_o = [\phi, \theta, \psi]^T$ (Attitude of roll, pitch, and yaw) is based on the globe inertial coordinate frame. Linear velocity vector $v_p = [u, v, w]^T$ (Surge speed, sway

speed and heave speed) and angular velocity vector $v_o = [p, q, r]^T$ (Angle velocity of roll, pitch and yaw) is based on the body-fixed coordinate frame.

If $v = [v_p^T, v_o^T]^T$ and $\eta = [\eta_p^T, \eta_o^T]^T$, the motion equation transition in the earth coordinate can be defined as the following:

$$\dot{\eta} = J(\eta_o)v, \quad (2-1)$$

$$J = \begin{bmatrix} J_1 & 0_3 \\ 0_3 & J_2 \end{bmatrix}, \quad (2-2)$$

$$J_1(\eta_o) = \begin{bmatrix} c\psi c\theta & -s\psi c\phi + c\psi s\theta s\phi & s\psi s\phi + c\psi c\phi s\theta \\ s\psi c\theta & c\psi c\phi + s\phi s\theta s\psi & -c\psi s\phi + s\theta s\psi c\phi \\ -s\theta & c\theta s\phi & c\theta c\phi \end{bmatrix}, \quad (2-3)$$

$$J_2(\eta_o) = \begin{bmatrix} 1 & s\phi t\theta & c\phi t\theta \\ 0 & c\phi & -s\phi \\ 0 & s\phi/c\theta & c\phi/c\theta \end{bmatrix}, \quad (2-4)$$

where $s \cdot$, $c \cdot$, and $t \cdot$ represent $\sin()$, $\cos()$ and $\tan()$.
(For example: $s\psi = \sin(\psi)$).

The angle range is defined as:

$$\phi \in [0, 2\pi[, \quad \theta \in \left] -\frac{\pi}{2}, \frac{\pi}{2} \right[\quad \text{and} \quad \psi \in [0, 2\pi[.$$

The velocity transform matrix J is the Jacobian matrix.

2. Underwater robot dynamics

Assuming the velocity of the underwater robot is relatively slow, the complete mathematic equation of underwater robot motion can be modeled by Euler theory based on the theory of the hydrodynamics etc. Here, we define six DOF body motion equation as, like [Fossen 1994] [Newman 1977][Shi 1995] [Shang 1988] :

$$m[\dot{u} - vr + wq - x_G(q^2 + r^2) + y_G(pq - \dot{r}) + z_G(pr + \dot{q})] = X, \quad (2-5)$$

$$m[\dot{v} - wq + ur - y_G(r^2 + p^2) + z_G(qr - \dot{p}) + x_G(qp + \dot{r})] = Y, \quad (2-6)$$

$$m[\dot{w} - uq + vp - z_G(p^2 + q^2) + x_G(rp - \dot{q}) + y_G(rq + \dot{p})] = Z, \quad (2-7)$$

$$I_x \dot{p} + (I_z - I_y)qr - (\dot{r} + pq)I_{xz} + (r^2 - q^2)I_{yz} + (pr - \dot{q})I_{xy} \\ + m[y_G(\dot{w} - uq + vp) - z_G(\dot{v} - wp + ur)] = K, \quad (2-8)$$

$$I_y \dot{q} + (I_x - I_z)rp - (\dot{p} + qr)I_{xy} + (p^2 - r^2)I_{zx} + (qp - \dot{r})I_{yz} \\ + m[z_G(\dot{u} - vr + wq) - x_G(\dot{w} - uq + vp)] = M, \quad (2-9)$$

$$I_z \dot{r} + (I_y - I_x)pq - (\dot{q} + rp)I_{yz} + (q^2 - p^2)I_{xy} + (rq - \dot{p})I_{zx} \\ + m[x_G(\dot{v} - wp + ur) - y_G(\dot{u} - vr + wq)] = N. \quad (2-10)$$

Here m is the mass of underwater robot in the air; x_G, y_G and z_G are the positions of the center of gravity in earth coordinate frame; X, Y, Z, K, M, N is the outside force and momentum. I_x, I_y etc. are the different inertia matrixs.

According to [Fossen 1994], the above complex equation can be simplified in body-fixed coordinate frame as:

$$M_v \dot{v} + C_v(v)v + D_v(v)v + g_v(\eta) = Bu. \quad (2-11)$$

Here, $v = [u, v, w, p, q, r]^T$ is the vector of the linear and angle velocity. $M_v, C_v(v)v, D_v(v)v$, and $g_v(\eta)$ represent the mass matrix, the centripetal and coriolis terms, the damping matrix, the vector of gravitational forces and moments, respectively. In the earth coordinate frame, the equation can be modified as:

$$M(\eta)\ddot{\eta} + C(\eta, \dot{\eta})\dot{\eta} + D(\eta, \dot{\eta})\eta + g(\eta) = J^{-T}(\eta)Bu, \quad (2-12)$$

where $\eta = [x, y, z, \phi, \theta, \psi]^T$ is the position and attitude vector; $M(\eta) \in R^{6 \times 6}$ is the inertial matrix including adding inertial part; $C(\eta, \dot{\eta})\dot{\eta} \in R^6$ is the centripetal and coriolis term; $D(\eta, \dot{\eta})\dot{\eta} \in R^6$ is the damping term including the quadratic and linear drag terms; $g(\eta) \in R^6$ is the hydrostatic restoring force terms; $J(\eta) \in R^{6 \times 6}$ is the transform matrix between the body-fixed reference and the earth reference; $B \in R^{6 \times P}$ is known constant propulsion parameter matrix; $u \in R^P$ is the thruster force matrix; P is the number of the thruster.

In our research, the equation $\eta = [x, y, z, \phi, \theta, \psi]^T$ is simplified to $\eta = [x, y, z, \psi]^T$ because the pitch and roll movement can be measured, but hardly be controlled.

3. Additional inertial force

The additional inertial forces are induced by pressure forces. They are proportional to the acceleration of the vehicle. The vehicle is continually displacing water, while it is moving. Thus, it creates these forces.

The kinetic energy T_A from the water displaced is calculated as:

$$T_A = \frac{1}{2} v^T M_A v,$$

where M_A is the added mass matrix, which is expressed as :

$$M_A = - \begin{bmatrix} X_{\dot{u}} & X_{\dot{v}} & X_{\dot{w}} & X_{\dot{p}} & X_{\dot{q}} & X_{\dot{r}} \\ Y_{\dot{u}} & Y_{\dot{v}} & Y_{\dot{w}} & Y_{\dot{p}} & Y_{\dot{q}} & Y_{\dot{r}} \\ Z_{\dot{u}} & Z_{\dot{v}} & Z_{\dot{w}} & Z_{\dot{p}} & Z_{\dot{q}} & Z_{\dot{r}} \\ K_{\dot{u}} & K_{\dot{v}} & K_{\dot{w}} & K_{\dot{p}} & K_{\dot{q}} & K_{\dot{r}} \\ M_{\dot{u}} & M_{\dot{v}} & M_{\dot{w}} & M_{\dot{p}} & M_{\dot{q}} & M_{\dot{r}} \\ N_{\dot{u}} & N_{\dot{v}} & N_{\dot{w}} & N_{\dot{p}} & N_{\dot{q}} & N_{\dot{r}} \end{bmatrix}. \quad (2-13)$$

The terms of M_A are defined in the SNAME (1950). For example, the hydrodynamic added mass force Z_A along the Z-axis is created by acceleration \dot{v} along the y-direction. It is written as:

$$Z_A = Z_v \dot{v}, \quad \text{when } Z_v = \frac{\partial Z}{\partial \dot{v}}. \quad (2-14)$$

According to [Fossen 1994], we can define the expression of the added mass forces and moments from T_A by applying Kirchhoff's equations. These forces can be defined as:

$$\tau_A = M_A \dot{v} + C_A(v)v. \quad (2-15)$$

4. Hydrodynamic damping

Hydrodynamic damping is caused by body forced oscillations, wave drift damping, vortex shedding damping as well as linear and quadratic skin frictions. If the body moves at large speeds, it creates a nonlinear and coupled damping term $\tau_D = D(v)v$. However, as a common ROV moves at low speed, we only approximately consider the damping terms of linear and quadratic skin friction term. Thus, the diagonal structure $D(v)$ is defined as:

$$\begin{aligned} D(v) &= -diag\{X_u, Y_v, Z_w, K_p, M_q, N_r\} \\ &= -diag\{X_{u|u}|u|, Y_{v|v}|v|, Z_{w|w}|w|, K_{p|p}|p|, M_{q|q}|q|, N_{r|r}|r|\}, \end{aligned} \quad (2-16)$$

where $X_{u|u} = \frac{\partial X}{\partial (u|u)}$, etc.

The linear damping force is much smaller than quadratic damping force, which can be neglected [Fossen 1994]. Some researchers propose to use the following equation as the quadratic damping equation [Conte 1996].

$$X_{u|u} u|u| = \frac{1}{2} \rho C_{D_x} A_x |u| u \quad (2-17)$$

Therefore, the hydrodynamic damping force can be defined as the following matrix:

$$F_D = D(\dot{q})\dot{q}, \quad (2-18)$$

$$D(\dot{q}) = -\frac{1}{2} \rho diag\{C_{D_x} A_x |u|, C_{D_y} A_y |v|, C_{D_z} A_z |w|, C_{D_r} A_r |r|\}. \quad (2-19)$$

5. Restoring forces and moments

Restoring forces and moments are hydrostatic forces and moments resulted from the combined action of the buoyancy and the gravity of the underwater robot. The gravitational force F_G acts on the centre of gravity G , while the buoyant force F_B acts on the centre of buoyancy. The buoyancy includes the measured one and the unmodeling motion force.

Let $r_G = [x_G, y_G, z_G]^T$ and $r_B = [x_B, y_B, z_B]^T$ as the vectors of the centers of gravity and buoyancy respectively in the body-fixed frame. The restoring force and moment $g(\eta)$ is presented as:

$$g(\eta) = - \begin{bmatrix} F_G(\eta) + F_B(\eta) \\ r_G \times F_G(\eta) + r_B \times F_B(\eta) \end{bmatrix} = \begin{bmatrix} (W - B)s\theta \\ -(W - B)c\theta s\phi \\ -(W - B)c\theta c\phi \\ -(y_G W - y_B B)c\theta c\phi + (z_G W - z_B B)c\theta s\phi \\ (z_G W - z_B B)s\theta + (x_G W - x_B B)c\theta c\phi \\ -(x_G W - x_B B)c\theta s\phi + (y_G W - y_B B)s\theta \end{bmatrix}, \quad (2-20)$$

where, $W = \|F_G\|$ and $B = \|F_B\|$.

6. Propulsion forces

Generally, the thruster's force and moment vector τ is a complex nonlinear function b . It consists of the underwater robot's velocity vector v and the rotational motor speed vector $n = [n_i]_{i \in \{1, p\}}$, where p is the number of motors [Fossen 1994].

$$\tau = b(v, n) \quad (2-21)$$

Forward and backward thrusters are generally non-symmetrical except for a special design. A classical first order model approximation of the thrust T and torque Q for a single screw propeller is defined in [Newman 1977].

7. Environmental forces

The environmental force τ_E includes sea currents force acting on the underwater robot body, outside disturbance such as cable force or the manipulator force etc. These forces are very complicate and we will give a detailed modeled method in the next section.

2.4. Theory, simulation and experimental of underwater robot motion control

The hydrodynamic motion control equation of underwater robot six DOF remains a challenging work. For a simple view to solve this problem such as only fluid mechanics, it is very difficult to get a satisfactory answer for stable motion control. Therefore, many scholars combine several theories such as control theory, fluid theory etc. to improve the abilities of underwater robot.

Based on the previous researches ([Fossen 1991][Fossen 2000][Fossen 1995][Goheen 1999]), adaptive control, PID control, sliding mode control theory, neural networks, robust control and many other types of control methods have been proposed for the robot motion control. These algorithms have been widely used in many areas. To solve different research problems in different research background, these algorithms have their own unique characteristics and are appropriate for different tasks. The choice of the algorithm is an important decision. Due to the different ideas of modeling, these algorithms are related to different boundary conditions and application fields. Therefore, we adopt a variety of control methods and propose new control algorithm to improve the special application of super-mini underwater robot in complex environment.

2.4.1. Theory of control algorithms and control algorithm design for underwater robots

Firstly, this section shows a simple theory introduction of the PID control algorithm. Then according to this theory, we propose an improvement for the control model design and analysis of underwater robot. Secondly, the sliding mode control algorithm and the improvement algorithms are proposed for underwater robot control; In the third step, we propose a totally new adaptive neural network and sliding mode controller based on the balance parameters control; Fourthly, a design of complex simulation environment is proposed for the test of these three algorithms; Finally, based on the actual experiments of the above algorithms, we compare and discuss the results and point out the method to solve the shortcomings and future works.

1. PID control theory and design of underwater robots

From the classic control theory, we can know that PID control algorithm is simple and has good, robust performance and characteristics of high reliability. It is now widely used in the industrial process control and motion control, vibration control. This algorithm is very appropriate for the deterministic control systems with accurate mathematical models. This control system can be shown as Fig.2-10.

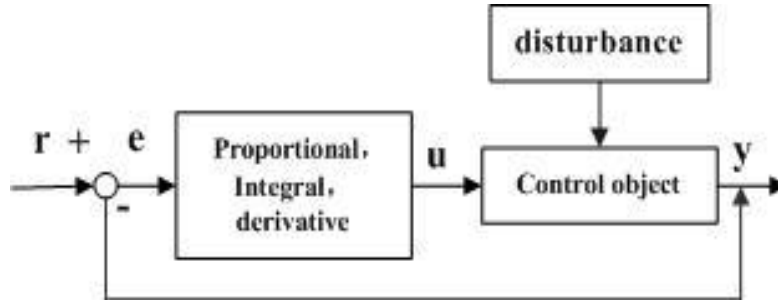


Fig.2-10 PID control theory diagram

PID controller is a linear control algorithm and an offset $e(t)$ is calculated between the predefined value $r(t)$ and the actual value $y(t)$:

$$e(t) = r(t) - y(t) \quad (2-22)$$

The control model consists of the proportional term (P), the integral term (I) and the derivative term (D) based on the offset value. For the model to control the objects, it is named as the PID controller in [Tan 1999][Van 2003]. It is defined as:

$$u(t) = k_p e(t) + k_i \int_0^t e(\tau) d\tau + k_d \frac{de}{dt}(t), \quad (2-23)$$

where k_p is the proportional term, k_i is the integral term, k_d is the derivative term, and t is time term.

PID parameters directly affect the control quality and performance by the regulation. Simply, the roles of the parameters in PID controller have the following characters:

- (1) Proportional term: This term for the deviation of the signal $e(t)$ is proportional to the performance of control system. When the error arises, the controller can quickly reduce the deviation of the control.

- (2) Integral term: The main integral part is used to eliminate static error, improve the system fine-tuning performance and reduce the errors.
- (3) Derivative term: Deviation of the signal errors reflects the trend of single. In large deviation between the signals, the amendments are added ahead of time to speed up system and stability for reducing the regulation time.

Therefore, we can clearly know the basic theoretical knowledge of PID control algorithm. We combine the motion control equation of underwater robot to create a PID equation control model.

Refer to section 2.3.2 of [Fossen 1994] and others introduced in the definition of motion equation of underwater robot (2.12), the motion parameters of the equations have the following characteristics:

- C.1 Inertia matrix is symmetric and positive, defined as $M(\eta) = M^T(\eta) \forall \eta \in R^6$. The positive constants m_m and m_M compose $m_m \leq \|M(\eta)\| \leq m_M$;
- C.2 $\dot{M}(\eta) - 2C(\eta, \dot{\eta})$ is a skew symmetric matrix;
- C.3 $\dot{M}(\eta) = C(\eta, \dot{\eta}) + C^T(\eta, \dot{\eta})$;
- C.4 Damping matrix $D(\eta, \dot{\eta})$ is strictly positive and within limited boundary;
- C.5 Coriolis matrix $C(\eta, \dot{\eta})$, η is in limited boundary and $\dot{\eta}$ is linear, as $x \in R^6$. $C(\eta, \dot{\eta}) = C(\eta, x)\dot{\eta}$ always exists. There is positive number k_c that keeps $\|C(\eta, \dot{\eta})\| \leq k_c \|\dot{\eta}\|$.

In general, the underwater robot simulation neglects the outside wave interference and considers the impact of water flow. The water density is assumed constant, and the sand stone effects are ignored. Meanwhile, the vertical inclination angle is assumed less than $\pi/2$ in this experiment.

Before the experimental model with different algorithms, we need to do the following assumptions:

- (1) The underwater robot moves at low velocity.
- (2) The damping force is non-coupling.
- (3) The linear damping force is negligible.
- (4) The gravity and the buoyancy are nearly in balance.
- (5) Water kinetic coefficient is constant.
- (6) In the parts of the roll and pitch angle, the system is stable, and therefore the hydrodynamic equations are not considered in these directions.

Since the kinetic knowledge of the underwater robot is limited, the design for precise control and navigation is very difficult. Therefore, the dynamic models of the underwater robot for the system simulation and control system kinematics are helpful. The parameters of underwater robot dynamic equation are non-linear, coupled, time-varying, and unstable. Thus, it is difficult to obtain accurate hydrodynamic equations. On the other hand, if there is the interference of drift etc., it is also difficult to get the accurate model. Here, we propose to use a large time varying disturbance mathematic model for simulation.

In the above mentioned assumptions and simulation conditions, the use of PID control method is adopted as the motion modeling equations of the underwater robot in [Smallwood 2004][Nguyen 2007] [Arimoto 1984]. Here, we list our PID control model for underwater robot and it is defined as:

$$\begin{cases} \tau = J^T(\eta)[-K_p \tilde{\eta} - K_I \int \tilde{\eta}(t) dt - K_D \dot{\tilde{\eta}} + g(\eta) + \delta] \\ u = B^T (BB^T)^{-1} \tau, \end{cases} \quad (2-24)$$

where δ is the disturbance of the cables, waves or etc, presented by a large time varying disturbance simulation model. $K_p, K_I, K_D \in \mathbf{R}^{6 \times 6}$ are the symmetric positive definite matrixes, $\tau \in \mathbf{R}^{7 \times 7}$ is a positive definite matrix, $\tilde{\eta} = \eta - \eta_d$ (η_d is predefined position) is the position error. The simulation diagram is shown in Fig.2-10.

2. Sliding mode control theory and control model design of underwater robot

In recent years, researches of the robust control have been improved a lot not only in theory but also in the application. Due to a the improvement of nonlinear robust control theory, sliding mode control theory ([Hu 2003][Edwards 1998][Utkin 1992]) has been studied a lot, and an important character is that the system has strong robustness.

Considering the following control system:

$$\dot{x} = f(t, x) + B(t, x)u, \quad (2-25)$$

where $f(t, x)$, $B(t, x)$ is the corresponding smooth continuous dimensional function.

For the general sliding mode control system, when the system of sliding mode happens, the breakpoints constitute non-zero measure sets in time, and the system is limited to the switch movement surface. Thus, the conventional method of solving the control input is not available and commonly the equivalent control method is used.

Ideally, after the system enters the sliding mode, as the system state trajectory maintains at the top, that is $S = 0$ and there is $\dot{S} = 0$. Thus, the system switch in the manifold should satisfy the following equation:

$$\dot{S} = \frac{\partial S}{\partial t} + \frac{\partial S}{\partial x} f(t, x, u) = 0. \quad (2-26)$$

If u is established or calculated, the resultant solution u can be regarded as an equivalent or average control effect on the switching manifold by system (2-26). u is considered as a value of the equivalent control. The equation control (2-25) is

$$u_{eq} = -G^{-1} \left(\frac{\partial S}{\partial t} + \frac{\partial S}{\partial x} f \right). \quad (2-27)$$

Thus, the control value is substituted to equation (2-25), the sliding mode need to satisfy the differential equations in the ideal condition:

$$\dot{x} = [I - BG^{-1} \frac{\partial S}{\partial x}] f - BG^{-1} \frac{\partial S}{\partial t}. \quad (2-28)$$

These systems only need to meet the appropriate conditions for the smooth and we can guarantee the existence and uniqueness of solutions. Thus, the above equation can be regarded as a dynamic system of sliding mode equation. Because the equation $S=0$ is satisfied, it can get the possible solutions of the m state variables. Therefore, equation (2-26) is essentially only $n-m$ dimension, and this is the reduced-order characteristics of sliding mode control.

How to design a sliding mode control law for the system in the limited time to reach the switching manifold is another important issue of the sliding mode. Only this problem is solved to guarantee the sliding mode to keep moving, and the sliding mode does exist.

For single variable systems, the intuitive point of view is to make the system trajectory to reach switch lines in a limited time. The switch vector must point to the switch curve, that is when $S > 0, \dot{S} < 0$. However, when $S < 0, \dot{S} > 0$. Therefore, the necessary and sufficient condition of the single variable system to realize sliding mode movement is: $S\dot{S} < 0$.

However, for multi-variable system, the arrival conditions of sliding mode is not so intuitive and it is equivalent to the stability of switching manifolds $S=0$ concerned to the nonlinear system state trajectory of switching manifolds. Proof of this sufficient condition is based on the theory of Lyapunov stability, while providing design base for a multi-variable sliding mode control system. Generally speaking, there are two following selections of $V(t, x, S)$:

- (1) When $\frac{\partial S}{\partial x} B$ is reversible, $V(t, x, S) = S^T S$.
- (2) When $\frac{\partial S}{\partial x} B$ is symmetric matrix or diagonal matrix $V(t, x, S) = S^T W(t, x) S$,

where $W(t, x)$ is positive definite symmetric matrix.

After the above conditions are satisfied, the following two law can be used:

- (1) $\dot{S} = -K \operatorname{sgn}(S), K = \operatorname{diag}(k_i), (k_i > 0)$.
- (2) $\dot{S} = -WS - K \operatorname{sgn}(S), K = \operatorname{diag}(k_i),$
 $W = \operatorname{diag}(\omega_i), (k_i > 0, \omega_i \geq 0)$.

To reach these two laws, $V(t, x, S) = S^T S$ is used, and we can see that derivative can keep negative state to ensure the realization of sliding mode. Moreover, the law can be arrived at by choosing the parameters of the system to reach the expectations of the time switching manifold, in order to achieve sliding mode movement.

From a simple presentation of the sliding mode control system theory, it can be seen that this design has two steps. Firstly, the design of switching function or switch surface allows the system to enter the manifold after the sliding mode movement has good dynamic properties. Secondly, the design of sliding mode control law can make the system in the limited time to reach the switching manifold and maintain movement on the manifold.

The sliding mode control design is a model-based design method. Algorithm is used in the kinetic equation to predict the error status of movement and the feedback. It can handle nonlinear characteristics of the system. It can also be used to solve the problems of speed independence and multi-axis coupling etc. Sliding mode control system for underwater robot motion control is of great practical value.

Sliding mode controller can eliminate the changes (For example, interference of the resiliency) of external environment by adding adaptive models. Of course, this method also has many shortcomings. It requires the dynamic model of the system has a clear and exact dynamic model and need for a complete closure of the state feedback. The model also needs to know a source of instability. However, generally speaking, the sliding mode control

algorithm is a high performance method, and the design performance can guarantee the combination characteristics etc.

We propose a multi-variable system of the sliding mode controller for underwater robots. Here, the sliding surface is designed to:

$$S = (d/dt + \lambda)^2 \int_0^t e(\tau) d\tau, \quad (2-29)$$

where $S \in R^6$ and λ is a constant positive definite matrix.

Here, $e(\tau) = \eta_d - \eta$. η_d is set as a reference value, η is set as the actual values. When $t > 0$, the surface of the manifold to maintain the system state meets the requirements of the path $\eta(t) \rightarrow \eta_d(t)$. Given any initial conditions $e(0)$, it forces the error vector to approach zero.

In order to calculate the size of control, consider the Lyapunov function:

$$V(s, t) = \frac{1}{2} S^T S. \quad (2-30)$$

Considering the time changes, differential $V(s, t)$ is calculated as:

$$\begin{aligned} \dot{V}(s, t) &= S\dot{S} \\ &= S(\ddot{e} + 2\lambda\dot{e} + \lambda^2 e) \\ &= S(\ddot{\eta}_d - M_\eta^{-1}[\tau_\eta(t) - C_\eta(\eta, \dot{\eta})\dot{\eta} - D_x(\eta, \dot{\eta})\dot{\eta} - g_\eta(\eta) - \delta(t)] + 2\lambda\dot{e}(t) + \lambda^2 e(t)), \\ &= S(\ddot{\eta}_d - U(t) + M_\eta^{-1}[C_\eta(\eta, \dot{\eta})\dot{\eta} + D_x(\eta, \dot{\eta})\dot{\eta} + g_\eta(\eta) + \delta(t)] + 2\lambda\dot{e}(t) + \lambda^2 e(t)) \end{aligned} \quad (2-31)$$

where $U(t) = M_\eta^{-1}(\eta)\tau_\eta(t)$ is the new definition of the control vector, $\delta(t)$ is used to describe the external disturbance and can not be the accurate dynamic model.

In order to ensure that Lyapunov function is less than zero and sliding mode control system can enter the sliding surface, the definition of equivalent U_{eq} is defined as:

$$U_{eq}(t) = \ddot{\eta}_d + M_\eta^{-1}(\eta)[C_\eta(\eta, \dot{\eta})\dot{\eta} + D(\eta, \dot{\eta})\dot{\eta} + g_\eta(\eta)] + 2\lambda\dot{e}(t) + \lambda^2 e(t), \quad (2-32)$$

to satisfying $\dot{S}(t)|_{(U=U_{eq})} = 0$.

$$\text{Let} \quad U_{sw} = -K \text{sgn}(s), \quad (2-33)$$

$$U = U_{eq} + U_{sw}, \quad (2-34)$$

where K is a positive constant vector, $K_{i,i} > |\delta_i| + \varepsilon$. ε approaches zero.

Through equation (2-32) ~ (2-34), we can ensure $V(s, t)$ less than zero and the system can guarantee the convergence.

Of course, Sign function can cause the system chatters. In order to avoid this phenomenon, a sliding mode fuzzy logic fuzzy switching surface is proposed, and U_{sw} is replaced by U_{fuzzy} . In this research, the design of the fuzzy controller is a single-input single-output fuzzy

controller. The fuzzy controller S is the input variable and the output variable is U_{fuzzy} . These fuzzy sets are defined as follows:

$$T(\tilde{S}) = \{NB, NM, ZR, PM, PB\} = \{F_Z^1, \dots, F_Z^5\}, \quad (2-35)$$

$$T(\tilde{u}) = \{NB, NM, ZR, PM, PB\} = \{F_u^1, \dots, F_u^5\}, \quad (2-36)$$

where NB, NM, ZR, PM, PB is negative big, negative middle, zero, positive middle, positive big. The corresponding membership function is shown in Fig.2-11, where $\varepsilon \in (0, 0.5]$.

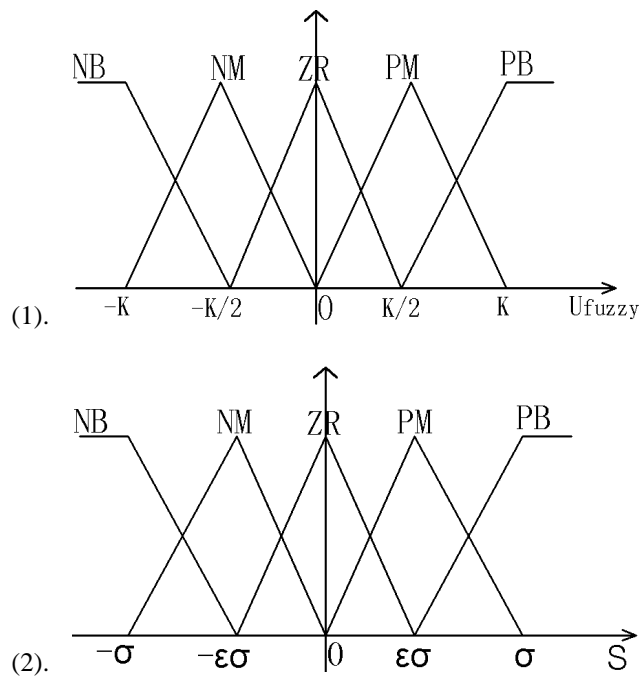


Fig.2-11 Membership function of S and U_{fuzzy}

In this research, we apply the weighted average algorithm for the U_{fuzzy} through the defuzzification calculation of the fuzzy data. The final U_{fuzzy} is corresponding to every S . They are shown as follows:

$$U_{fuzzy} = -K_s \cdot fuz(S / \sigma). \quad (2-37)$$

Here $q = 2\varepsilon \in (0, 1]$ where $fuz(\mu)$ is

$$fuz(\mu) = \begin{cases} -1 & \mu < -1 \\ \frac{\mu + q - 1}{2 - q} & -1 \leq \mu < -q/2 \\ \frac{\mu}{q} & -q/2 \leq \mu < 0 \\ \frac{\mu}{q} & 0 \leq \mu < q/2 \\ \frac{\mu + 1 - q}{2 - q} & q/2 \leq \mu < 1 \\ 1 & \mu \geq 1 \end{cases} \quad (2-38)$$

Therefore, we propose the sliding mode control functions of underwater robot and they are listed as follows:

Define the simple fuzzy sliding mode controller (SMSFC):

$$U(t) = \ddot{\eta}_d + M_\eta^{-1}(\eta)[C_\eta(\eta, \dot{\eta})\dot{\eta} + D(\eta, \dot{\eta})\dot{\eta} + g_\eta(\eta)] + 2\lambda\dot{e}(t) + \lambda^2 e(t) + U_{fuzzy} \quad (2-39)$$

Define the common sliding mode controller (SMC):

$$U(t) = \ddot{\eta}_d + M_\eta^{-1}(\eta)[C_\eta(\eta, \dot{\eta})\dot{\eta} + D(\eta, \dot{\eta})\dot{\eta} + g_\eta(\eta)] + 2\lambda\dot{e}(t) + \lambda^2 e(t) + U_{sw} \quad (2-40)$$

The above two designs do not consider the compensation of the outside disturbance $\delta(t)$. Here, we propose to apply an adaptive fuzzy control method [Wong 2001][Liang 2003][Ha 2001] to enhance this underwater robot system. The adaptive fuzzy system design is zero order TSK(Takagi-Sugeno-Kang) and the rules can be described as follows:

$$\text{If } s \text{ is } S_d, \hat{\delta}_r = \hat{D}_d \text{ and } d = 1, 2, \dots, N,$$

where S_d is fuzzy set, \hat{D}_d is each output value from N fuzzy rules.

Considering each output from each fuzzy rule, we define the output δ as:

$$\hat{\delta}(s) = \frac{\sum_{r=1}^N \omega_r \cdot \hat{\delta}_r}{\sum_{r=1}^N \omega_r} \quad (2-41)$$

$$\hat{\delta}(s) = \hat{D}^T \psi(s) \quad (2-42)$$

Here, $\hat{D} = [\hat{D}_1, \hat{D}_2, \dots, \hat{D}_N]^T$ contains the eigenvalue vector \hat{D}_d corresponding to each rule d . $\psi(s) = [\psi_1(s), \psi_2(s), \dots, \psi_N(s)]^T$, where $\psi_N(s) = \omega_r / \sum_{r=1}^N \omega_r$ and ω_r is the length of each rule. Here, the adaptive fuzzy adjustable parameters are defined as:

$$\dot{\hat{D}} = -\varphi s \psi(s), \quad (2-43)$$

where φ is the corresponding positive constant to adaptive velocity.

Therefore, this adaptive fuzzy sliding mode control (AFSMC) is proposed as:

$$U(t) = \dot{\eta}_d + M_\eta^{-1}(\eta)[C_\eta(\eta, \dot{\eta})\dot{\eta} + D(\eta, \dot{\eta})\dot{\eta} + g_\eta(\eta) + \hat{\delta}] + 2\lambda\dot{e}(t) + \lambda^2 e(t) + U_{fuzzy}. \quad (2-44)$$

Theorem 1. When underwater robot uses the AFSMC controller for the motion control, the system can enter the sliding surface $S(t)$ and normally carry out track movement.

Proof 1: Given Lyapunov function V

$$V(t) = \frac{1}{2} S^T S + \frac{1}{2M_\eta(\eta)\varphi} H^T H, \quad (2-45)$$

where $H = \hat{D} - \hat{D}^*$ and \hat{D}^* are the optimal parameter vectors associated with the optimal estimates.

$$\begin{aligned} \dot{V}(t) &= \frac{1}{2} S^T \dot{S} + \frac{1}{2M_\eta(\eta)\varphi} H^T \dot{H} \\ &= S(\dot{\eta}_d - U(t) + M_\eta^{-1}[C_\eta(\eta, \dot{\eta})\dot{\eta} + D_x(\eta, \dot{\eta})\dot{\eta} + g_\eta(\eta) + \delta(t)] \\ &\quad + 2\lambda\dot{e}(t) + \lambda^2 e(t)) + \frac{1}{M_\eta(\eta)\varphi} H^T \dot{H} \\ &= -SM_\eta^{-1}[U_{sw} - (\hat{\delta}^*(s) - \delta) - (\hat{\delta} - \hat{\delta}^*)] + \frac{1}{M_\eta(\eta)\varphi} H^T \hat{D} \\ &= -SM_\eta^{-1}[U_{sw} - (\hat{\delta}^*(s) - \delta)] + \frac{1}{M_\eta(\eta)\varphi} H^T [\hat{D} + \varphi s \psi(s)] \\ &= -SM_\eta^{-1}[U_{sw} - (\hat{\delta}^*(s) - \delta)], \end{aligned}$$

where K is positive vector of U_{sw} , $K_{i,i} > |(\hat{\delta}^*(s) - \delta)| + \varepsilon$. ε approaches zero.

Therefore, $\dot{V}(t) < 0$, $V(t) < V(0)$. This theorem is proven.

Above all, we have proposed three sliding mode controllers:

1. Sliding mode control (SMC);
2. Simple fuzzy sliding mode control (SMSFC);
3. Adaptive fuzzy sliding mode control (AFSMC).

(3) Adaptive neural network sliding mode control theory and a new control design of underwater robots

Theory of sliding mode algorithm is briefly described above and an improved fuzzy logic based algorithm applied to the sliding mode controller is proposed for the motion of underwater robot. This part continues to explore a new type of motion controller by the neural network and sliding mode joint structure. [Wai 2003] made his first sliding mode control based on neural network controller (SMNN) for the operation of the robot arm movement. In this research, we propose a smart learning function to strengthen the convergence rate of the system and estimate bounds of parameter uncertainties. It is a balanced controller that is proposed to control the parameter size. Thus, a new controller ANNSMB is proposed for the controller design of the underwater vehicle. ANNSMB underwater robot controller framework is shown in Fig.2-12.

At the beginning, a three layer neural network function and an active function are defined as follows:

$$\begin{aligned} y &= U_{NN}(e, V, K, n, s) = KT(Ve), \\ T(Ve) &= \exp[-(Ve - n)^2 / s^2] \in R^{ix^1}, \end{aligned} \quad (2-46)$$

where e is error vector between the command trajectory and the real position; $V \in R^{ix^j}$ is the weight matrix between input layer and hidden layer, i is the hidden layer nodes; $K \in R^{jxi}$ is the weights matrix between hidden layer and output layer; n and s are the adjustable parameter vectors of Radial Basis Functions (RBF); y is the output of neural network. Then, we define U_{eq} as follows:

$$U_{eq}(t) = U_{neural}^*(e, V^*, K^*, n^*, s^*) + \varepsilon = K^* T^*(V^* e) + \varepsilon, \quad (2-47)$$

where ε is a minimum error vector; V^*, K^*, n^* and s^* are the optimal neural network parameters of V, K, n, s . The definition of ANNSMB control rules are as follows:

$$U(t) = \hat{U}_{Neural}(e, \hat{V}, \hat{K}, \hat{n}, \hat{s}) + U_s, \quad (2-48)$$

where \hat{U}_{Neural} is the neural network controller. It is a control parameter in accordance with dynamic equation of the uncertain system. U_s is a robust controller including a parameter balanced controller. $\hat{V}, \hat{K}, \hat{n}, \hat{s}$ are estimate values of optimal parameter vectors.

The sliding surface is defined as $S(t) = (d/dt + \lambda)^2 \int_0^t e(\tau) dt$, where λ is a positive constant vector and S is a vector of sliding surface. According to the general calculation steps of the sliding mode control algorithm, We can easily derive $U_{eq} - U = \dot{S}(t)$ to satisfy the equivalent control law $\dot{S}(t)|_{U=U_{eq}} = 0$.

$$\begin{aligned} \tilde{U} &= U_{eq} - U = K^* T^* + \varepsilon - \hat{K} \hat{T} - U_s = \tilde{K} T^* + \varepsilon + \hat{K} \tilde{T} - U_s \\ \text{Let } \tilde{K} &= K^* - \hat{K} \\ \tilde{T} &= T^* - \hat{T}. \end{aligned} \quad (2-49)$$

Considering the active function is nonlinear, the Taylor algorithm is applied to \tilde{T} :

$$\tilde{T} = T_v \tilde{V} e + T_n \tilde{n} + T_s \tilde{s} + O_n \quad (2-50)$$

Here

$$\begin{aligned} T_v &= \left[\frac{\partial T_1}{\partial (Ve)} \quad \frac{\partial T_2}{\partial (Ve)} \quad \dots \quad \frac{\partial T_k}{\partial (Ve)} \right] \Big|_{Ve=\hat{V}e} \in R^{ix^i}, \\ T_n &= \left[\frac{\partial T_1}{\partial (n)} \quad \frac{\partial T_2}{\partial (n)} \quad \dots \quad \frac{\partial T_k}{\partial (n)} \right] \Big|_{n=\hat{n}} \in R^{ix^i}, \end{aligned}$$

$$T_s = \left[\frac{\partial T_1}{\partial(s)} \quad \frac{\partial T_2}{\partial(s)} \quad \dots \quad \frac{\partial T_k}{\partial(s)} \right] \Big|_{s=\hat{s}} \in R^{i \times i},$$

$$\tilde{V} = V^* - \hat{V}, \quad \tilde{n} = n^* - \hat{n}, \quad \tilde{s} = s^* - \hat{s}, \quad O_n \in R^{K \times 1}. \quad (2-51)$$

Redefine the equation (2-50)

$$T^* = T + T_v \tilde{V} e + T_n \tilde{n} + T_s \tilde{s} + O_n \quad (2-52)$$

Substituting the equation (2-52) by (2-43)

$$\begin{aligned} \tilde{U} &= K^* T^* + \varepsilon - \hat{K} \hat{T} - U_s \\ &= K^* [\hat{T} + T_v \tilde{V} e + T_n \tilde{n} + T_s \tilde{s} + O_n] + \varepsilon - \hat{K} \hat{T} - U_s \\ &= (K^* - \hat{K}) \hat{T} + (\tilde{K} + \hat{K}) T_v \tilde{V} e + (\tilde{K} + \hat{K}) T_n \tilde{n} + (\tilde{K} + \hat{K}) T_s \tilde{s} + \varepsilon - U_s + K^* O_n \\ &= \tilde{K} \hat{T} + \hat{K} T_v \tilde{V} e + \hat{K} T_n \tilde{n} + \hat{K} T_s \tilde{s} - U_s + \tilde{K} T_v \tilde{V} e + \tilde{K} T_n \tilde{n} + \tilde{K} T_s \tilde{s} + K^* O_n + \varepsilon, \end{aligned} \quad (2-53)$$

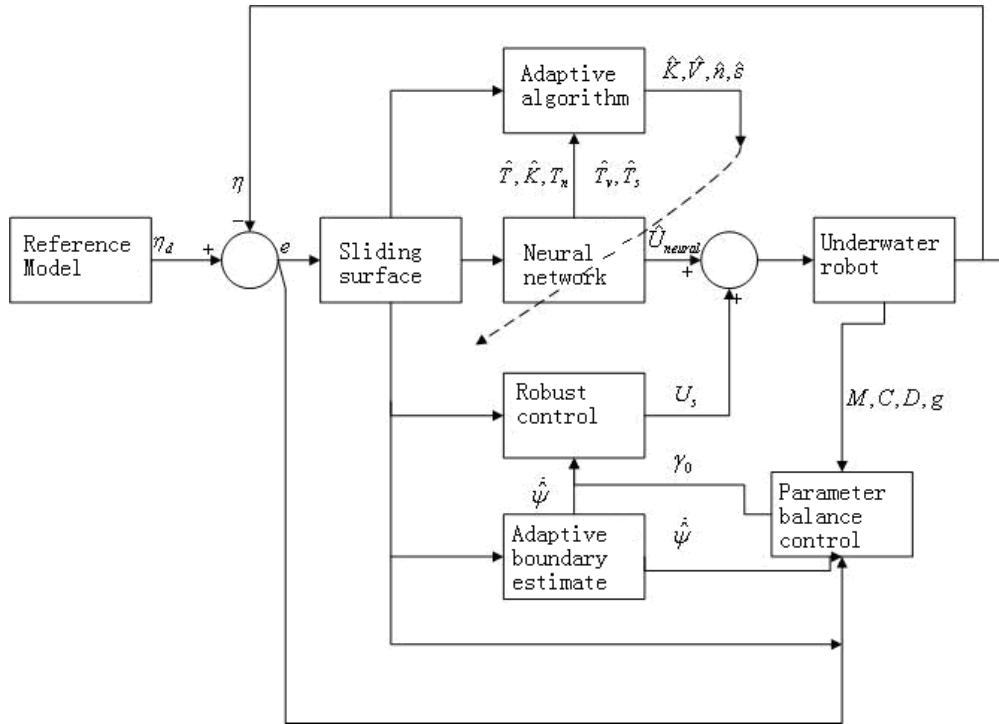


Fig.2-12 ANNSMB Controller Diagram

where uncertain boundary is given as

$$\| \tilde{K} T_v \tilde{V} e + \tilde{K} T_n \tilde{n} + \tilde{K} T_s \tilde{s} + K^* O_n + \varepsilon \| < \psi.$$

Then, we define:

$$\hat{K} = \eta_1 (\hat{T} S^T)^T, \quad (2-54)$$

$$\hat{V} = \eta_2 (e S^T \hat{K} T_v)^T, \quad (2-55)$$

$$\hat{n} = \eta_3 (S^T \hat{K} T_n)^T, \quad (2-56)$$

$$\hat{s} = \eta_4 (S^T \hat{K} T_s)^T, \quad (2-57)$$

$$\hat{\psi} = \frac{\eta_5 S^T \text{sat}(S)}{\sum_{i=1}^n S_i^2 + 1}, \quad (2-58)$$

$$U_s = \left(\frac{\hat{\psi} + \gamma_0}{\sum_{i=1}^n S_i^2 + 1} \right) \text{sat}(S), \quad (2-59)$$

where the parameter balanced controller γ_0 is defined as:

$$\gamma_0 = M \sqrt{\sum_{i=1}^n \lambda_i e_i} + \sqrt{\sum_{i=1}^n \dot{e}_i} + \sqrt{\sum_{i=1}^n \ddot{e}_i} + \frac{N}{M} + \hat{\psi} \times \sum_{i=1}^n S_i^2 \quad (2-60)$$

$$M = \|M_\eta(\eta)\|_2 = \sqrt{\max\{\rho(M^T M)\}}, \quad (2-61)$$

$$N = \|C_\eta(\eta, \dot{\eta})\dot{\eta} + D_\eta(\eta, \dot{\eta})\dot{\eta} + g_\eta(\eta)\|_2,$$

where $\rho(M^T M)$ is the largest eigenvalue of $M^T M$ matrix; $\hat{\psi}$ is the uncertainty of the boundary ψ ; $\eta_1, \eta_2, \eta_3, \eta_4, \eta_5$ is positive; γ_0 has increased the robustness and fast convergence, through calculating the external states to estimate the values of the uncertain borders and to guarantee the control system's dynamics on the sliding surface.

Saturation function is introduced here. It is a commonly used function in the sliding mode control, the main role is to smooth the signum function discontinuous terms, and eliminate chatter phenomena.

$$\text{sat}\left(\frac{s}{\phi}\right) = \begin{cases} \text{sgn}(S) & \text{if } \left|\frac{s}{\phi}\right| > 1 \\ \frac{s}{\phi} & \text{ot her s} \end{cases} \quad (2-62)$$

where sat function is instead of sgn function.

Therefore, we propose an adaptive neural network and sliding mode controller with a balanced parameter contrller (ANNSMB):

$$U(t) = \hat{U}_{Neural}(e, \hat{V}, \hat{K}, \hat{n}, \hat{s}) + U_s$$

Theorem 2. When underwater vehicle adopts this ANNSMB controller, the system can enter and keep on the sliding surface. The desired trajectory tracking can be guaranteed.

Proof 2: Firstly define Lyapunov V

$$V = \frac{1}{2} S^T S + \frac{1}{2\eta_1} \text{tr}(\tilde{K}\tilde{K}^T) + \frac{1}{2\eta_2} \text{tr}(\tilde{V}^T\tilde{V}) + \frac{1}{2\eta_3} \tilde{n}^T \tilde{n} + \frac{1}{2\eta_4} \tilde{s}^T \tilde{s} + \frac{1}{2\eta_5} \tilde{\psi}^2(t), \quad (2-63)$$

where $\text{tr}(\cdot)$ is the trace of the matrix, $\tilde{\psi}(t) = \psi - \hat{\psi}$ is the estimate error of the boundary. Derivation of V:

$$\dot{V} = S^T \dot{S} + \frac{1}{\eta_1} \text{tr}(\tilde{K}\dot{K}^T) + \frac{1}{\eta_2} \text{tr}(\tilde{V}^T \dot{V}) + \frac{1}{\eta_3} \dot{\tilde{n}}^T \tilde{n} + \frac{1}{\eta_4} \dot{\tilde{s}}^T \tilde{s} + \frac{1}{\eta_5} \dot{\tilde{\psi}}(t) \tilde{\psi}(t) \quad (2-64)$$

Given the terms in (2-59)

$$\tilde{K}T_v \tilde{V}e + \tilde{K}T_n \tilde{n} + \tilde{K}T_s \tilde{s} + K^* O_n + \varepsilon = L.$$

Thus, we can calculate:

$$\begin{aligned} \dot{V} &= S^T (\tilde{K}\hat{T} + \hat{K}T_v \tilde{V}e + \hat{K}T_n \tilde{n} + \hat{K}T_s \tilde{s} - U_s + L) - \frac{1}{\eta_1} \text{tr}(\tilde{K}\dot{K}^T) - \frac{1}{\eta_2} \text{tr}(\dot{V}^T \tilde{V}) \\ &\quad - \frac{1}{\eta_3} \dot{\tilde{n}}^T \tilde{n} - \frac{1}{\eta_4} \dot{\tilde{s}}^T \tilde{s} - \frac{1}{\eta_5} \dot{\tilde{\psi}}(t) \tilde{\psi}(t) \\ &= \text{tr}\{\tilde{K}[\hat{T}S^T - \frac{1}{\eta_1} \dot{K}^T]\} + \text{tr}\{[eS^T \hat{K}T_v - \frac{1}{\eta_2} \dot{V}^T] \tilde{V}\} + [S^T \hat{K}T_m - \frac{1}{\eta_3} \dot{\tilde{n}}^T] \tilde{n} + \\ &\quad [S^T \hat{K}T_s - \frac{1}{\eta_4} \dot{\tilde{s}}^T] + S^T (L - U_s) - \frac{1}{\eta_5} \dot{\tilde{\psi}}(t) \tilde{\psi}(t). \end{aligned} \quad (2-65)$$

Substituting equation (2-65) by (2-54)~(2-59):

$$\begin{aligned} \dot{V} &= S^T L - S^T \left(\frac{\gamma_0}{\sum_{i=1}^n S_i^2 + 1} \right) \text{sat}(S) - S^T \left(\frac{\psi}{\sum_{i=1}^n S_i^2 + 1} \right) \text{sat}(S) \\ &\leq \|S^T\| \|L\| - \|S^T\| (\gamma_0 + \psi) \\ &\equiv -\beta \|S^T\| \leq 0, \end{aligned} \quad (2-66)$$

where $\beta = (\gamma_0 + \psi) - \|L\| > 0$ is a small positive constant. Because $\dot{V} \leq 0$, $V(t) < V(0)$.

Thus, the control system can become asymptotical stable.

In this section, we have proposed PID controller, common sliding mode controller (SMC), simple fuzzy sliding mode controller (SMSFC), adaptive fuzzy controller (AFSMC) and adaptive neural network and sliding mode balanced controller (ANNSMB) for the control design of the underwater robot. Their theories have been described and proven in detail, which constitutes the basis for the analysis and results comparison of the simulation and experiment in the next section.

2.4.2. Simulations, experiments and discussions of underwater robot motion control algorithms

This section carries out the design controllers in previous section to control an underwater robot movement in the simulation. Firstly, we propose a predefined model of a large time varying disturbance. Then we implement several corresponding simulation and discuss and analyze the results.

Step 1: Design of simulation experiments:

In the earth coordinate system, the parameters are as follows:

$$\begin{aligned} M &= \text{diag}\{120.0, 128.0, 126.0, 14.2\}, \\ D &= \text{diag}(120|u|, 175|v|, 200|w|, 10.18|r|), \\ g &= [0, 0, 0, 0]. \end{aligned}$$

Here, in the process of movement, we set the parameters M, D following with about 5 kilos periodic disturbance, which is given as follows:

$$\begin{aligned} M &= M_0 + M_s, \\ M_s &= 5 * \cos(4t) * \text{diag}(1, 1, 1, 1), \\ D &= D_0 + D_s, \\ D_s &= 5 * \sin(4t) * \text{diag}(1, 1, 1, 1), \end{aligned}$$

where M_0, D_0 are estimate values, M_s is an outside value.

Here, only yaw control is discussed and analyzed, as there will be too much thesis contents if all the motions are simulated and experimented. The initial yaw angle motion trajectory is:

$$\psi(t) = 2 * \sin(\pi * t).$$

Let periodic large interference model:

$$\begin{aligned} \delta &= 0.1 * M * [\sin(8\pi t) + \sin(3\pi t) + \sin(2\pi t) + \sin(6\pi t) + 1 \\ &\quad \sin(8\pi t) + \sin(3\pi t) + \sin(2\pi t) + \sin(6\pi t) + 1 \\ &\quad \sin(8\pi t) + \sin(3\pi t) + \sin(2\pi t) + \sin(6\pi t) + 1 \\ &\quad \sin(8\pi t) + \sin(3\pi t) + \sin(2\pi t) + \sin(6\pi t) + 1]^T \end{aligned}$$

Step 2: The results of simulation:

The figures of simulation results include 4 parts. The left top corner part of the figure is the results of track, that $\psi(t)$ is predefined motion trace depicted in solid line and the dotted line is the practical motion trace. The right top corner part is the input control force U . The left bottom part is the phase value. The right bottom part is the trace error e .

<1> Yaw motion trace simulation of PID controller

Initialize the parameters of PID control:

$$K_p = 800, K_d = 100, K_i = 30 \quad (\text{Best choice of parameters by the regulation})$$

The simulation results are shown in Fig.2-13.

<2> Yaw angle movement simulation with sliding mode controller (SMC)

The results are shown in Fig.2-14.

<3> Yaw angle movement simulation with simple fuzzy sliding mode controller (SMSFC)

Let the parameters $q = 0.6$, $K_s = 35$, and $\sigma = 1.5$. The results are shown in Fig.2-15.

<4> Yaw angle movement simulation with adaptive fuzzy sliding mode controller (AFSMC)
Define equation (2-48)

$$\Delta = \hat{\delta}(s) = \hat{D}^T \psi(s) \quad (2-67)$$

$$\varphi = 0.7.$$

Considering fuzzy system, we set triangle function, gradient function to define the membership function S_r , and the center is given as $C = \{-5.0; -1.0; -0.5; 0.0; 0.5; 1.0; 5.0\}$. We choose the property of fuzzy as NB, NXM, NM, ZR, PM, PXM, PB, as shown in Fig.2-16.

The results of simulation are given in Fig.2-17. The simulation results include a), b) parts. Here, the first figure of b) part is the output value from equation (2-67) that is the estimate output value $\hat{\delta}$ of adaptive sliding mode controller, and the second figure is the proposed large time varying disturbance model δ .

<5> Adaptive neural network and sliding mode balanced parameter controller (ANNSMB)

Let $\eta_1 = 28, \eta_2 = 28, \eta_3 = 5, \eta_4 = 3, \eta_5 = 39$. The simulation results are given in Fig.2-18.

Step 3: Comparative analysis of simulation results:

Based on previous works, we add a large disturbance to the model such as the flow and the cable, as well as the parameters M, D, etc. in the motion equation of underwater robot. These parameters are considered with the instability from a time varying disturbance. From the above mentioned assumption, the environment has a strong impact for each controller for this simulation experiment. Thus, various controller parameters are very important indicators in the simulation experiments.

Fig.2-13 shows the results of PID controller. The system involves three initial parameters which have been adjusted for the best results. From the results, the follow-up speed of the input and output value from PID tracker controller is always a little slow, and the cyclical errors always exist. The right part of results shows the input control. The initial control force is large and it gradually reduces. However, because of the existence of disturbance, the force has a sharp increase and then it can come to a new stable status gradually.

Fig. 2-14 shows the results of a simple SMC controller. From the simulation, we can see that the track of the sliding mode controller is close to the desired track. However, it is worth noting that the input force of the system shown in right top of Fig.2-14 has a number of chatters, which is the shortcoming of this traditional SMC algorithm. After taking use of SMSFC to reduce the chatters etc., we can see that the chattering phenomena can decrease a little and remain exist, as shown in Fig.2-15.

Comparison with Fig.2-13, though there is a small decline of the system static error rate and the overshoots decline too, the static error still exists. From Fig.2-14~Fig.2-15, we can see that there are some small advantages of sliding mode controller for the static error and overshoot compared with PID controller. For simulation, the limitations of sliding mode controller lead to frequent switching chatter response. Taking into account the simple structure of the sliding mode controller ignores outside complex disturbance, a new adaptive fuzzy sliding mode controller AFSMC is proposed to improve the system anti-chatter capability and further reduce the static error, and the chatter phenomena.

Fig.2-17 shows the results, we can see clearly AFSMC controller performance has been improved. The reason of longer simulation time is to show the results of AFSMC with disturbance model and give full expression of the control performance to the disturbance. From the second picture of 2) part in Fig.2-17, the outside disturbance is shown. Comparing the second part to the first part, we can see that the input is changing rapidly due to the disturbance model and the adaptive fuzzy controller can not output high frequency tracking movement. However, these results are acceptable, which are equivalent to do an average

calculation to the disturbance. In a) part of the results, we can see the output of simulation reduces a lot to the static error $-0.15 \sim 0.15$. For the phase output figure (the lower-left corner of a) part), we can see that the overshoot is also reduced etc.

AFSMC controller can very well reduce the static error, the overshoot and speed up the convergence of the system. Compared to SMSFC controls, there has been a great decline in chatter phenomena but remain existed.

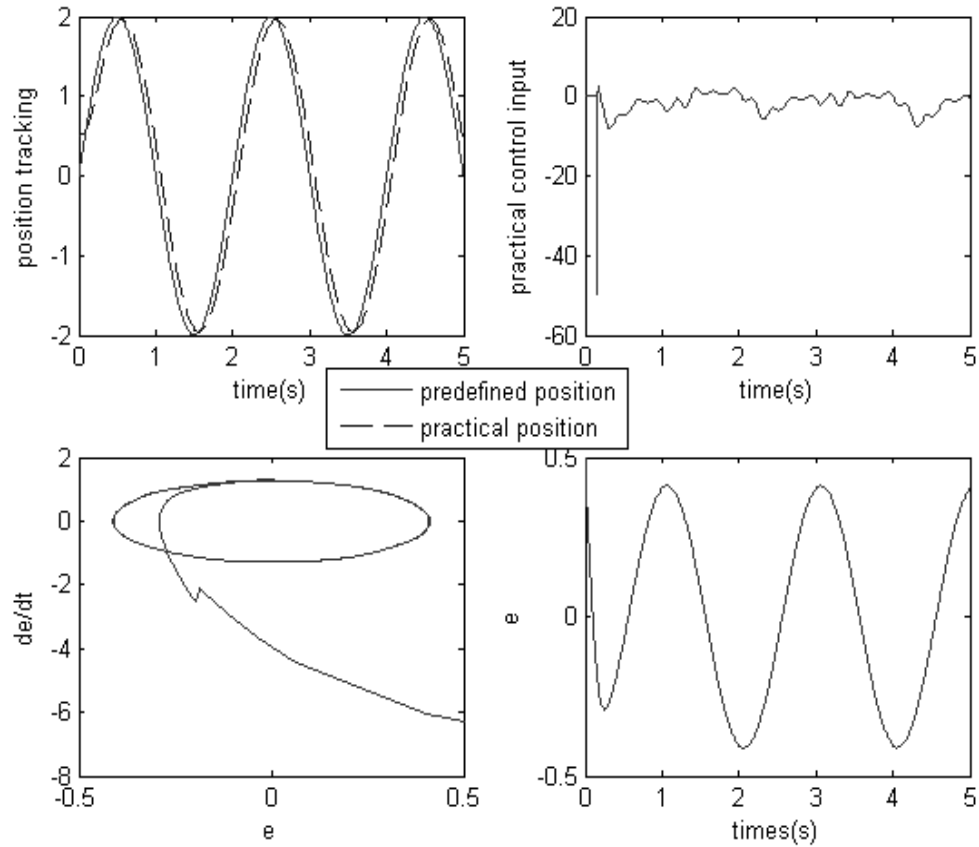


Fig.2- 13 Results of PID controller

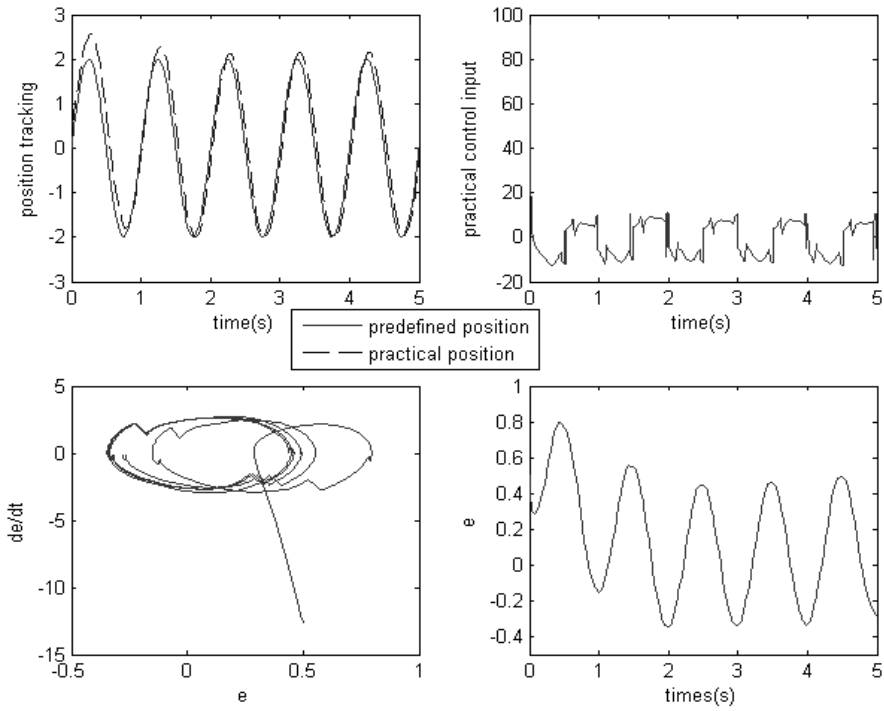


Fig.2-14 Results of SMC controller

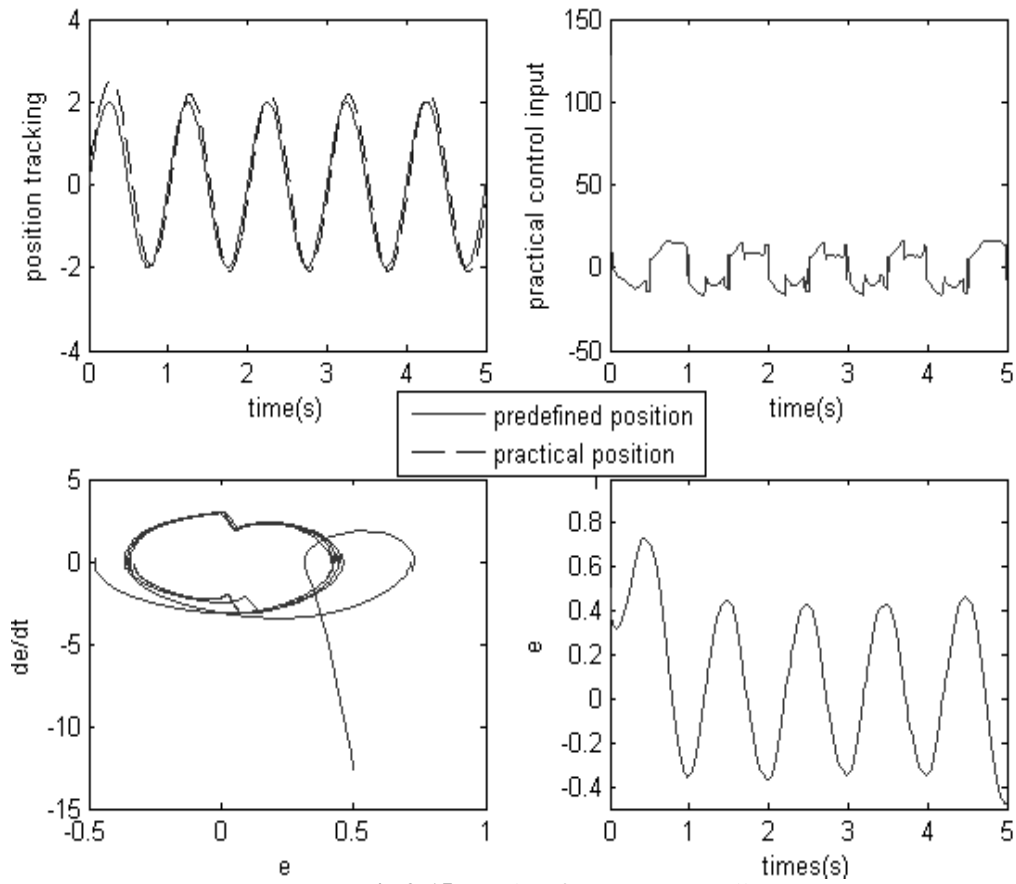


Fig.2-15 Results of SMSFC controller

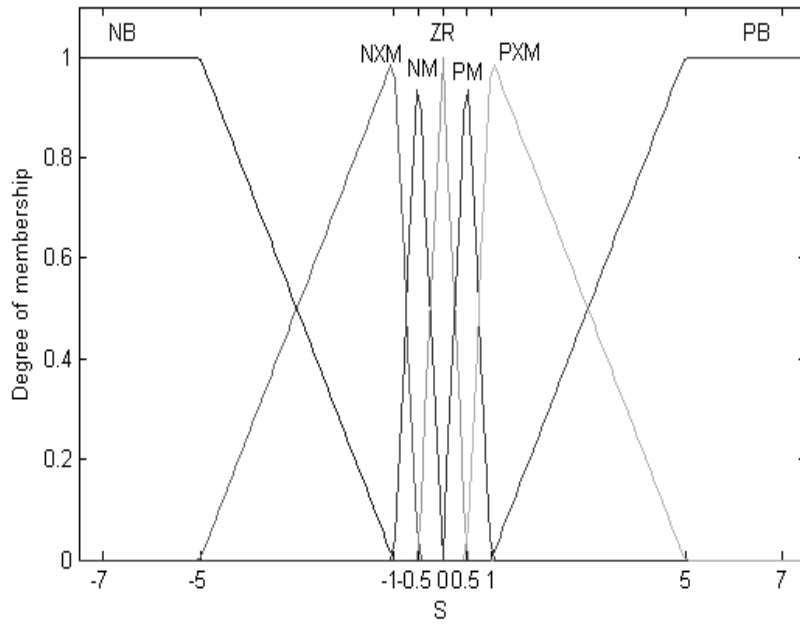
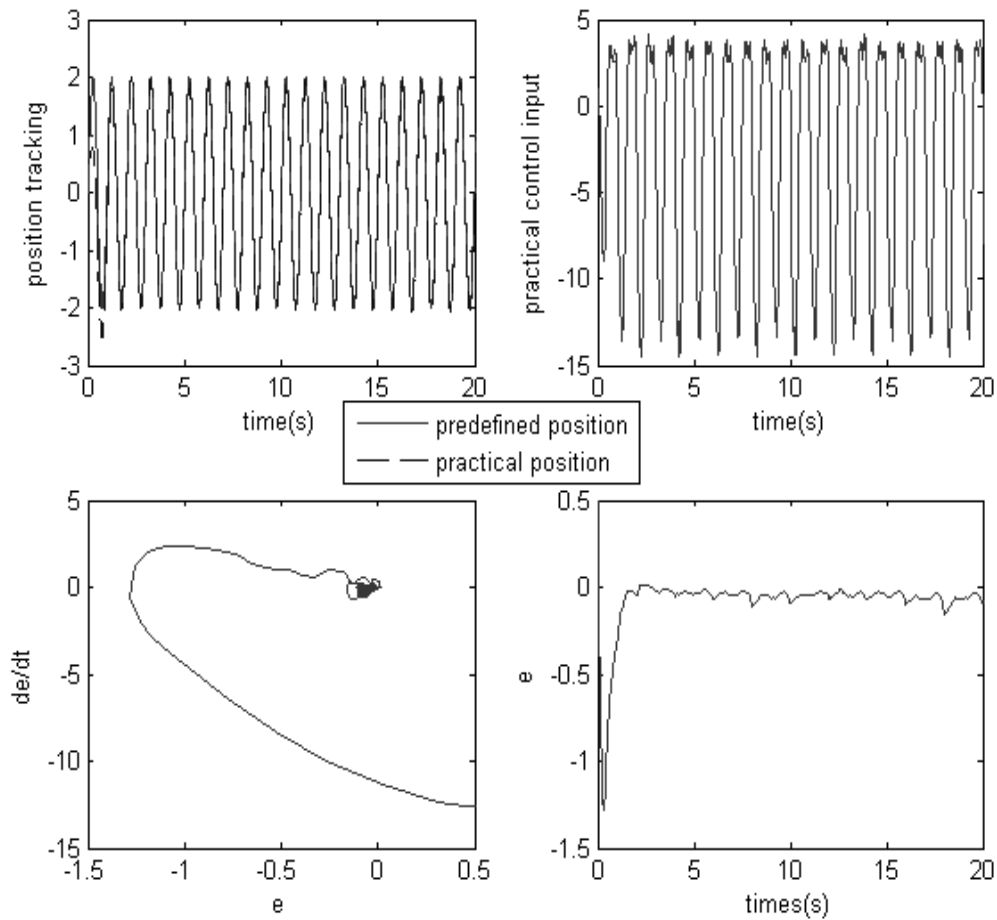
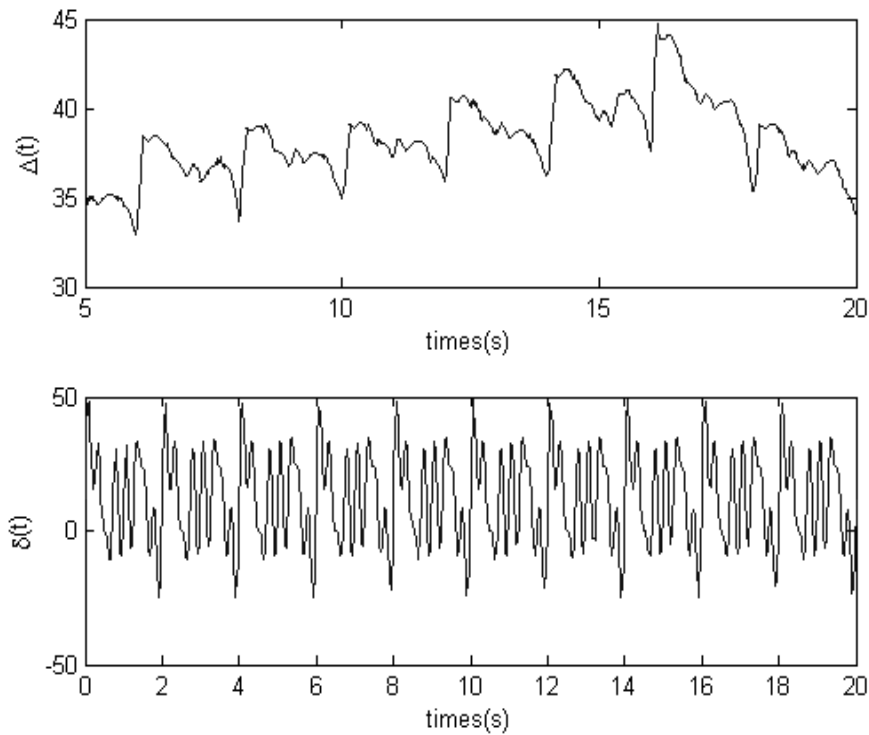


Fig.2-16 Membership function



a. Result of Position, control input, error



b. Results of real disturbance and estimated disturbance

Fig.2-17 Results of AFSMC controller

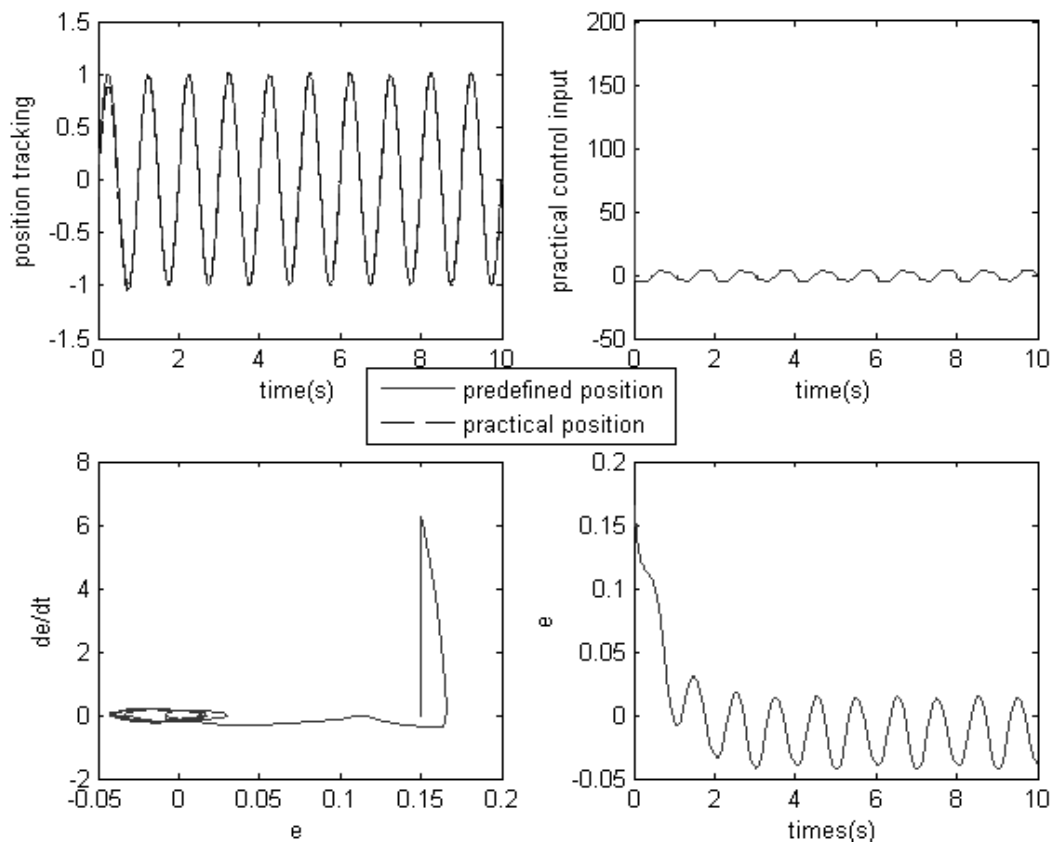


Fig.2-18 Results of ANNSMB controller

Based on a new type of ANNSMB controller proposed in this research, we collect the data from the simulation, as shown in Fig. 2-18. Tracking trajectory of the figure shows that the new controller almost eliminate the basic error and the error has fallen to $-0.05 \sim 0.05$. At the beginning, the error is slightly higher. After a period of time, the error reduces to a very small value through the online learning. In spite of the existence of large time varying disturbance, the system is able to enter a relatively stable state. Moreover, it is clear that the input force enter a state of stability, and there is no-chattering generation from the result of upper right part of the Fig.2-18.

From the simulation results above, the results are analyzed under the same external environment. The sliding mode controller has improved anti disturbance ability, static error is slightly lower, and the amount of overshoot is reduced. But it causes the chattering input commands to the underwater robots. AFSMC controller further reduces the static errors, improves the anti disturbance ability, and reduces the size of overshoot and the chatters. ANNSMB controller reflects its excellent performance in the simulation, not only to reduce the static error to a small extent, but also can significantly reduce the chatters.

Based on the above theories and simulations, different algorithms are applied for the design of super-mini underwater robot and the experiments have been carried out. The experiment was shown in Figure 2-19. The parameters of this super-mini robot in this research are given as follows: The size is 31 cm*22.5 cm*21 cm; the weight in the air is 60 kg; the max navigation speed is 2.6 knot; the max diving depth is 152 cm.

The inertia matrix includes the mass and moments of inertia. In this research, the common oscillation experiment with a small swing angle around the principle axis has been performed to determine the moment of inertia I_{xx}, I_{yy}, I_{zz} . (See Table 2.1). Generally, the other hydrodynamic derivatives are calculated experimentally in towing tank tests or in flumes with controlled flowing water. The hydrodynamic forces are recorded and the data is sampled by the data acquisition system under the condition of the controlled flowing water.

Table 2.1 Moment of inertia

	Value	Units
I_{xx}	0.02512	$kg.m^2$
I_{yy}	0.02687	$kg.m^2$
I_{zz}	0.02875	$kg.m^2$

In this research, there are five thrusters in the underwater robot. Each one has the individual driver that controls the rotational speed. Since the propeller diameter, mass and the motors are small, the speed of the thruster is much faster than the underwater robot. So the dynamics are neglected. Only the parameter C_i needs to be identified. Here, the least square method is applied to compute the coefficients for the different thrusters. The results are shown in Table 2.2.

Table 2.2 Thruster coefficients

Thruster	$C_i (N)$	
	Forward	Backward
Horizontal	2.6210×10^{-4}	1.2310×10^{-4}
Lateral	3.2774×10^{-4}	1.7314×10^{-4}
Vertical	1.1532×10^{-4}	0.8134×10^{-4}

Following the traditional identification methods, a series of experiments have been done to get the drag coefficients etc. Some coefficients that cannot be estimated by the experiment are estimated by the theoretical calculation. Note that the linear drag is much smaller than quadratic drag. Therefore, the linear drag can be neglected. Some coefficients are listed in Table 2.3.

Table 2.3 Coefficients

Added mass			
$X_{\dot{u}}$	1.8357	$Y_{\dot{v}}$	6.1483
$Z_{\dot{w}}$	3.5402	$K_{\dot{p}}$	0.0285
$M_{\dot{q}}$	0.0153	N_r	0.0314
Quadratic drag coefficients			
$X_{u u }$	7.2056	$Y_{v v }$	27.671
$Z_{w w }$	25.260	$K_{p p }$	0.0032
$M_{q q }$	0.0073	$N_{r r }$	0.0095

We command the super-mini underwater robot yaw angle rotation from the 100 -> 60 -> 20 degrees and the time interval of this command is 80s. Speed of water flow in the experiment is time varying. The experimental results are shown in Figure 2-20. From the experiment results, though the parameters of the model can not be completely accurate known, these four controllers can finally achieve the location of the command after different times' regulation through different closed-loop control algorithms with some other estimated parameters from the [Pepijn 2006] identification method. For the measurement of propeller force, an experienced database is stored as a reference to estimate a proper ratio between the input current value and the output force value. As the complex compact of the water, the propeller force can only be estimated in advance.



Fig.2-19 Experiment of the Super-mini Underwater robot

In the experimental results, it can be seen that two new AFSMC and ANNSMB controllers have stronger abilities to work. In the practical work, PID SMC, SMSFC controllers have longer regulation times and larger overall errors than the two new controllers. These indicate their larger overshoot. Here, Fig.2-21 shows a standard deviation value of the underwater robot yaw angle. It shows that the highest value is PID controller, the lowest one is ANNSMB. The results are in accordance with the simulation results of algorithm theory.

The weight of this super-mini underwater robot is small. The disturbance from the cables and others are relatively large. When the yaw angle is at 180 degrees, the cable is rightly behind the underwater robot. Thus, the smallest disturbance is attached to the yaw motion. However, when the underwater robot reduces angle, its front part is moving toward the cable. The angle errors increase and the vibration becomes bigger as the resistance and its moment of the cable grow up. When the command angle is at 20 degrees, the disturbances are beyond the controllers' abilities of regulation. Thus, the underwater robot keeps a small range of swing in a relatively stable state, rather than the other two situations that the underwater robot can finally stabilize and keep the yaw angle after a period of adjustment.

Through simulation and experimental verification of the applicability of several algorithms, the simulation results are similar to the experimental results. These provide a solid basis for the controller development of the super-mini underwater robot.

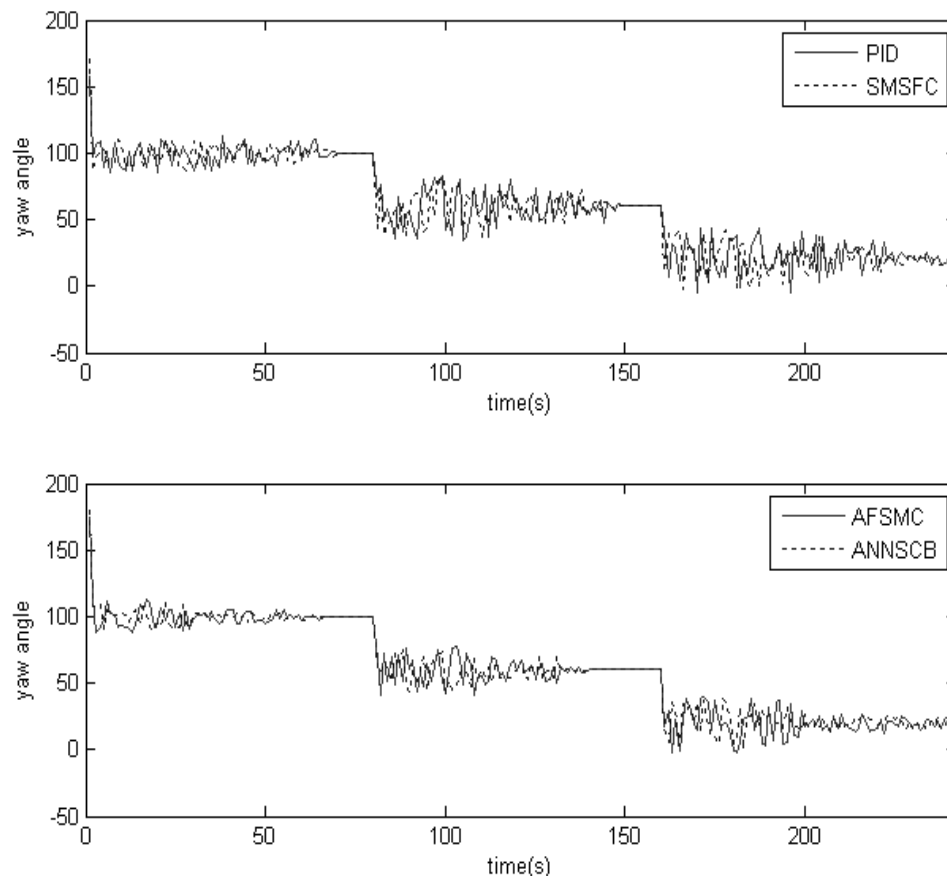


Fig.2- 20 Experimental record of the yaw angle

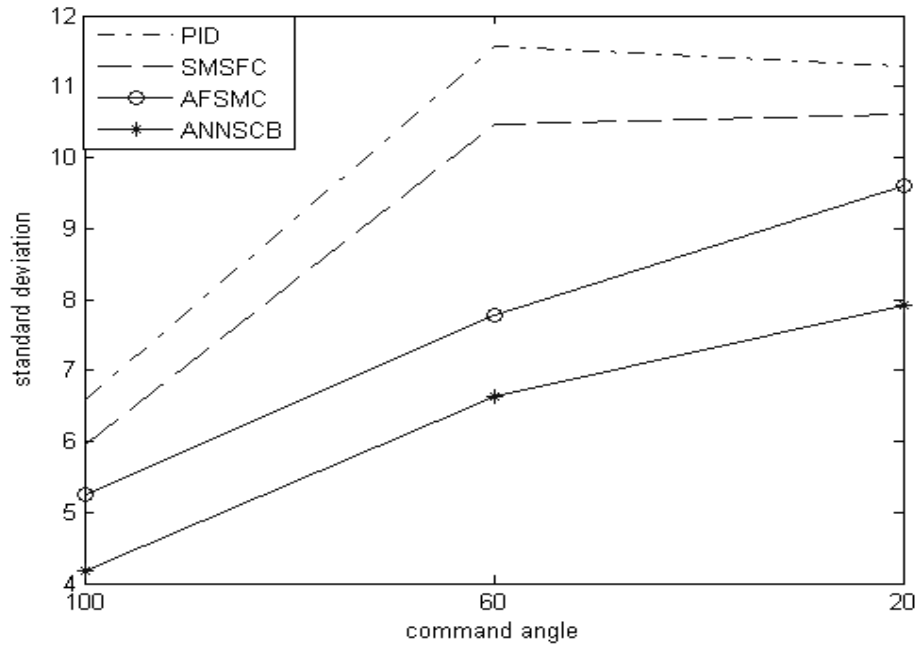


Fig.2-21 Standard deviation of yaw angle

2.5. Summary

First of all, this chapter in detail introduces the development of super-mini design of underwater robots. It contains the basic theory and related design framework of the system. Then, a number of motion controllers are described for the underwater robot in theory. Considering a large time varying disturbance model, the simulations are implemented and the results are compared and analyzed based on several new controllers. We carry out many experiments of different controller for underwater robot in this research. Finally, we present the analysis and comparison of the experimental results from multiple controllers in detail.

PART II

RECOGNITION AND PATH RECONSTRUCTION

Chapter 3 ALGORITHMS OF THREE-DIMENSIONAL PATH TRACKING

Summary

3.1. Introduction.....	59
3.2. Streamline Algorithm Theory	60
3.3. Theory of maximum energy tracking approach.....	61
3.4. Stochastic tracking algorithm based on Bayesian theory	66
3.5. Summary	66

3.1. Introduction

In different research areas, the principles of path tracking algorithms are different to the different purposes of tracking application. This chapter mainly focuses the path tracking algorithm on the high dimensional space, which is applied to track the human myocardium distribution in medical imaging and the underwater robots path tracking in the underwater environment. Based on these goals, we try to find a suitable theory of three dimensional path reconstructions for these two particular applications.

In the current path planning algorithm, we can understand that some algorithm does the whole optimal path selection based on the known nodes and the space environment, such as the A^* algorithm [Huyn 1980]. The advantages of these algorithms are that you can find the shortest path to complete the optimal closed-loop path based on the known nodes. Thus, the algorithm is widely used in transportation etc. However, as the specificity of tracking experiment in the myocardium, the space vector directions of the myocardial tracking can be calculated and the directions are reliable. The need for strengthening the reliability of processing is necessary. When underwater robots move in the environment, the disturbance from the external obstacles and the limitations of scanning images sonar sensors can cause the uncertainty information of the entire spatial distribution. When underwater robots are doing exploration in the actual experiment, the external sudden disturbance should be added to the algorithm at some time. Thus, the complexity of the path tracking algorithm is largely increased. Many algorithms take into account of the two dimensional space for the optimal path. We are more concerned about the problems of how to walk in three-dimensional space, adapt an effective algorithm and keep the high real-time. Therefore, the optimal path selection algorithm of the traditional low-dimensional space can not be enough to be applied to these two special applications. For real applications, we do not want to find the shortest path for the underwater path tracking and are more interested to locate a simple, stable, high reliability, real time algorithm to complete the journey for space planning. Reference on the high dimensional tracking path experience of mobile robot, a simple algorithm based on the random routing theory is proposed for the path exploration of the underwater robots.

In this chapter, we propose to categorize these algorithms into two types. One type is called inactive tracking algorithm, and the other type is called active tracking algorithm. The first type of algorithm is based on known space, through the high dimensional data, such as tensors or other means. It deals with the known direction information field and the path from any starting point moves forward to find the known information to achieve tracking paths. The latter type of algorithm solves the problems of a number of unknown space information fields. Based on some simple and practical algorithm ideas, it takes use of a small amount of information from the outside world and explores the path of maximum probability field step by step. Both above-mentioned classifications are applied to the current studies. These will

also be discussed and applied in the follow-up chapters. The theory in this chapter will be applied to DT-MRI myocardial tracking and underwater robot's tracking movement to the destination and return to the starting points, as well as emergencies treatment method etc. The starting point of algorithm is to construct a reliable, simple, feasible, and real-time path algorithm. This chapter first presents the theory such as the streamline algorithm shown in section 3.2. Then we propose in detail a new maximum energy tracking algorithm in section 3.3. A Bayesian theory algorithm is simply quoted in section 3.4 and this new detailed proposed algorithm will be described in Chapter 5.

3.2. Streamline Algorithm Theory

Streamline is a simple integral algorithm for solving the path and is also an inactive algorithm. Streamline uses a series of vector field data and streamline surface is describing the idea of the complexity of vector field distribution.

This algorithm finds out the path from the vector field. The path $s(\tau)$ is the bending line in three-dimensional space. It is a linear integral calculation based on the series of characteristics from the initial vector field, and its equation (3-1) is as follows:

$$s(\tau) = \int_0^\tau \bar{e}_1(t) dt, \quad (3-1)$$

where t is the curved line parameter, $t = t(x, y, z)$ and \bar{e}_1 values are the position function of initial vector field. Here, vector field is a unit vector field.

Based on DT-MRI, we introduce diffusion tensor field \bar{T}

$$\bar{T}\bar{e}_1 \iff \bar{\lambda}_1\bar{e}_1, \quad (3-2)$$

where $\bar{\lambda}_1$ is the largest eigenvalue of the tensor. The integration calculation of the equation (3-1) can use discrete method. The numerical solution is dominant or recessive and this depends on the convergence or divergence of tensor. For the bifurcation of the fiber distribution, a most simple algorithm is to use the forward algorithm

$$r_{new} = r_{old} + \bar{e}_1 \left[\bar{T}(r_{old}) \right] \Delta t \quad (3-3)$$

The fiber distribution convergence takes use of inverse Euler algorithm:

$$r_{new} = r_{old} + \bar{e}_1 \left[\bar{T}(r_{new}) \right] \Delta t \quad (3-4)$$

Of course, we can use high order solution to solve the integration problem, but we have to consider tensor field characteristics. The divergence or compactness of the fiber field calculated from the tensor field is according to the stickiness and bifurcation of the equation.

The algorithm steps of streamline algorithm for the application of DT-MRI images can be concluded as follows:

- (1) Definition of starting points as a seed set;
- (2) Calculate the tensor data for each corresponding point;
- (3) Determine if the anisotropy value in the corresponding points is satisfied.

If satisfied, we set it as the track direction and use the streamline integration algorithm for

$e_1, -e_1$ directions of the fiber path. Then calculate the sum of the two paths for preservation. If not satisfied, we select the next calculation point and return to step (2).

The advantage of the streamline algorithm is characterized by fast path tracking space method from the known vector distribution. If the vector field data is not reliable and the boundary conditions are easy, these may lead to the wrong fiber path. Therefore, we need to strengthen the processing conditions. Taking the trend analysis for example, we consider multiple vector fields around the original direction, and then update the vector direction of the points, or through the interpolation algorithm to repack the vector.

For the application of underwater robots in the underwater environment, the beginning of movement is unable to establish a predetermined distribution of field vectors based on this algorithm. The algorithm of underwater robot should be an active type. However, when the underwater robots reach the target, the robots explore the surrounding environment and deal with the information storage during the movement process. Combined with the presentation path algorithm of underwater robots for exploration, the direction of spatial distribution can be easily acquired through the movement of underwater robots. Although there is no tensor field, a priori probability, a likelihood distribution, and a posteriori probability distribution that are calculated from the statistics, can be used for the replacement of tensor data into the equation¹. Combined with the storage direction of information, we can easily construct several paths.

3.3. Theory of maximum energy tracking approach

This new algorithm is inspired for DT-MRI medical imaging applications background, and then is extended for the application of underwater robots.

In DT-MRI images, the fiber path may not track along the principle vector field from the tensor field. It may be in accordance with the other directions of the collected images due to the deformation from the noise, chatter etc. Compared with the previous described streamline algorithm, the maximum energy method is based on the new energy field from the potential path to find out the most proper and reliable paths. The algorithm goal is to locate the most appropriate point of balance between the reliability of fiber track and the complexity of algorithms.

We define a new energy field which is used for the statistical summarization of the influence from the other voxels around the current voxel. We assume that if there is only one voxel, it will follow the main principle vector direction that we can get from the tensor. However, the voxel is not a single one in the region and its neighborhood voxels will also impact the current voxel orientation. So how can we propose a way to describe this physical feature in our assumption, this is the main job in this part. Here, we introduce the following energy field to describe this feature.

Firstly, we need a region which is a predefined constrained sliding tri-dimension window around the current voxel. All voxels in the window are defined as X_0, \dots, X_n . For example, this window is 5*5*5 grids. The reciprocal distance between the current voxel and the other

voxels inside the region is individually set to be the weights $\omega_1, \omega_2 \dots \omega_n$. $\omega_i(x) = \frac{1}{d(X_0, X_i)}$,

where $i=1 \dots n$ and $d(\cdot)$ is the distance between two voxels. Each coordinate plane individually divides the whole region into two regions. For example, YZ coordinate plane divides the voxels into two parts. Ω_{x+} is defined as the voxel set along the positive half of the X-axis. Otherwise, Ω_{x-} is the one along the negative half of the X-axis. Like $\Omega_{x\pm}$, we can define $\Omega_{y\pm}, \Omega_{z\pm}$.

¹ Detailed description in Chapter 5 section 5.3

Then, we calculate the average value in each region and store these values as $I_{x\pm}$, $I_{y\pm}$, $I_{z\pm}$. These values are defined as

$$I_{x\pm} = \frac{\sum_{i \in \Omega_{x\pm}} I_i \omega_i}{\sum_{i \in \Omega_{x\pm}} \omega_i}, \quad I_{y\pm}, I_{z\pm} \text{ are alike,} \quad (3-5)$$

$$I_x = [I_{x+} \ I_{x-}], \quad I_y, I_z \text{ are alike,}$$

where I_i is the voxel image intensity value. We consider that every MR signal from the voxel is the sum of the signal from arbitrarily small sub-voxel.

The variable average value vector \mathcal{V} is pointed out to be the common robust distribution around the current voxel along each axis. It is derived in

$$r_x = (I_s - \left\| \vec{I}_x \right\|), \quad r_y \text{ and } r_z \text{ are alike} \quad (3-6)$$

$$\vec{r} = [r_x \ r_y \ r_z], \quad (3-7)$$

where I_s is the current voxel image intensity value. Then we assemble the current voxel with other voxels from different areas into six individual clusters $\Omega_{x\pm}$, $\Omega_{y\pm}$, $\Omega_{z\pm}$. These areas of voxels are partitioned along the cubic plane around the current voxel. Thus, the standard deviation $\alpha_{v_{\pm}}$ in those clusters can be calculated. The new variable average deviation matrix σ is also defined to be a diagonal norm standard deviation value matrix which is constructed for describing the differential deviation variety. The equation can be written as

$$\sigma_x = [\sigma_{x+} \ \sigma_{x-}], \quad \sigma_y, \ \sigma_z \text{ are alike,}$$

$$\sigma = \text{diag}(\|\sigma_x\|, \|\sigma_y\|, \|\sigma_z\|), \quad (3-8)$$

where the standard deviation σ_{x+} takes on voxel values I_s, I_{x+} , the others are similar.

Based on some previous experiments, Gaussian densities model is an efficient way to describe the estimation of the region properties. So we adapt the vector Gaussian model to construct the variable average value gradient distribution

$$p_1(I) = \frac{1}{(2\pi)^{\frac{1}{2}} |\sigma|^{\frac{1}{2}}} e^{-\frac{1}{2} \vec{r}^T \sigma^{-1} \vec{r}}. \quad (3-9)$$

The purpose of p_i is to obtain the differences between the original point and the surrounding points and store them as factors for the variable average value distribution energy. At each gradient direction, diffusion weighted MR images signal values represent the intensity map following corresponding direction. So we need consider all those sub-voxel values and calculate the sum of the variable average value distribution energy from different direction which can be considered to be the first energy field

$$\xi_1 = \sum_{i=1}^N (\ln p_1)_i, \quad (3-10)$$

where N is the number of diffusion weighted image volumes.

In equation (3-10), the first energy ξ_1 describes the influence products from the nearby voxels. Alternatively, we also move to measure the current voxel own energy

$$\begin{aligned} p_2 &= \beta I_s / \bar{I} \\ \xi_2 &= \sum_{i=1}^N (\ln p_2)_i. \end{aligned} \quad (3-11)$$

where average value \bar{I} is the average intensity value of all the points in the predefined sliding window except for the current one.

Here, we set $\beta = \frac{1}{|I_s - \bar{I}| + 1}$. The principle of this energy is to encourage the large value

of the current voxel as it appears to be areas including fibers in black-white DT-MRI images. However, the weight parameter can punish the unexpected voxel value if the special voxel value is deviated largely from the average value in the current region. Hence, this energy is pointed out to record the fibers possibility in the current voxel.

Although the uncertainties may deflect the principle direction, its distribution still plays an important role. So we are looking for the special energy which can record the information from the principle direction distribution. This third energy is written as

$$\begin{aligned} p_3 &= \left| \frac{1}{(n-1)(n-2)} \sum_{\substack{j=1\dots n-1 \\ k=j+1\dots n}} (v_j \cdot v_k) \right|, \\ \xi_3 &= \sum_{i=1}^N \ln(p_3)_i, \end{aligned} \quad (3-12)$$

where v_j, v_k are the principle directions of the points in the sliding window which are calculated from the tensor matrix. ‘ \cdot ’ is the standard Euclidean vector inner product. Fig.3-1 shows the maximum and the minimum direction energy of two types of vector connections. If the two vector directions are opposite, the result is the minimum. If the two vector directions are same, the result is the maximum. Thus, the parameter ξ_3 is the average value of the whole coupled voxel directions that defines the principle direction distribution energy. The value of this energy encourages the homogeneous principle vector in the region and the vector direction should be fixed in the same coordinate system.

In view of the equation (3-10) ~ (3-12), the whole energy field ξ is constructed from these three parts

$$\xi = \xi_1 + \xi_2 + \xi_3 \quad (3-13)$$



Fig.3-1 Voxel direction energy

Here, one is presented for the nearby voxels influence energy, one stands for the current voxel own energy, and the final one is used to describe the principle voxel directions distribution in the region. However, this definition of three parts are deficient, more works should be considered in the future.

After the construction of the energy field, we can now know the possible influence which is calculated from the voxel value and the average connection between the directions in each region. Each region is a constant voxel cluster which is the same size of the overlapping sliding window. Then we define ϕ which presents the possible direction function of each fiber and it is shown as

$$\phi = F(x, D, \xi), \quad (3-14)$$

where x is the coordinate value, D is the tensor matrix of the voxel. The initial direction ϕ_0 is set to be the principle vector direction of every fiber current voxel. This gives

$$\phi_0 = v \quad (3-15)$$

Then, we propose an idea to describe the fiber directions that vary according to the energy field influence. Fiber direction ϕ is updated from two parts, one is the normalized gradient direction ϕ and the other part is the projection vector of the tensor matrix along the normalized energy gradient direction. The equations are written as

$$\dot{\phi} = a \left(\frac{\nabla \phi}{|\nabla \phi|} + D \frac{\nabla \xi(x)}{|\nabla \xi(x)|} \right). \quad (3-16)$$

Equation (3-16) describes those two parts. The second part is to construct the connection between the energy field disturbance and the fiber orientation. Here, a is the weight parameter and its value is defined as the product of the norm value of the upper two normalized gradient parts. It is given by

$$a = \left\| \frac{\nabla \phi}{|\nabla \phi|} \right\| \times \left\| \frac{\nabla \xi(x)}{|\nabla \xi(x)|} \right\|. \quad (3-17)$$

The principle of this weight parameter is set as the threshold value which can record the variety from both two parts. If no variety or little variety, the accumulation of the direction should be stopped. Following the steps of updating fiber orientation, we can believe that the local fiber orientation is always trying to record the available directions at each point along the path.

Obviously, it is not enough if we only consider the local voxel energy or the local line energy. So we introduce Equation (3-18) to obtain all the feature status value E along every fiber line

$$E(x, \phi) = \sum \xi(x)H(\xi) - \sum \operatorname{div}\left(\frac{\nabla \xi(x)}{|\nabla \xi(x)|}\right)H(\xi) + \sum_{i=2\dots n} \phi_i \cdot \phi_{i-1} \quad (3-18)$$

where $H(\xi)$ is a Heaviside function. We calculate the Euclidean vector inner product of the two near fibers as an angle standard which is stored as values for the final part of Equation (14), shown in Fig.3-2. $\operatorname{div}\left(\frac{\nabla \xi(x)}{|\nabla \xi(x)|}\right)$ is defined as the divergence of the energy gradient field. In general physical interpretation, if the divergence of a three dimensional vector field is considered, the vector field flow behaves as a source or a sink. Thus, a vector field with constant zero divergence means no net flow can occur across any closed surface. Hence, this feature of the divergence part is to describe the isotropic and homogeneous level of the energy field.

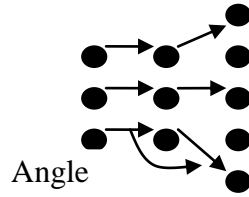


Fig.3-2 Angle between two near vector direction

If this special homogeneous level is small, the energy field is flat, stable. We can see that the fiber orientation is also stable and without too much uncertainties disturbance. If the special homogeneous level is big, the energy field seems to be bended. We should punish this status as it means unstable energy field. These features are shown in Fig.3-3. According to this part in Equation (3-18), the principle is encouraging stable and flat energy field. The shape of this energy distribution manifold can also be an efficient criterion for the final fiber orientation. Meanwhile, for a reasonable fiber tracking results, we choose 90 degree as the threshold of fiber angle.

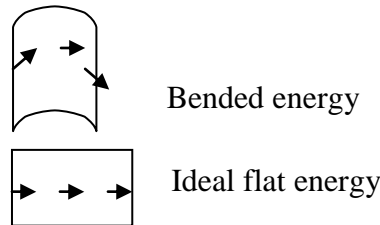


Fig.3-3 Homogeneity level of the Energy field

Here, the tracking process is following the possible vector direction. We should record the available fiber orientations calculated from the updated steps in Equation (3-16) and keep the initial points, to find the next points in the fiber lines. As the time steps pass, the tracts are updated following the new possible vector direction ϕ_i . Compared with the former types of PDD tracking approach or streamline approach which are local continuous algorithms, the globe constraints for the fiber lines which can get the maximum energy from all the fiber paths and the tract of the max one is the final fiber path. This globe constraints equation is written as

$$\sup\{E(x, \phi)\} \quad (3-19)$$

In this view, the idea of this tracking approach consider not only principle direction but also the other possible direction and the constraint of the globe features in fiber line that can help to improve the certainties and robustness.

In the above mentioned algorithm, the detailed tracking algorithm of the maximum energy for the DT-MRI applications is described. In this inactive tracking algorithm, a combination of the original image features and characteristics of the vector direction is proposed to strengthen the effectiveness of the tracking algorithm.

For the return path tracking applications of underwater robot, the algorithm is similar to the proposed algorithm. The characters of original image map, the priori probability distribution, the distribution of likelihood function, the posterior probability distribution of maps and the vector distribution by the exploration space process can be stored and put to use. Based on the above algorithm characteristics, for the return path of the underwater robot, we propose to combine the posterior probability distribution and the direction of the distribution of vector. Thus, in the equation (3-16), the projection tensor data is changed to the probability distribution as the weight value.

Of course, every algorithm can not be perfect and it has the shortcomings. In the algorithm of underwater robots to find the path of return movement, if in the return process, the underwater environment is ideal for space with no great changes, the algorithm will find out the largest energy value to maintain the desired track initialization vector field. However, the speed of streamline algorithm is faster and more proper. If in the return process, there is a large change in the underwater environment or as a result of the limitations of the experimental device, these cause an incorrect distribution of the space vector in the beginning exploration. The errors always exist. In this case, the combination of the probability distribution is known and the maximum energy can be used to identify a more reliable method to track the path.

Above all, this section describes a new maximum energy tracking algorithm theory and it is the establishment of a global path to find the way through the construction of different energy field. The combination of the new type of energy field to and the path of innovation is aimed to enhance the reliability of the path tracking algorithm. Compared with the single vector tracking algorithm, the robustness and reliability of the algorithm can be guaranteed.

3.4. Stochastic tracking algorithm based on Bayesian theory

This algorithm takes use of Bayesian theory to the realization of an underwater robot working in unknown underwater space environment and completing the path tracking from the starting points. Through a simple calculation of the probability in high-dimension, it is unique in practice compared to the commonly used Markov chain Monte Carlo theory (MCMC) algorithms. Algorithm derived from the idea of DT-MRI fiber uncertain direction tracking theory and the algorithm can greatly improve the robustness and the reliability of an underwater robot in unknown space.

In order to give more specific description of the algorithm, the chapter 5 section 5.3 concerns underwater robot path reconstruction algorithms and applications, and the detailed description of algorithms and related mathematical proof are proposed. Therefore, this section do not discuss in detail.

3.5. Summary

Under the premise of DT-MRI and the underwater robot path tracking options, this chapter introduces three types of practical and theoretical path tracking algorithms, which are used for the base works of the applications in follow-up sections.

Chapter 4 APPLICATION OF THREE DIMENSIONAL MYOCARDIAL FIBER RECONSTRUCTION AND ITS REFERENCE VALUE FOR UNDERWATER ROBOT

Summary

4.1. Introduction.....	67
4.2. DT-MRI images and derived data types, characteristics	68
4.3. Application of tracking algorithms and their results comparison.....	75
4.4. Myocardial fiber structures study and the parameters	91
4.5. Reference value of myocardial tracking algorithms to the underwater robot path tracking methods	97
4.6. Summary.....	99

4.1. Introduction

Reconstruction technology of cardiac medical image is currently a hot research field. Because the space model of the heart can help people improve their understanding of the internal anatomy of the heart structure and the common understanding of the physical phenomena. People can have a better view of heart common physiological and path physiological aspects. Such knowledge has been widely used in biological research, education and training, as well as drugs, medical equipment development. The most important application of the research in the biomedical field of the heart space model is to understand the structural defects of heart that can easily lead to human deaths. Taking use of the appropriate model, it can simplify the drug and medical device development and validation process, which verifies that this technology is crucial and important. Modeling heart provides a simple method to describe the heart and can be combined with theoretical physics and mathematics. For example, the general clinical studies of human heart are taking the heart of animal experiments for comparison. Mathematical models are generally using the computer numerical simulation. The heart modeling generally refers to the calculation of the surface, and usually a number of research methodologies are based on academic and commercial fields. Methods of these studies are the reconstruction of the general molecular structure and the relationship between the anatomies of the heart with the electrical, mechanical behavior.

Myocardial structure is a special composition of the heart muscle cells, the cells in other organs in the body does not exist. The heart muscle like other muscles can shrink, but it can also be the sportive potential (for example: transmission of electrical conductivity), that is the same as nerve can be composed of the neurons. Further, it can be known that some cells could have a potential capacity of movement, such as the movement of the heart muscle. Myocardial blood supply is by coronary vascular transport. Myocardium is divided into two opposing sets of control power. The first cardiac electrical control is generated by the sinoatrial node. The second type of cardiac electrical control is closely connected with the cone of spinal ganglia and vagus nerve in the sympathetic nerve.

For the medical images in the current research area of the physical structure of the human body, the diffusion tensor magnetic resonance imaging (DT-MRI) is a new and hot research technology. DT-MRI is to provide a number of information of the nervous system and heart medicine and other disciplines of the subject to provide a more direct fiber anatomy in the tracking technology. Different types of methods have been applied to show the fiber path and

have the interesting part of connecting fiber distribution. This allows people to be more intuitive to understand the structure of the composition of the human body. Fiber tracking in DT-MRI or diffusion tensor imaging (DTI) offers a unique and nondestructive technique to obtain the three-dimensional organization of myocardial fibers.

From theory of DT-MRI cardiac imaging, through the water molecules of Brown's process, the multi-angle magnetic field direction information is calculated from the distribution of the data. However, there is a lot of instability. Thus, how to reduce the uncertainty of information and increase the stability of the information field of cardiac DT-MRI is the target of the path tracking algorithm. They are significant for the entire heart structure and heart pathology.

In the underwater movement of the underwater robots, there also exist in a lot of instability. The explored direction that is known as the return path information criteria is the same as an instable direction distribution map due to instable underwater environment. Myocardial fiber tracking can be regarded as a space field in return movement of underwater robot that consists of a multi-state-space field, a variety of non-stability field, and a wide range of stability field. Its path selection ideas can be referenced as a 'real simulation' environment that is similar to the complex underwater space field.

Therefore, the return path tracking algorithm of the underwater robot and myocardial fiber tracking algorithm are faced to solve similar problems. Based on these ideas, we discuss the examples and applications of myocardial fiber tracking reconstruction. Then we in detail explain its reference value to the underwater robots of the return path reconstruction. Therefore, the contents of this chapter are listed as follows:

Section 4.2 introduces DT-MRI image processing and the basic processes for tensors and the anisotropy described in DT-MRI data, such as FA, RA and the theory of tensor data etc. Section 4.3 discusses the data source and give a detailed qualitative and quantitative comparison of the maximum energy algorithm and commonly used algorithm from the tracking results, as well as the advantages and disadvantages and the relationship of these algorithms; In section 4.4, the reference value and significance of myocardial track are described for the application of the underwater robot return movement; Section 4.5 is the summary.

4.2. DT-MRI images and derived data types, characteristics

This section introduces basic processes of DT-MRI image processing, as shown in Fig.4-1.

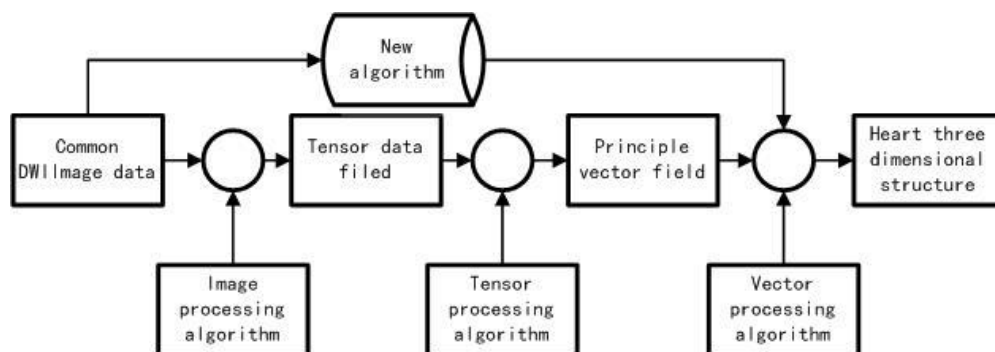


Fig.4-1 DT-MRI Image Processing Basic Process

Commonly DT-MRI calculation steps are based on the general diffusion weighted magnetic resonance imaging (DWI) data. After the calculation of tensor field data, the direction of the principle vector distribution can be analyzed. Combination of the basic algorithm of three dimensional reconstructions, the final three dimensional myocardial reconstructions can be obtained.

Therefore, based on the basic steps above, we can introduce a three-layer data-processing algorithm to enhance the reliability of images and data stability, robustness etc in this basic process of image processing. This three layer data processing algorithms include image processing algorithms, tensor field data processing algorithms and vector data processing algorithms. These processing algorithms can be categorized into: segmentation algorithm, noise reduction algorithm, interpolation algorithm, and enhancement algorithm.

For the special problem of this research, we propose a new maximum energy approach to raise a bridge between the original image characters and the final vector direction field, which is one major contributions of this algorithm. In section 4.5, we can see the experimental results of the maximum energy track approach, the traditional streamline methods and the improved streamline methods. In order to better analyze the merits and weaknesses of the results and we put forward the relevant evaluation criteria, and in the final data the qualitative and quantitative comparisons have been discussed. Our experimental goal is to identify and find out the most closely ways with the pathology, linked to the means of three-dimensional computer imaging technology to reconstruct the most likely distribution of the myocardium.

Generally speaking from the diffusion-weighted magnetic resonance imaging (DWI), the diffusion tensor data calculations have two kinds of algorithms. One is the use of H matrix and the other is a matrix algorithm that uses b matrix. This section describes in more detail H matrix algorithm, and processed data in this article from the H matrix is calculated by the algorithm [Peter.I 2006][Peter.II 2006][Peter.III 2006].

1. H matrix algorithm

Firstly, the tensor data is defined as a six dimensional column vector d :

$$d = [D_{xx}, D_{yy}, D_{zz}, D_{xy}, D_{xz}, D_{yz}]^T. \quad (4-1)$$

Each independent six row matrix H_i is derived from the normalized gradient terms g_{xi} , g_{yi} and g_{zi} . H_i is defined as:

$$H_i = [g_{xi}^2, g_{yi}^2, g_{zi}^2, 2g_{xi}g_{yi}, 2g_{xi}g_{zi}, 2g_{yi}g_{zi}]. \quad (4-2)$$

H_i vector is combined to the matrix, H is

$$H = [H_1^T H_2^T \dots H_M^T]^T \quad (4-3)$$

Thus, H is calculated as:

$$H = \begin{bmatrix} g_{x1}^2 & g_{y1}^2 & g_{z1}^2 & 2g_{x1}g_{y1} & 2g_{x1}g_{z1} & 2g_{y1}g_{z1} \\ g_{x2}^2 & g_{y2}^2 & g_{z2}^2 & 2g_{x2}g_{y2} & 2g_{x2}g_{z2} & 2g_{y2}g_{z2} \\ & & & \dots & & \\ & & & \dots & & \\ & & & \dots & & \\ g_{xM}^2 & g_{yM}^2 & g_{zM}^2 & 2g_{xM}g_{yM} & 2g_{xM}g_{zM} & 2g_{yM}g_{zM} \end{bmatrix}. \quad (4-4)$$

DWI experiment data is described as an independent obvious diffusion coefficient (ADCs) and not single log distribution information.

$$Y_i = \ln(S_0 / S_i) / b \quad (4-5)$$

$$Y = [\ln(S_0 / S_1) / b, \ln(S_0 / S_2) / b, \dots, \ln(S_0 / S_M) / b]^T \quad (4-6)$$

In equation (4-5),(4-6), $i = 1, \dots, M$,

S_0 : Signal data when $b = 0$ (T2 image).

S_i : Signal data when $b = 1000$ (diffusion image).

Y : Diffusion obvious ADC coefficient.

b : Diffusion weight factor, that is set according to data of DWI image collection.

There are noise effects in collection experiment. Thus, Y is defined as

$$Y = Hd + \eta, \quad (4-7)$$

where η is the noise data.

There four different solutions to solve Equation (4-7). Firstly, if there are only six directions, we can use the precise calculation method. Secondly, a nonlinear weighted least squares algorithm can be applied. Thirdly, we can use a weighted linear least squares calculation. Fourthly, a nonlinear least square method can be used.

Taking into account the gradient direction has 12 and 30 the directions, the non-linear weighted least square method is considered to calculate the tensor data.

2. Pseudo-inverse matrix and tensor calculation

Because the gradient direction is larger than 6 and H matrix is not square, there is no real existence of inverse matrix H^{-1} . Therefore, we take use of a pseudo-inverse matrix to calculate

$$H^\phi H = I_{6 \times 6}. \quad (4-8)$$

Though $H^\phi H$ is not equal to $I_{M \times M}$, one method is to construct a 6×6 matrix to solve this inverse calculation

$$H^T Y = H^T H d, \quad (4-9)$$

$$(H^T H)^{-1} H^T H d = d = (H^T H)^{-1} H^T Y, \quad (4-10)$$

$$H^\phi = (H^T H)^{-1} H^T. \quad (4-11)$$

This is in non-weighted linear least square method for the logarithmic signals. Pseudo inverse calculation can be used for the singular value decomposition algorithm (SVD). This algorithm factorize H matrix to become three matrixes.

$$H = U W V^T. \quad (4-12)$$

Here W is diagonal matrix, H matrix calculation is as follows

$$V W^{-1} U^T H = V W^{-1} U^T U W V^T = I_{6 \times 6}. \quad (4-13)$$

Obviously speaking, the pseudo inverse calculation is given as follows:

$$(H^T H)^{-1} H^T = V W^{-1} U^T = H^\phi \quad (4-14)$$

After we solve the pseudo inverse matrix H^ϕ , take use of the least square method and combine with the equations (4-6), (4-7), the most proper tensor data can be calculated. This algorithm is very quickly (results can be quickly calculated even in large data sets). Thus, it can be applied for the calculation of DWI image tensor data.

Then, we continue apply the following tensor analysis to the singularity of the tensor data as well as the micro structures:

I. Anisotropy

DT-MRI is an imaging measurement method of the micro-observation. The voxel dimension of the images can directly affect the measured value of the diffusion tensor. The size of several factors in images can directly affect the diffusion tensor data shape (the diffusion ellipsoid shape), including density of fiber, fiber angle, the average fiber diameter and angle similarity of fiber etc. These measured diffusion tensor geometric shape of the fiber tracking is important for the final fiber tracking path results. Diffusion tensor imaging technology can provide a large number of methods of the anisotropy description. Therefore, [Basser 1996] proposes that it is essential to relate the diffusion anisotropy to the geometric structure information. This section highlights some common standardized parameters, including the mean diffusion coefficient (MD), related anisotropy coefficient (RA), the fraction anisotropy coefficient (FA).

$$MD = \frac{Trace(D)}{3} = \frac{\lambda_1 + \lambda_2 + \lambda_3}{3}, \quad (4-15)$$

$$RA = \frac{1}{\sqrt{2}} \frac{\sqrt{(\lambda_1 - \lambda_2)^2 + (\lambda_2 - \lambda_3)^2 + (\lambda_1 - \lambda_3)^2}}{(\lambda_1 + \lambda_2 + \lambda_3)} \quad (4-16)$$

$$= \frac{\sqrt{3}}{\sqrt{2}} \frac{\left| D - \frac{1}{3} trace(D) I \right|}{trace(D)},$$

$$FA = \frac{1}{\sqrt{2}} \frac{\sqrt{(\lambda_1 - \lambda_2)^2 + (\lambda_2 - \lambda_3)^2 + (\lambda_1 - \lambda_3)^2}}{\sqrt{\lambda_1^2 + \lambda_2^2 + \lambda_3^2}} \quad (4-17)$$

$$= \frac{\sqrt{3}}{\sqrt{2}} \frac{\left| D - \frac{1}{3} trace(D) I \right|}{|D|},$$

where I is a unit tensor. RA is quantitative and non-dimensional constant. For the isotropy tensor D , $RA = 0$. RA is represented as the ratio between the sample standard deviation value $\sqrt{\text{var}(\lambda)}$ that is calculated from the three eigenvalues of tensor and the expectation value $E(\lambda)$.

FA records tensor intensity to describe the performance of the fractional anisotropy. For a cylindrical symmetric anisotropy tensor data (For example, $\lambda_1 \gg \lambda_2 = \lambda_3$), $FA = 1$. [Pierpaoli 1996] present that when the anisotropic structure is obvious, the intensity of human brain FA image are bright. Meanwhile, when the isotropy is strong, the image intensity of FA is relatively dark. Thus, we can know the value of FA in the human brain is a useful parameter. The relative anisotropy of heart is not very high in comparison with brain.

However, in the application process, FA values remain valuable as a criterion. In this research, how to find the most obvious features of the anisotropy value is a problem that is worthy of studying.

II. Microstructure tensor data

Diffusion tensor as the principle direction is in accordance with the direction of characters, it can be described by the ellipsoid. [Westin 2002] pointed out that the symmetry properties of ellipsoid tensor and diffusion tensor can be defined as several different types of geometric structures.

When $\lambda_1 \geq \lambda_2 \geq \lambda_3 \geq 0$ is set as the symmetric diffusion tensor D and \hat{e}_i is the corresponding standardized eigenvector to λ_i . Tensor D can therefore be described as

$$D = \lambda_1 \hat{e}_1 \hat{e}_1^T + \lambda_2 \hat{e}_2 \hat{e}_2^T + \lambda_3 \hat{e}_3 \hat{e}_3^T \quad (4-18)$$

Based on the dimension of diffusion tensor, the characters of diffusion can be categorized into three types.

Linear tensor ($\lambda_1 \gg \lambda_2 \cong \lambda_3$): the main diffusion refers to the largest eigenvalue that represents the direction of the characteristics.

$$D \cong \lambda_1 D_l = \lambda_1 \hat{e}_1 \hat{e}_1^T \quad (4-19)$$

Planar tensor ($\lambda_1 \cong \lambda_2 \gg \lambda_3$): diffusion is restricted to two of the largest eigenvalue of the two corresponding eigenvectors that constitute the plane.

$$D \cong \lambda_1 D_p = \lambda_1 (\hat{e}_1 \hat{e}_1^T + \hat{e}_2 \hat{e}_2^T) \quad (4-20)$$

Ball tensor ($\lambda_1 \cong \lambda_2 \cong \lambda_3$): with the isotropy diffusion

$$D \cong \lambda_1 D_s = \lambda_1 (\hat{e}_1 \hat{e}_1^T + \hat{e}_2 \hat{e}_2^T + \hat{e}_3 \hat{e}_3^T) \quad (4-21)$$

The diffusion tensor equations can be extended as

$$\begin{aligned} D &= \lambda_1 \hat{e}_1 \hat{e}_1^T + \lambda_2 \hat{e}_2 \hat{e}_2^T + \lambda_3 \hat{e}_3 \hat{e}_3^T \\ &= (\lambda_1 - \lambda_2) \hat{e}_1 \hat{e}_1^T + (\lambda_2 - \lambda_3) (\hat{e}_1 \hat{e}_1^T + \hat{e}_2 \hat{e}_2^T) + \lambda_3 (\hat{e}_1 \hat{e}_1^T + \hat{e}_2 \hat{e}_2^T + \hat{e}_3 \hat{e}_3^T) \\ &= (\lambda_1 - \lambda_2) D_l + (\lambda_2 - \lambda_3) D_p + \lambda_3 D_s. \end{aligned} \quad (4-22)$$

In equation (4-21), $(\lambda_1 - \lambda_2)$, $(\lambda_2 - \lambda_3)$ and λ_3 are the coordinates of tensor D data set $\{ D_l, D_p, D_s \}$. The similarity analysis of tensor shape is very useful to the computer graphics applications.

Because the coordinates are based on tensor eigenvalues, they are rotation invariance constants and these values do not need to specify a reference coordinate system. In order to access the calculation of anisotropy, these coordinates need to be standardized for the measurement of various geometric shapes.

Tensor data using the maximum eigenvalue can be used to calculate the standardized linear, planar, spherical three parameters.

$$c_l = \frac{\lambda_1 - \lambda_2}{\sqrt{\lambda_1^2 + \lambda_2^2 + \lambda_3^2}} \quad (4-23)$$

$$c_p = \frac{2(\lambda_2 - \lambda_3)}{\sqrt{\lambda_1^2 + \lambda_2^2 + \lambda_3^2}} \quad (4-24)$$

$$c_s = \frac{3\lambda_3}{\sqrt{\lambda_1^2 + \lambda_2^2 + \lambda_3^2}} \quad (4-25)$$

In order to ensure the measurements result is between 0 and 1 and the sum is 1, the second and third parameter are defined as plane and spherical parameters. The measurement of a new geometry to the anisotropy alike FA is to describe the spherical error that is defined as follows

$$c_a = 1 - c_s = c_l + c_p \quad (4-26)$$

If the tensor trace data is to do a standardization calculation rather than norm, it is like RA parameter. [Westin 1997][Westin 2002][Behrens 2003] in the human brain DT-MRI data, applied three types of restrictions and constraints on the whole tensor data. Using the following algorithm:

$$D = \begin{cases} c_l D_l, & \text{if } c_l > c_p, c_s \\ c_p D_p, & \text{if } c_p > c_l, c_s \\ c_s D_s, & \text{if } c_s > c_l, c_p \end{cases} \quad (4-27)$$

Therefore a standardized data field tensor can be calculated, the introduction of this method can be used to optimize the tracking algorithm. The space of diffusion tensor and the different performance of tensor shape, can determines DT-MRI information distribution. For the common algorithms, the most concerned characters of the image determine the direction of fiber tracking track path. Thus, the tensor shape of the entire late stage imaging is very useful.

III Definition of fiber angle information and the system coordinates

In order to describe the angle of ventricular fiber orientation and fiber layer angle, DTI data in Cartesian coordinate system is transformed to a new cylindrical coordinate system, shown as Fig. 4-2 (a). The central apex-base axis of the left ventricular in each heart is the longest axis. Polar coordinate system is based on different sections of the long axis and radial axis is perpendicular to the apex-base axis and connects with the central point and voxel (shown as a circle in Fig.4-2). The third tangential axis is defined as a vertical axis that is perpendicular to the apex-base axis and the radial axis in Fig.4-2(b).

According to these three polar coordinates, the definition of three reference planes is listed as follows:

1) Horizontal plane (transverse plane):

The shortest side of the heart and apex-base axis is perpendicular to this plane.

2) Circumferential surface (circumferential plane):

Epicardial tangent plane and the radial axis are perpendicular to this plane.

3) Radial surface (radial plane):

This plane is perpendicular to the horizontal plane and the circumference surface.

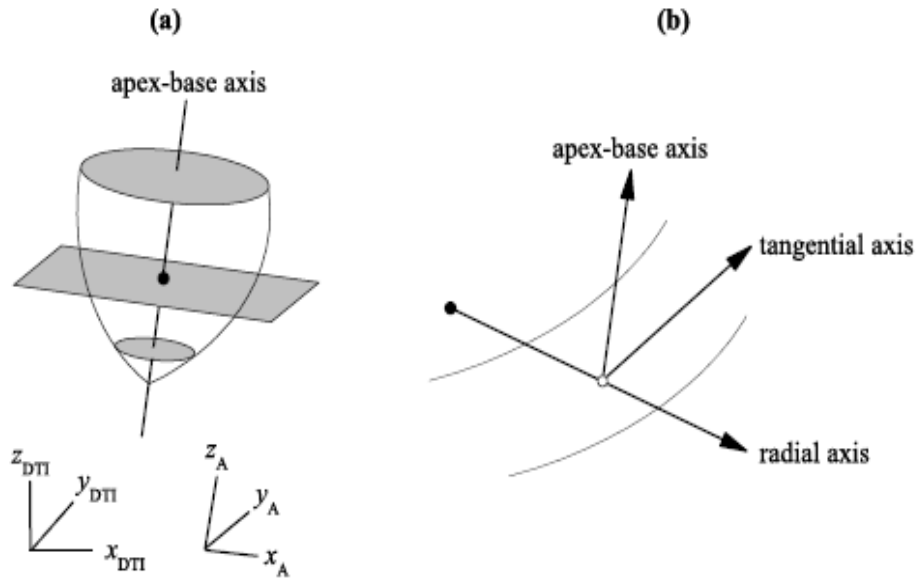


Fig.4-2 Heart Coordinate system description

The coordinate system in Fig.4-2 is used to describe the heart of myocardial fiber orientation and layer direction of the heart. In Fig.4-2(a), apex-base axis is through the center of left ventricle. This axis is orthogonal to the horizontal plane. The gray slice displays the central horizontal plane and the black central spots are the center of the new coordinates. The notation DTI in Fig.4-2 shows the absolute coordinates of diffusion tensor. The notation A in Fig.4-2 shows the anatomical coordinates.

Fig.4-3(b) describes the definition of three orthogonal axes for each voxel (shown in circle). Base-apex axis has been introduced. The radial axis (radial apex) comes through the voxel and center. Tangent axis (tangential apex) in the horizontal plane is vertical to the other two axes. Fig.4-3 shows the definition of the fiber orientation angles. (a) Fiber inclination angle (α_I) and horizontal angle (α_T). (b) Myocardial angle (α_S).

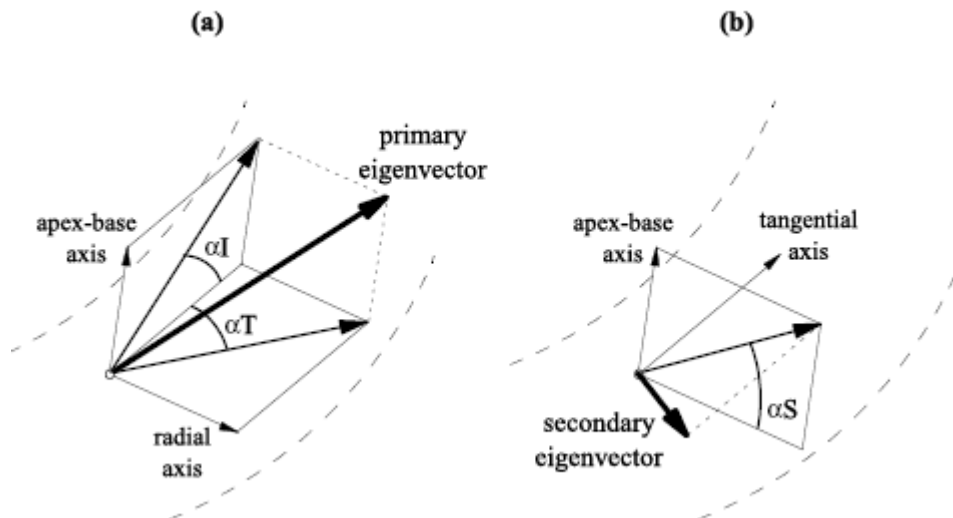


Fig.4-3 Angle Definition

4.3. Application of tracking algorithms and their results comparison

In this study, the size of primary vector fields is $56 \times 56 \times 1$, which is calculated from cardiac diffusion weighted (DW) images that have been acquired on Siemens 1.5 T Magnetom Sonata in the hospital of Neuro-Cardiology of Lyon. The healthy human heart fixed by the gel was placed in the center of the coil and located in a plastic box to avoid artifacts such as susceptibility and motion during acquisition. The acquisition parameters were: TE = 98 ms, TR = 8600 ms, FOV = 256×256 mm², slice thickness = 2 mm, slice spacing = 2 mm, slice duration = 142.5 ms, number of slices = 52, slice size = $128 \times 128 \times 1$, diffusion sensitivity b = 1000 s/mm², gradient directions = 12 and 30, the time of average is 4.

Chapter 3 gives a detailed discussion of several three-dimensional reconstruction technologies. The superiority of DT-MRI technology makes it possible to gradually realize the heart and other human organs, such as three-dimensional fiber tracking technology. This section focuses on the proposed new maximum energy tracking algorithm on cardiac DT-MRI data for three-dimensional reconstruction and the streamline method. At the end of this section, the results are compared and analyzed.

This section describes a new tracking algorithm for the largest energy. We firstly summarize three energy image values from the original DWI images. Secondly, we calculate the distribution of the energy field, and then construct the final fiber tracking direction field. The following contents can describe the steps of new algorithm and traditional algorithms, and comparison and discussions of their advantages and disadvantages from the results.

1. The application of maximum energy tracking algorithm

For the maximum energy tracking algorithm, the normal human DT-MRI images that are created from one time imaging and have 30 gradient directions are used for three-dimensional heart fiber tracking. We compare the experimental data in the human heart with the United States John Hopkins University's data that cost a few days for the dog heart data collection. The time of data collection in this experiment is more applicable for normal medical treatment, because a shorter acquisition time and we do not spend a lot of time to get the heart images. This type of data collection is more suitable for further research.

Maximum Energy tracking method is the processing method based on DWI original gray value image data. Because each piece of DT-MRI is not only corresponding to the original T2 images, but also the image is different in accordance with different gradient direction. Thus, for the energy field of each image, the total energy is considered as the sum of all images.

In order to test the reliability of the algorithm and experimental performance, this section of the experimental contrast design does not include too many images preprocessing steps, such as the enhancement of the original border of DWI image, interpolation and other methods. Design of the contents of this section has only considered means commonly used to determine the threshold conditions.

1) Flow chart of Maximum energy tracking algorithm

Tracking method to calculate the maximum energy is listed as these steps:

Firstly, we collect the initial DWI data by DICOM image data and import gradient direction data. After using tensor data calculation algorithm introduced in section 4.2 to get the tensors, we calculate the eigenvectors and corresponding eigenvalues etc., as shown in Fig.4-4.

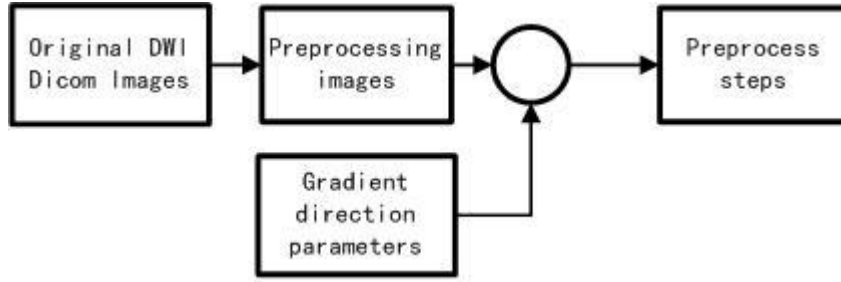


Fig.4-4 DWI image preprocess procedure

Threshold value such as FA, RA etc., and the initial minimum threshold of the images, fiber length and the parameters of integral calculations are necessarily determined at the beginning.

The maximum energy tracking method has to construct the voxel intensity gradient distribution of the energy field, target own energy field of voxels, the energy field of voxel direction. The entire energy field of images is summarized in Fig.4-5.

Through the equation of the energy field model, we can get the possible impact for the direction of fiber tracking. Due to the unbalanced energy distribution, this algorithm can be interpreted as a continuous cycle of looking for the cardiac fiber path. The paths sum the directions of fiber tracking and distribution. Thus, the starting point of each fiber tracking can be defined for the fiber tracking trajectory.

$$\Phi \{L_1 \{l_{11}, l_{12}, l_{13}, \dots, l_{1n}\}, L_2 \{l_{21}, l_{22}, l_{23}, \dots, l_{2n}\}, \dots, L_n \{l_{n1}, l_{n2}, l_{n3}, \dots, l_{nm}\}\} \quad (4-28)$$

where $L_1 \dots L_n$ refer to the initial point for each possible fiber trajectory. $l_{n1} \dots l_{nm}$ consist of the fiber size and the direction of each fiber.

Thus, we believe that each track sets constituted by a number of possible paths, and each path consist of a number of lines. Therefore, how to find the optimal path is very important. In order to find optimization route criteria, the total energy value of each fiber from every initial point in each possible path is recorded. Thus, it can be defined for each energy track as

$$\Phi \{E_1 \{e_{11}, e_{12}, e_{13}, \dots, e_{1n}\}, E_2 \{e_{21}, e_{22}, e_{23}, \dots, e_{2n}\}, \dots, E_n \{e_{n1}, e_{n2}, e_{n3}, \dots, e_{nm}\}\}, \quad (4-29)$$

where $E_1 \dots E_n$ refer to the energy of each path. $e_{n1} \dots e_{nm}$ refer to each fiber energy value.

Taking use of iterative conditions model (ICM) for the energy optimization, it is easy to get the maximum energy trajectory, which can access to a fiber path.

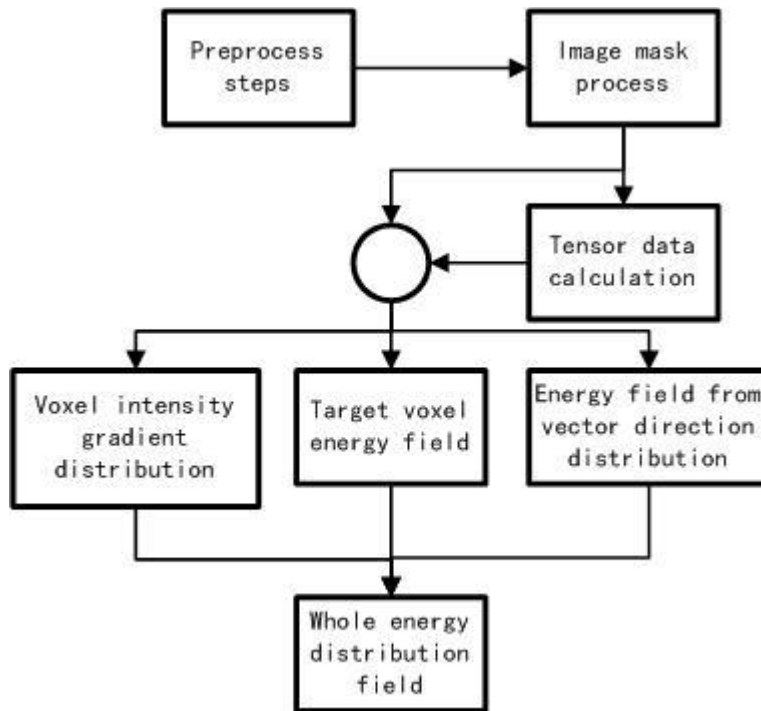


Fig.4-5 Construct Energy Distribution Field and Tensor Data Calculation

Of course reference to the criteria of determining the path, the threshold is also important, such as FA, RA. We calculate the initial vector field, tensor field etc. The image masks are to select the appropriate and the region of interest (ROI) of heart. We apply the angle constraints for the fiber tracking and improve the rationality of fiber tracks to get rid of the unreasonable excessive angle of fiber trajectories. The flow of maximum energy tracking algorithm is as shown in Fig.4-6.

2) Comparative analysis and process of common track algorithms

The steps of traditional tracking algorithm (traditional PDD tracking algorithm)(Fig.4-7) are written as follows:

Reference to the maximum energy tracking algorithm steps, we do the comparison directly from the pre-processing algorithm steps. After receiving the pre-processing image data, the tensor data field is calculated. We do not have to do anything with the tensor field data. In accordance with section 4.3.2, tensor data processing algorithms are classified.

In the post-classification tensor field, the parameters FA, MD, RA are treated as the threshold, and then do the threshold statistics, the tensor field filtering pre-processing, to get the tensor data.

For the received tensor data, we do the eigen decomposition for tensor data matrix to get the eigenvalues and corresponding eigenvectors. Then the largest eigenvector is stored, as the direction distribution of points to track the fiber trajectory.

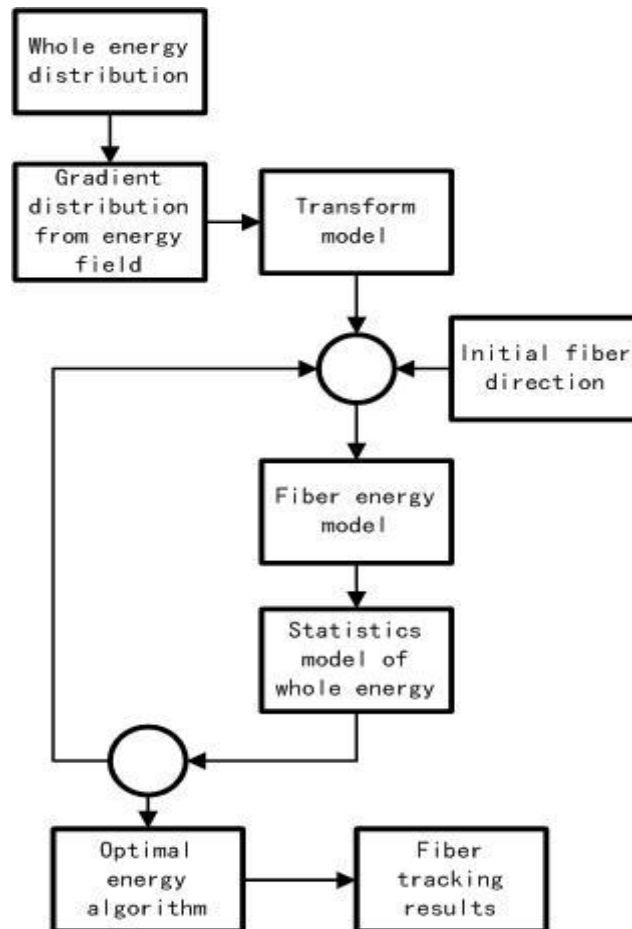


Fig.4-6 Flow Chart of Maximum Energy Tracking Approach

The traditional methods or improved streamline methods are used to gradually track the final trajectory. The fiber angle threshold, the maximum and minimum length of fibers, the largest number of fiber etc. are defined at the beginning.

From the above steps, the maximum energy tracking algorithm takes into account not only the traditional tensor of the distribution of data statistics, but also consider the original image information in DWI cases. This method compared to traditional tracking methods, not only increases the optimization functions, but also improve the global statistical information. Meanwhile, the new algorithm is also pioneering at building a impact bridge between DWI images and the direction field. The difference of these algorithms can be well interpreted with the results comparison.

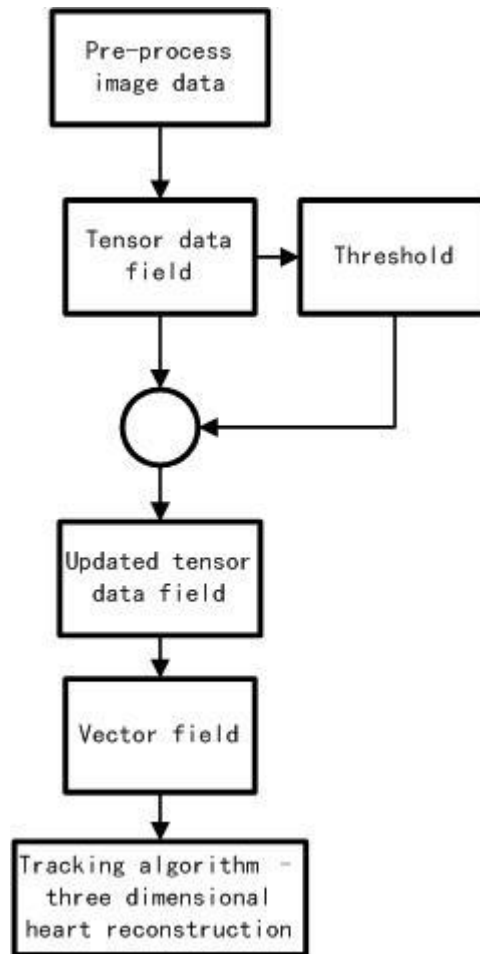


Fig.4-7 Flow Chart of Traditional Tracking Approach

2. Experiment environment and the criteria of results

In order to compare with the common DT-MRI fiber tracking methods, the same set of experimental data is used in the experiment, the same initial points set, as well as the same thresholds are listed as follows.

Experimental data:

Acquisition parameters: TE = 98 ms, TR = 8600 ms, FOV = 256×256 mm², slice thickness = 2 mm, slice spacing = 2 mm, slice duration = 142.5 ms, number of slices = 52, slice size = 128×128×1, diffusion sensitivity b = 1000 s/mm², gradient directions = 12 and 30, the time of average is 4. Heart samples =2.

Threshold parameters:

FA = 0.06, background threshold = 200, the minimum fiber length = 10, the maximum fiber length = 1000, RA = 0.01, the cosine value of largest fiber angle = 0.5, the maximum number of fibers = 8000;

Experimental algorithm categories: Experiment I uses the most energy tracking method; Experiment II considers the improved streamline method; Experiment III takes use of the traditional streamline method.

(1) Evaluation criteria of fiber tracts

Giving the different parameters as criterions (such as FA etc.), the fiber tracts are always treated as tradeoff. Till now, there are no golden criteria for determining the exact structure of human heart fibers. However, a measure to detect the whole fiber length in different regions is necessary and this is given by

$$\eta = \text{Vol}(\sum_{i=1..n} L_i) , \quad (4-30)$$

where η is the length of the fibers in the region, Vol is the current region and L represents the length of individual fiber.

Due to the previous study of the cardiac structures, the special helix fiber structures play an important role. Therefore, detailed information about the fibers shape of the human heart is an interesting and necessary observed part. Two different types of the fiber tracts smoothness are proposed and applied to summarize the globe attribute and the local attribute of the individual fiber in different regions. These two smoothness types S_1, S_2 are given as:

Smoothness Type I:

$$S_1 = \sum_{k=1..m} \text{vol}(\sum_{i=2..n} v_i \cdot v_i) \quad (4-31)$$

Smoothness Type II:

$$S_2 = \sum_{k=1..m} \text{Vol}(\sum_{\substack{i=1..n-1 \\ j=2..n}} v_i \cdot v_j) . \quad (4-32)$$

In Smoothness type I, fiber angle vector of the first point is stored as a persistent role which can determine one whole fiber tract growing attribute. From the study of the different tracts, the tracts can keep in a constrained angle bound as in traditional fiber tracking approach, a fiber angle threshold is supposed to remove the sharp vector movement of the nearby two points. However, after certain number of steps, the tracts may be far away from the original vector direction. It appears different features i.e. walks straight, turn round, or even walks back to the region around the seed point. Smoothness type II represents the sum of those nearby vector direction values along one fiber.

However, only considering the threshold value may neglect the whole tract attribute. Thus, smoothness type I can help to understand much more about the attributes of the fibers. By the way, in the cardiac tracts, different tract lines are always walking in a circle round way or the straight way. Therefore, only considering the length of the fibers in different regions, it is not enough to get the information to determine the straight forwarding tracts or the circling round tracts. Smoothness type I can distinguish this fiber feature in an easy way. If there are more circling round fibers in the region, the S_1 value is small. If there are more straight forward fibers in the region, the S_1 value is big. Given the information above, we can quantitatively describe the fiber structure from these criterion parameters and qualitatively display the fibers in the three dimensional visual view.

3. Experiment results and analysis

Before showing the human fiber tracking results, we take one heart data for example and compare the behavior of the energy field and investigate how the energy field behaves in the heart images. Then we analyze its relation to the uncertainties of fiber orientation and examine the fibers length distribution. Two different smoothness values are applied and quantitatively analysis of the results between the maximum approach and streamline approach

are also discussed. Finally, we pay attention to show the examples of the human heart fiber tracts from three different approaches including maximum energy method, traditional streamline method, and advanced streamline method.

(1) Energy field

We begin with showing the energy field values in Fig.4-8 and Fig.4-9 which is calculated from the original DTI images. In Fig.4-8, the energy values are picked from the 10th slice and the lateral plane view of the energy values in Fig.4-9 are selected when y-axis of the image is 63. The results display different color of the final energy values and all points are picked from the seed points. Thus, we can have a compact view of the values. A small part of the values in the images display special higher values, some of them are lower, and the main parts of the energy value are between 150~330.

Energy Value -- Top view of the heart images

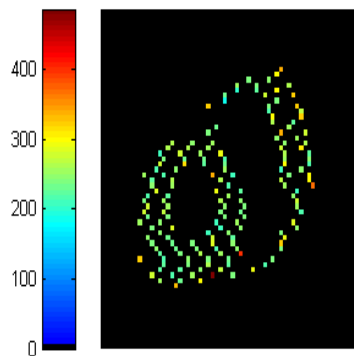


Fig.4-8 Energy Value of heart images (Top view)

Energy Value -- Lateral view of the heart images

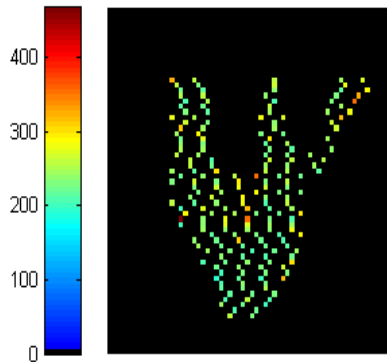


Fig.4-9 Energy Value of heart images (Lateral view)

However, the energy values show the inner difference among the points of the images, the coherence calculated from this field can be applied to reinforce the certainties of the fiber orientation. Thus, the energy diversity and its values located in the current regions can be supposed to improve the ability of finding the best path of heart fibers which presents the water molecule movement.

(2) Fiber Length and Smoothness

In our experiments, the number of slices is 52 and one slice image size is 128×128 . We use the Fractional anisotropy (FA) as one criterion, set the maximum length of the fibers, exclude the short fibers, and define the same max angle threshold between the nearest two fibers. In energy maximum fiber tracking approach, α is set as 0.5. Then we individually calculate the fiber tracking results in streamline fiber tracking approach and the energy

maximum fiber tracking approach. Both approaches deal with the same imaging data and the same seed points.

Under the predefined above conditions, the length rates are estimated to see the whole tracking fibers distribution in the human heart. Then, two fiber smoothness types are calculated to see the detailed fiber shapes. Finally, the whole three dimensional fiber tracking results of the human heart are observed and compared in two approaches.

At the beginning, 52 slices are divided to be 13 regions (4 slices in one region). The fiber length rates η in different regions are calculated. Then we compare the results from two approaches and compare the normalized lengths to see the fiber distribution varieties in different regions. Fig.4-10 and Fig.4-11 show the results. From the results of the fiber lengths of different slice region, every fiber length of maximum energy approach is longer than the streamline approach. However, the trend of the distribution of the normalized fiber length is almost the same, which guarantee the fiber occupation in the dimension and keep the whole structure of the heart without deformation. By the way, from the results, the fiber length is gradually increased from the apex to middle of the heart, and then decrease after the 6th region. However, the maximum energy approach can always keep the steps and length variety trend. It can show much more robustness in finding the tracts that can not be tracked by the streamline approach due to the uncertainties which are caused by artifacts, noise or low SNR images.

The study of the heart fiber structure is more interested in the whole structure and the detailed fiber shapes information of every volume is also necessary for understanding the confidence of the fibers in the human heart. As in the previous studies, the streamline approaches always give an impression of false certainty. Thus, two smoothness types are compared to see more about the fibers and give the proof of the certainties for two approaches. In Fig.4-12 and Fig.4-14, the value results of smoothness type are following the same trend as the fiber length distribution. So compared with the streamline approach, we can see that the fibers of the maximum energy approach are mainly straight parts which are similar to the primary fiber vector direction instead of the circle round fibers. In Fig.4-13 and Fig.4-15, the normalized values are almost the same so we can know that the fibers are gradually changing which can keep the same whole shape as the streamline fiber results.

(3) Fiber tracking

The three dimensional result comparisons are displayed in Fig.4-16~Fig.4-19. Fig.4-16~Fig.4-18 shows the experimental results from one heart. Fig.4-19 shows the results from another heart. The fiber tracts are displayed in top view and the lateral view. The color of the fibers is according to the fiber angles (Fig.4-19) or anisotropy values (Fig.4-16~Fig.4-18). All the approaches can keep the similar heart fiber tracts shape. However, the traditional streamline method shows a poor result as many fibers are lost. The advanced streamline method improves the tracking results and can locate more fibers. The maximum energy approach shows the best results that it can find out the most tracts which are neglected by the streamline approach and discard the erroneous fiber tracts compared to the advanced streamline method (i.e. the erroneous fiber pointed out by the black arrow in Fig.4-19. panel (2)). These results correspond with the previous statistical results. From the final results, we can see that the previous streamline fiber tracking approach is more sensitive to the disturbance of the diffusion tensor imaging data, because the fibers are easily hampered in many low SNR (Signal to Noise Ratio) parts and may cause some wrong fiber tracts as the uncertainties existed in the calculations. The number of the fibers in the previous fiber tracking approach is lower than the new energy maximum approach. Under the same preconditions, in the streamline fiber tracking approach, we can see the fibers are much shorter than the fibers in energy maximum approach. The energy maximum approach is much smoother, lower confusion and can provide much more confidence for finding the fiber tracts compared with the streamline fiber tracking approach.

In the heart studies, we are always interesting in the whole shape of the heart. Here, the quantificational criterions are proposed for the statistics of the heart fibers. The final stat.

results take the whole heart fibers tracking for examples and the maximum energy approach shows higher abilities in tracking the humane heart fibers than streamline approach. First, the fiber length in each region is longer in the novel approach. The fiber tracking in the streamline approach is always blocked by some disorganized principle vector areas which may be caused by noise, image artifacts or other uncertainties factors. Although some interpolated approaches are adopted, the disorder principle vector areas still existed and the fibers are stopped. Though some denoise approaches can be adopted to improve the homogeneity of the principle vector, the uncertainties still happens as the shortcoming of the streamline approach which is only based on the principle vector. The ambiguity of the fiber direction caused by the partial volume effect can also produce the error short tracking path but the globe constraint can decrease the possibility and keep the largest tracking probability. Subsequently, two novel smoothness types are compared. These results can tell us the shape of the heart and the varieties trend of the fibers pathways in different region. From the previous results, we can see that two smoothness types of the maximum energy approach are higher. These show that the fibers are longer and the fiber direction of the new method is always following the fiber direction in each beginning seed point which is blocked in the fiber tracking progress of the streamline approach. However, all the normalized results of the fiber length and two smoothness types can prove that the fibers in each algorithm can keep the similar varieties trend. Hence, the shape results of two whole heart fiber tracking approaches are really similar and the final three dimension visualization of the humane heart prove them. From the final three dimension results, we can also easily see that some true fibers are present in the new approach which can not be displayed in the streamline approach and some erroneous fibers in the left ventricle from the streamline approach are absent in the maximum energy approach. These confirm the previous statistic results and testify the certainties improved by the maximum energy approach to noise and partial volume effects.

Therefore, in this new approach, we can not only get the relationship from the tensor field but also the imaging data and this maximum energy approach is a globe tracking optimization method to locate the proper paths which are reliable and robust in finding the final tracts from the original DT-MRI images. However, this maximum energy method in describing the energy field, the expression of updating the fiber direction and the whole energy math equation may be imperfect to describe all complex system. From the results compared in Smoothness Type I, a weakness of this new approach can be found that the novel fiber tracking trends to have a “straightening fiber effect”, i.e., a bias toward straight fibers. The tensor operator in Equation (3-16) may deflect this gradient energy vector towards the major eigenvector direction, which limits the curvature of the deflection. The first part in Equation (3-16) may decrease this effect but not enough. Meanwhile, this weakness also exists in the traditional PDD tracking methods and the probabilistic or stochastic approaches. Refer to [Lu 2006], this weakness can be decreased as the smaller step size (and higher imaging spatial resolution). Though the better tract sensitivity is gained as the smaller step size, the power against the effect of uncertainties will be decreased. So the trade-off between robustness to uncertainties and tract sensitivity is appeared. So there comes the further research and also more work should be done to improve this idea of locating the fiber paths to be a much more efficient and reliable way. The calculation speed of the maximum energy approach in locating the whole heart fibers is lower than the streamline approach. In our experiments, the maximum energy approach takes 20 minutes and the streamline approach takes 4 minutes. However, it is still can be received. By the way, the time costs of the Bayesian approach or stochastic tracking approaches are much higher so they are proper and suitable for locating the fiber connection between two points as the less calculation of the fibers. The two fiber tracking approaches and its visualization are programmed by the C++ with the ITK and VTK toolkits and the fiber tracts results are analyzed and calculated under the Matlab.

Therefore, we can know that the energy maximum approach is more robust and become much more available to obtain the final fibers.

Above all, in the study of heart myocardium path tracking, the path distribution can be accessed by the adoption of qualitative and quantitative approach based on various means.

Experimental proof of the qualitative or quantitative algorithm of human heart is to describe a certain degree of regularity of the heart muscle.

Meanwhile, comparison of the experiment results of these algorithms, we can see the fiber tracking results in the non-stable direction field, which can also be thought as a very good 'real simulation scene' for the return process of underwater robots' experiment. DT-MRI images of the myocardium can prove these characteristics due to the similar random disturbance environment. In the section 4.5, the reference value of the cardiac path tracking technology of DT-MRI images for the underwater robot tracking algorithm will be discussed.

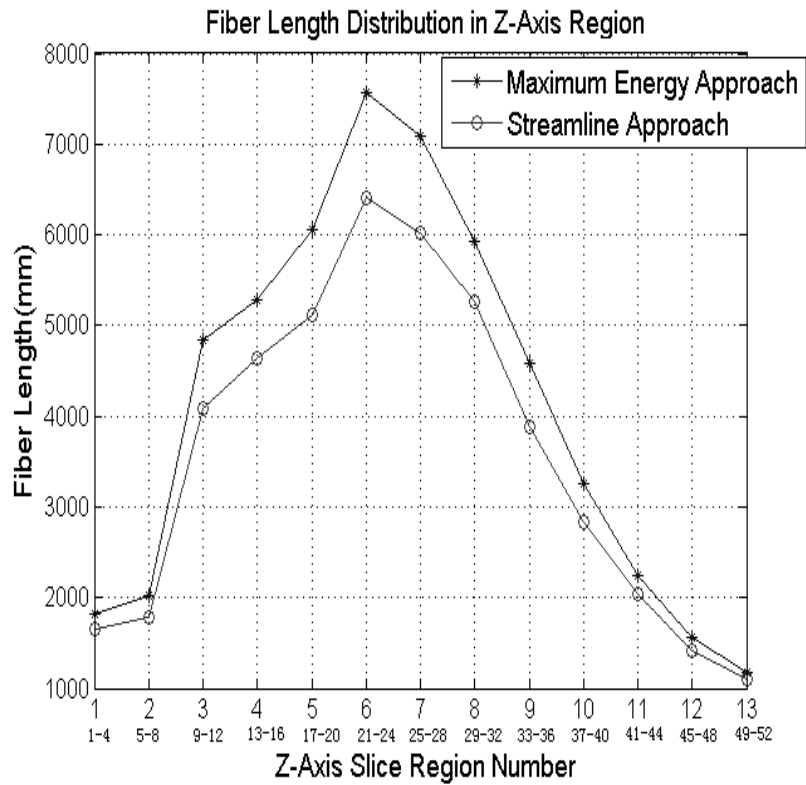


Fig.4-10 Fiber Length Distribution in Z-Axis Region

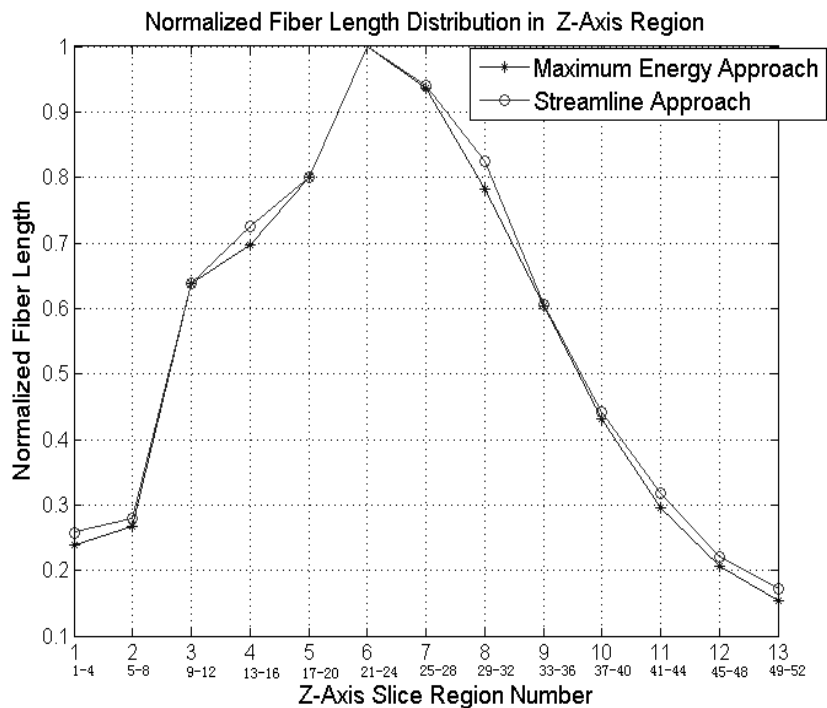


Fig.4-11 Normalized Fiber Length Distribution in Z-Axis Region

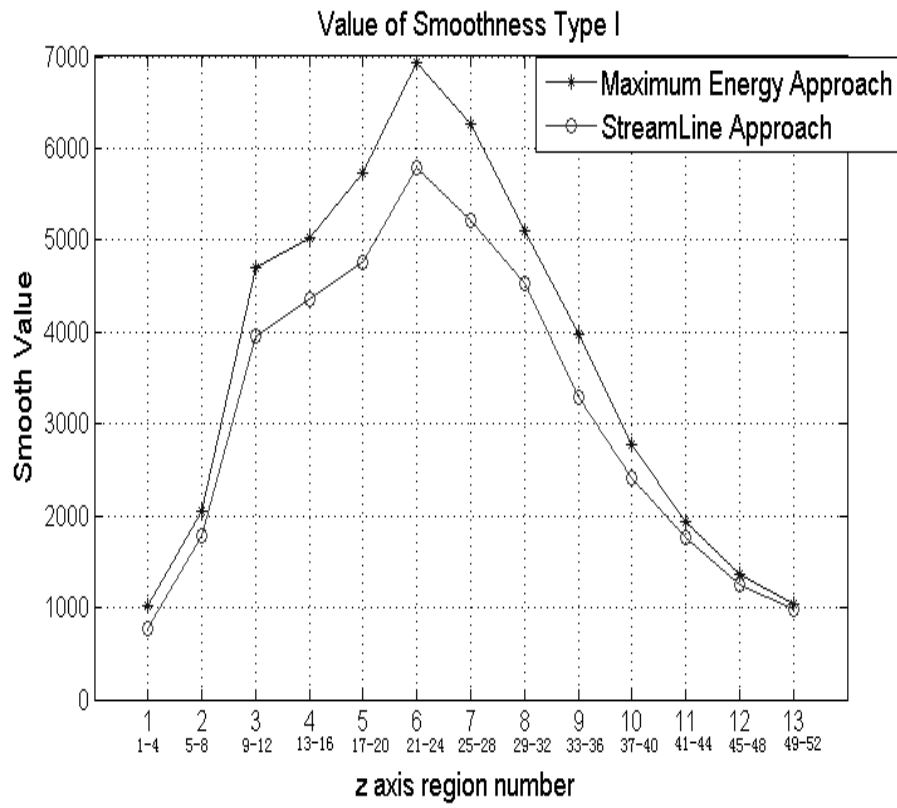


Fig.4-12 Value of Smoothness Type

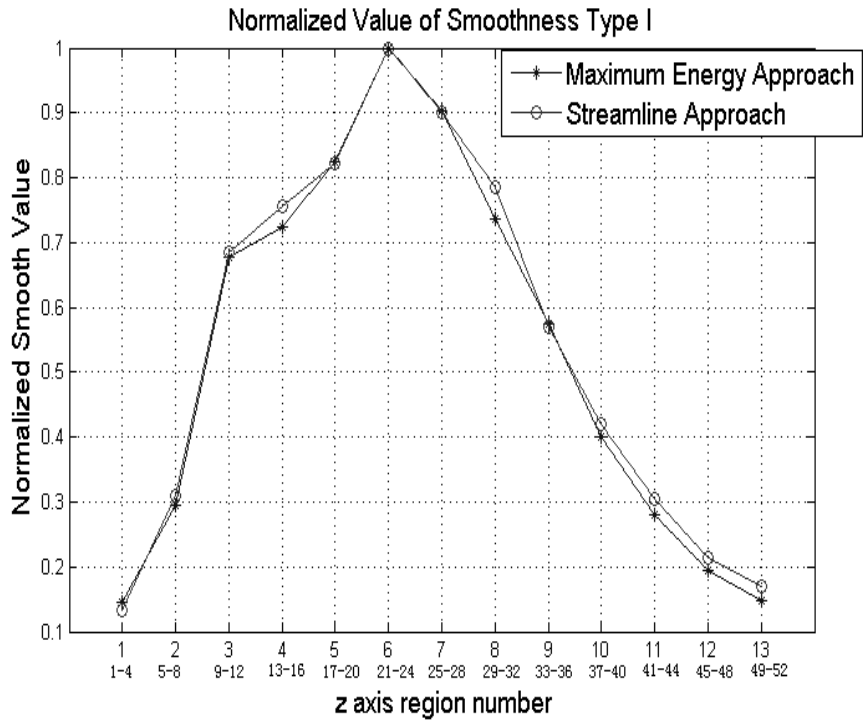


Fig.4-13 Normalized Value of Smoothness Type I

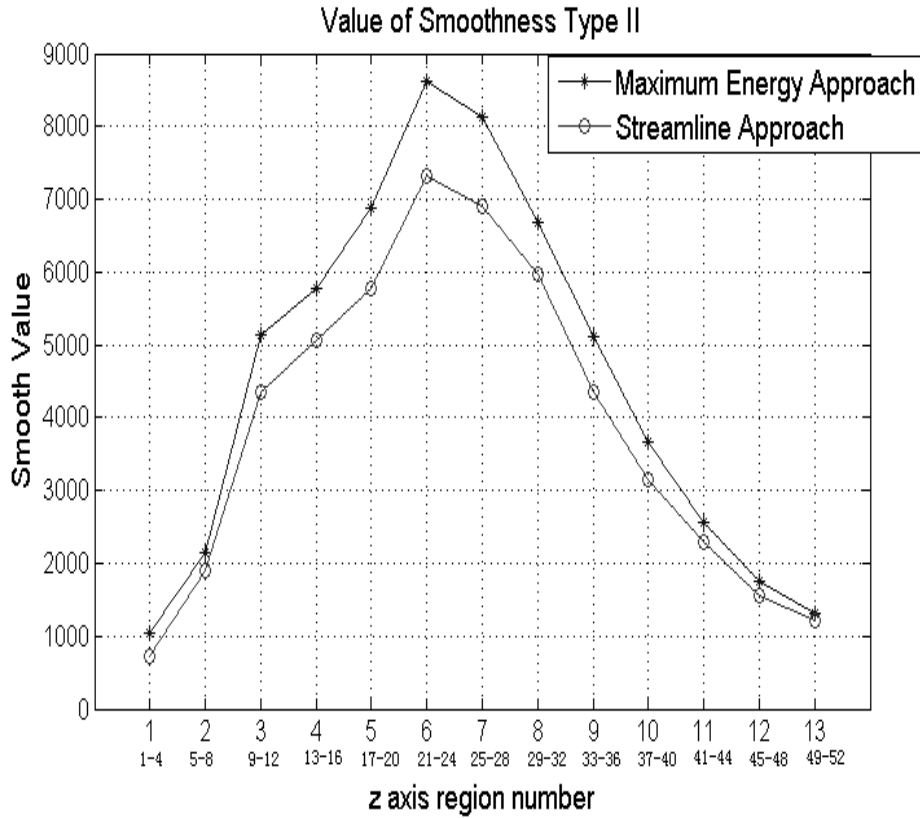


Fig.4-14 Value of Smoothness Type II

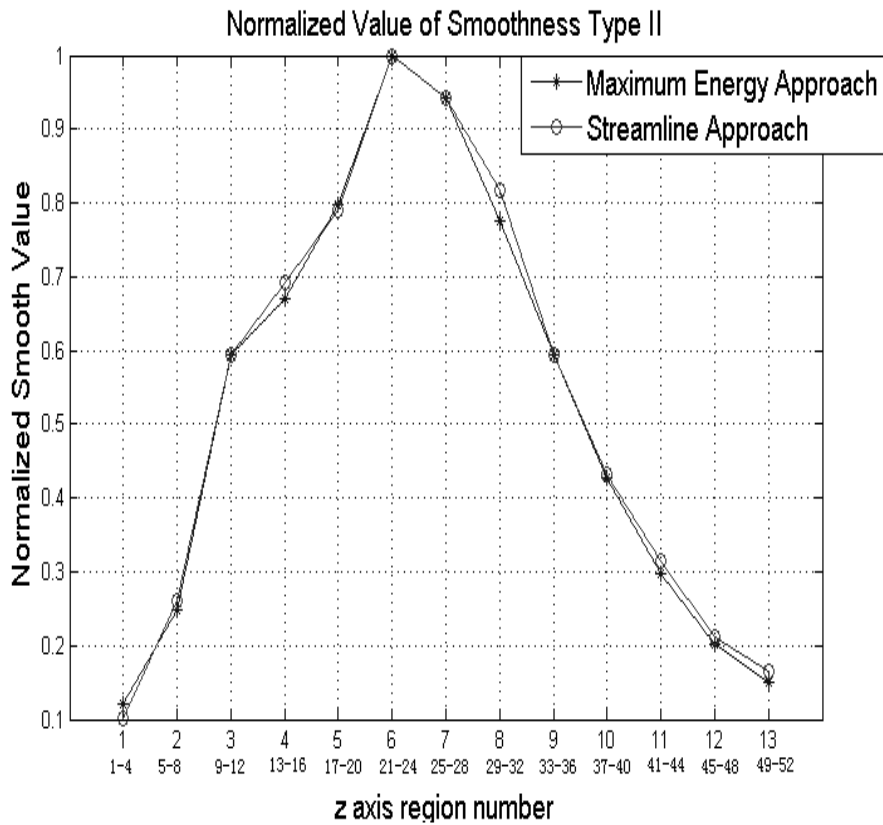
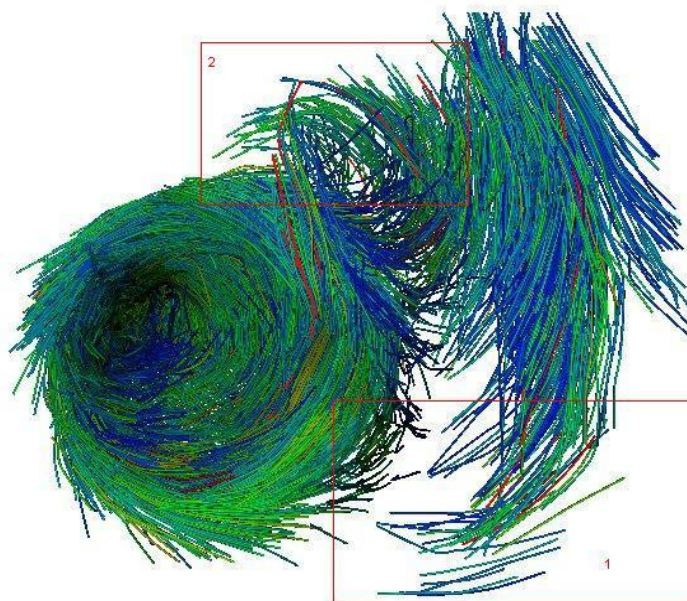
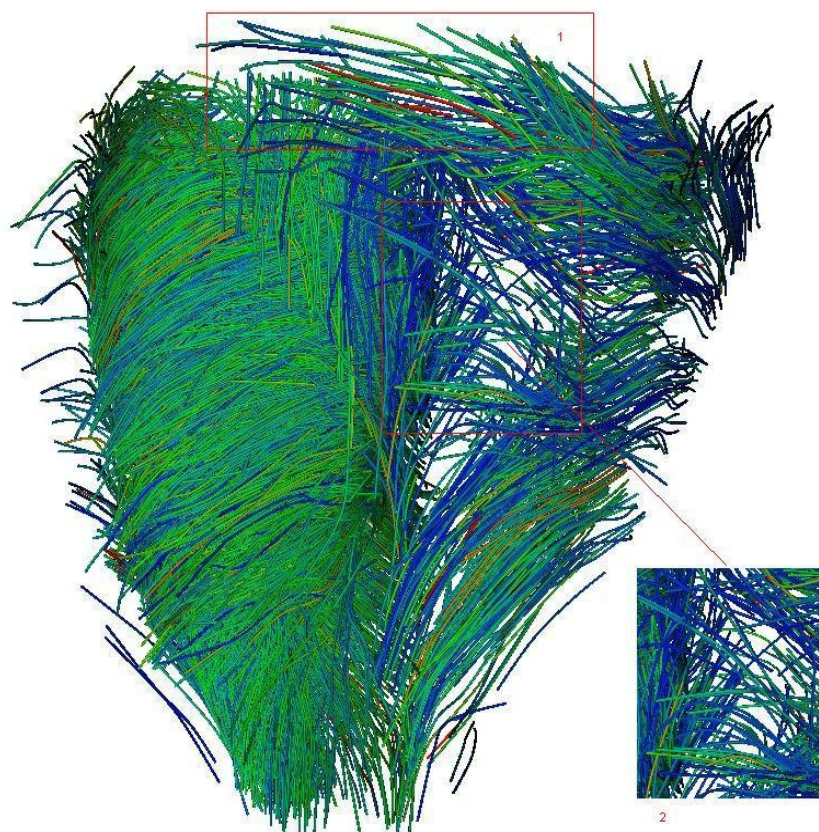


Fig.4-15 Normalized Value of Smoothness Type II

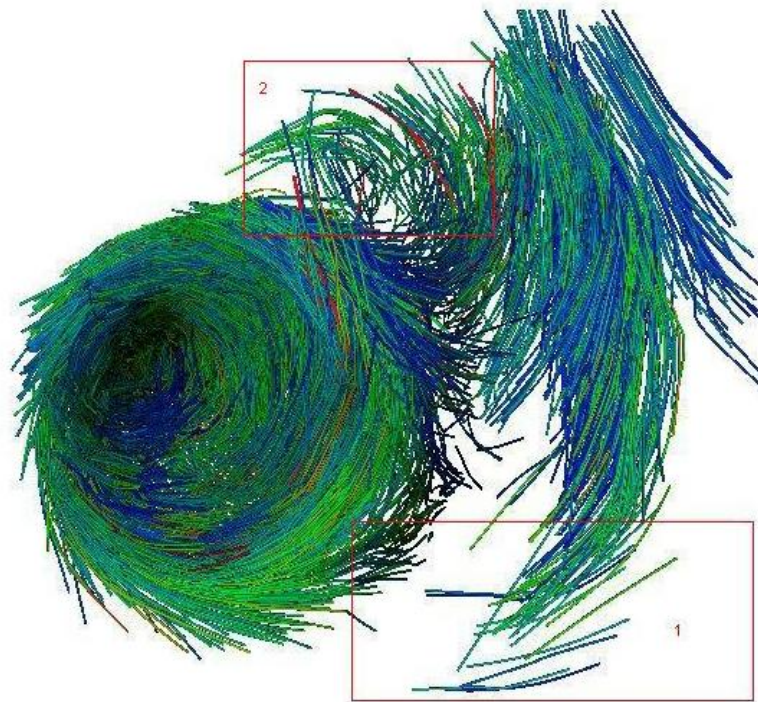


(1) The top view result of the Maximum Energy Tracking Approach

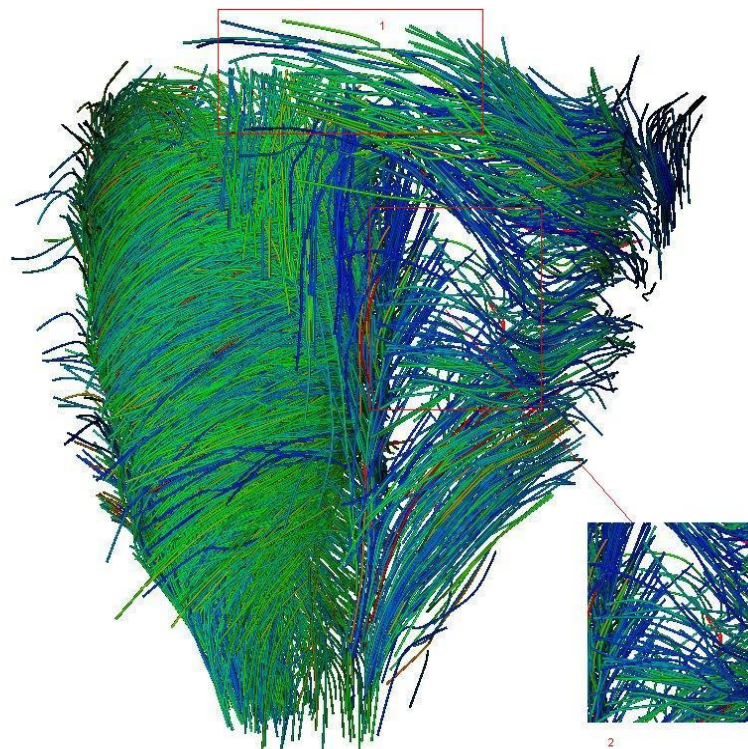


(2) The lateral view result of the Maximum Energy Tracking Approach

Fig.4-16 Fiber tracking result of the Maximum Energy Tracking Approach

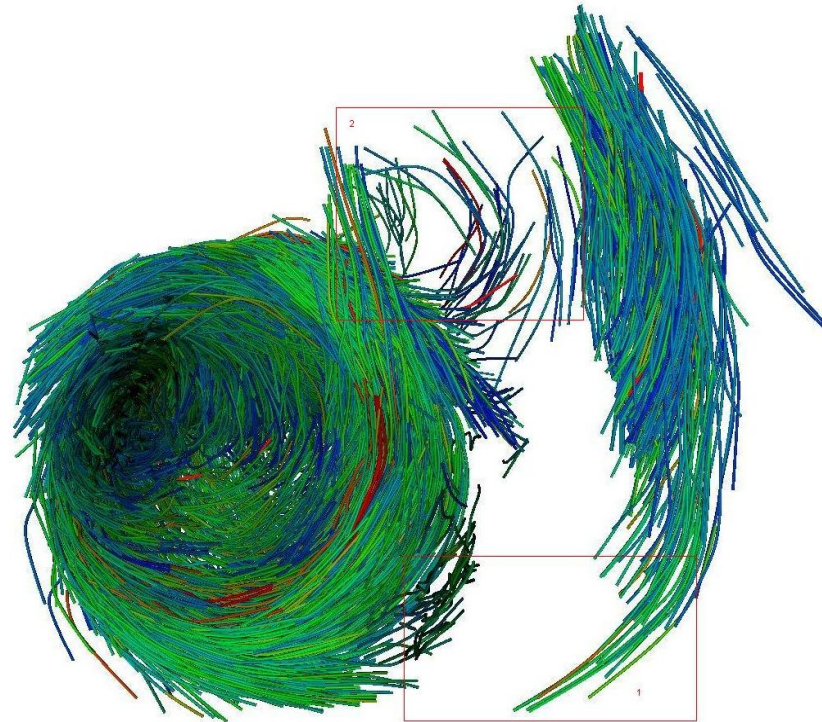


(1) The top view result of the advanced Streamline Approach

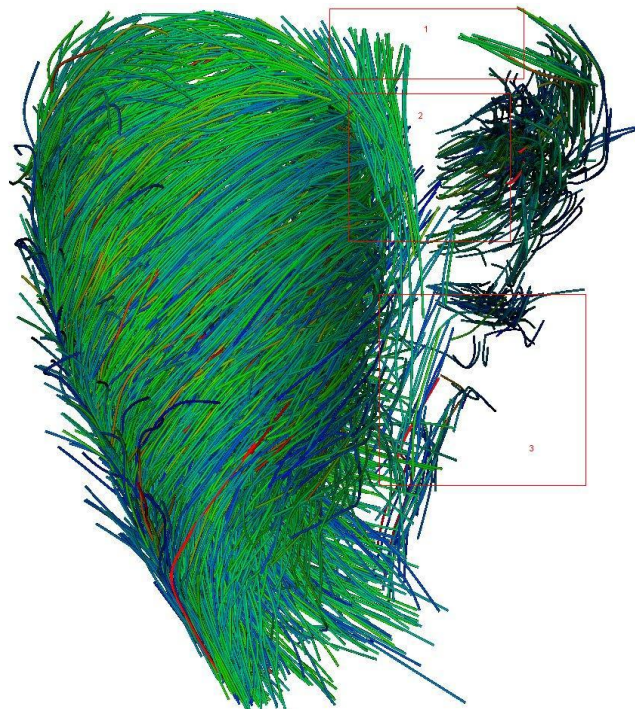


(2) The lateral view result of the advanced Streamline Approach

Fig.4-17 Fiber tracking result of the advanced Streamline Approach



(1) The top view result of the traditional Streamline Approach



(2) The top view result of the traditional Streamline Approach

Fig.4-18 Fiber tracking result of the traditional Streamline Approach

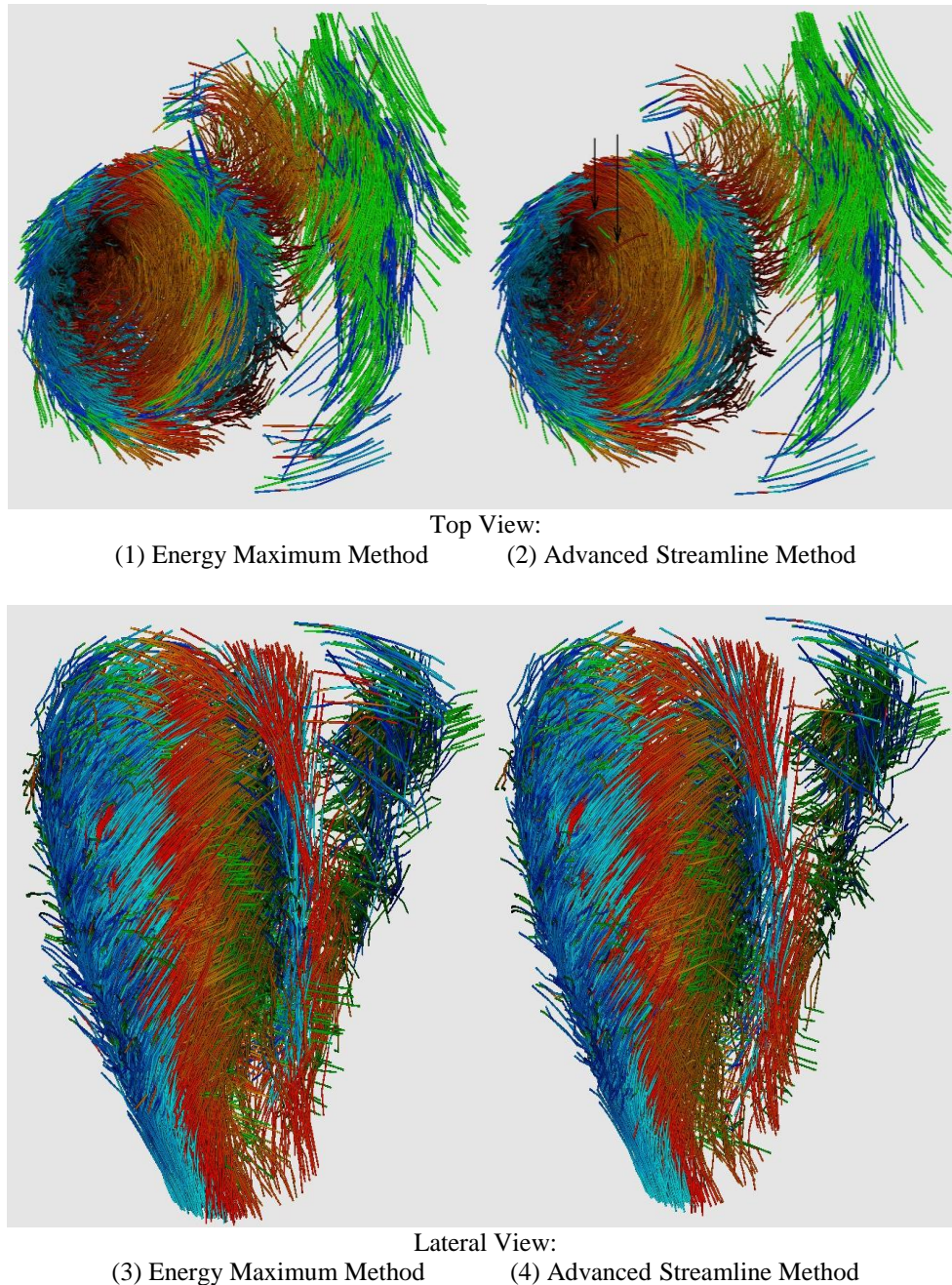


Fig.4-19 Fiber tracking results comparison (The left two images are calculated by energy maximum method, the right two images are calculated by advanced streamline method)

4.4. Myocardial fiber structures study and the parameters

In this section, fiber orientation and structure of muscle fibers are recovered and compared in the entire heart by fiber reconstruction method. Although there is intensive research on DTI visualization in the last few years, the accumulated uncertainties during the DTI fiber tracking pipeline are paid little attention so far, especially for the study of myocardial fiber. However, fiber tracking is sensitive to a number of parameters since they are playing a role of stopping criteria. A small change in the threshold values can lead to different output results. Little effort has however been reported in the literature on the evaluation of the stability of these

parameters or the effect of variations of the parameter that are used in fiber tracking, such as the length or the number of fibers. The results obtained from fiber tracking can remain ambiguous and it is not always easy to evaluate the tracking results quantitatively. To clarify the quantitative features of fiber tracking, it is important to compare the fiber features as a function of anisotropy threshold and elucidate how the corresponding feature is sensitive to threshold variations.

The goal of this section is to study different parameters involved in fiber tracking such as fractional anisotropy, medium anisotropy and related anisotropy, and the myocardial fiber pathway distribution in the human heart. To this end, different results from DTI fiber tracking are compared in a systematic and detailed manner, the uncertainties of the parameters involved in fiber tracking are analyzed, and the effect of parameter variation on the group studies is investigated.

Fiber tracking results are assessed in terms of the length and the number of fibers, which are studied as a function of different predefined parameters: FA, RA, MD, c_l , c_p , c_s . These results are shown in Table 4.1 and Table 4.2, where the different predefined parameters were chosen close the average value of the whole heart from 0.01~0.1. The results show that the trends of the length and the number of fibers are almost the same. They are gradually reduced when the parameter values are growing up. However, MD parameter value has more impacts on the fiber characters. The length and the number of fibers decrease largely when small changes occur in MD values. This implies that the parameter MD might not be suitable for this heart data in the experiment. The results in Table 4.1 and Table 4.2 also show that the uncertainties are caused by the sensitivity of the parameters values. To further get insight into the variation of fibers, fiber length is computed in different regions along the apex-base axis. The 52 slices of the DTI volume are divided into 13 regions. Each region contains 4 slices. The normalized fiber length and the normalized number of fibers can then be readily calculated. Fig. 4-20 illustrates the normalized fiber length, when FA is chosen as the parameter criterion.

Table 4.1 Variation of Fiber Lengths as a function of FA, RA, MD, c_l , c_p , c_s

FA Value	0.03	0.05	0.08	0.1
Length (mm)	264252.145010	223668.982510z29	179382.713809	160116.126987
MD Value	0.02	0.03	0.05	0.1
Length (mm)	279471.175495	179905.299050	20987.390893	2347.654231
RA Value	0.02	0.04	0.07	0.08
Length (mm)	251426.048660	193265.675171	142116.812962	127652.944840
c_l	0.01	0.03	0.05	0.07
Length (mm)	271138.354998	198141.956204	152582.075771	120451.344736
c_p	0.02	0.04	0.07	0.08
Length (mm)	199698.841659	123112.651196	70529.553612	61134.299298
c_s	0.06	0.07	0.08	0.09
Length (mm)	219083.930078	204364.515884	190234.519200	179748.078662

From Fig.4-20, it is seen that the maximum fiber length is found in the region 6. The fiber length is increasing in the regions 1~6. After the region 6, it gradually reduces.

Through these results, the change of different parameter values can be located. This may provide a reasonable way to verify the feasibility of choosing appropriate parameter values. In the future work, more information needs to be compared, such as the uncertainties of the myocardial helix angle, the distribution of fibers in different ranges of helix angles, etc.

Due to the complex interrelation between myocardial fiber direction and the propagation of electrical activity, it is rather difficult to completely describe the mechanical properties of the whole cardiac structure. To deal with this problem, during fiber tracking, we investigate in an individual manner the fibers of different regions and choose in an adaptive manner the values of anisotropy. Based on the studies of DTI fiber tracking results, we propose an effective procedure to estimate the appropriate anisotropy value, which consists of averaging the corresponding values of the all the myocardial parts of interest. Then, the averaged value is used as the initial threshold value. To verify and update this value, an error bound - 0.01~0.01 is calculated. The tracking results are compared by the number of fibers. If the number of fibers varies within relatively small error bound, this anisotropy value is considered to be a appropriate threshold value. In the present study, this anisotropy value is taken as fractional anisotropy (FA). It is known that lower FA can bring more fibers, but these fibers might be caused by noise or artifacts. Therefore, there is a tradeoff between the FA and noise. In this experiment, after the averaging and updating steps, the estimated fractional anisotropy value is 0.06.

Table 4.2 Variation of the Number of Fibers as a function of
FA, RA, MD, c_l , c_p , c_s .

FA Value	0.03	0.05	0.08	0.1
Number	7698	6722	5835	5412
MD Value	0.02	0.03	0.05	0.1
Number	8489	7315	2181	294
RA Value	0.02	0.04	0.07	0.08
Number	7402	6099	4976	4635
c_l	0.01	0.03	0.05	0.07
Number	8014	6355	5411	4682
c_p	0.02	0.04	0.07	0.08
Number	7136	5566	4211	3852
c_s	0.06	0.07	0.08	0.09
Number	6788	6516	6272	6061

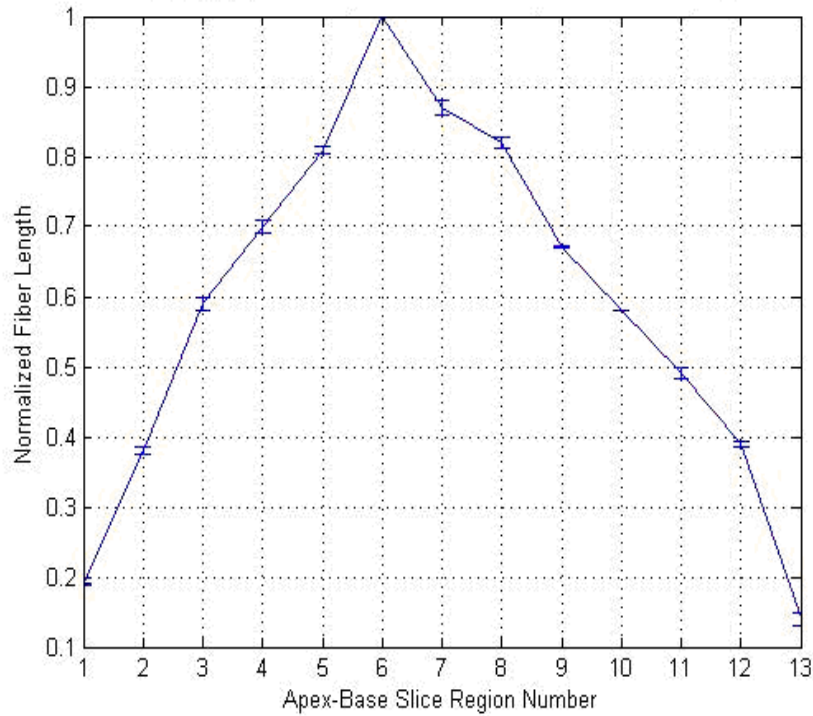


Fig.4-20 Normalized fiber length distribution along the apex-base axis.

The fiber length of individual cardiac muscle is known to play a key factor in characterizing the mechanical properties of a single cardiac muscle, such as the maximum tension created from the muscle. There always exists a close inherence factor between fiber structure and electromechanical activation. To describe the fiber length distribution, we categorize every 4 slices as a region along the apex-base axis. Therefore, the whole region number is 13, considering the number of slices. Each region is divided into $8 \times 8 \times 1$ parts along every axis. Since the whole slice size is $128 \times 128 \times 52$, the size of each part is $16 \times 16 \times 4$. Fig.4-21 shows the normalized fiber length distribution.

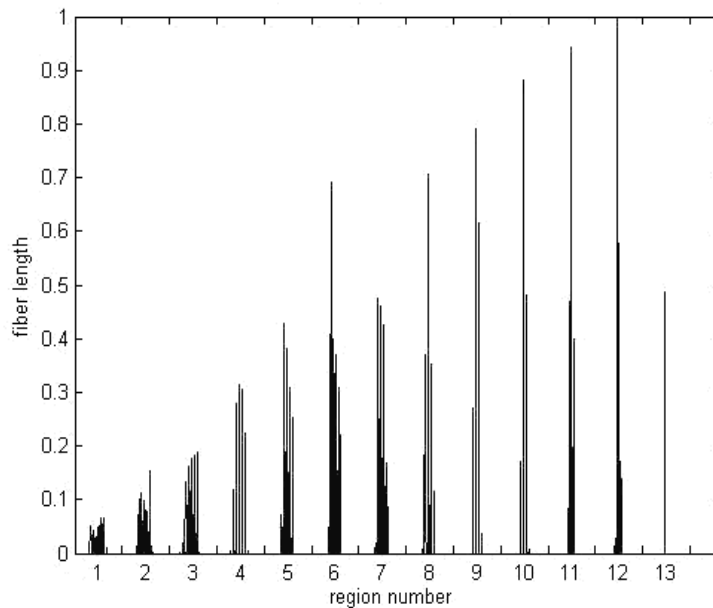


Fig.4-21 Normalized fiber length distributions

In region 1~8, the number of parts that contain fibers is larger than that in the regions 9~13. The fibers are mainly distributed in the medium myocardium, i.e. the regions from 4 to 9. The

fiber having the maximum length in the parts is located in the region 12, but the number of parts that have fibers is small. Moreover, Fig.4-22 illustrates five longest fibers in the whole cardiac muscle. We observe that these fibers consist of both circumferential fibers and longitudinal fibers.

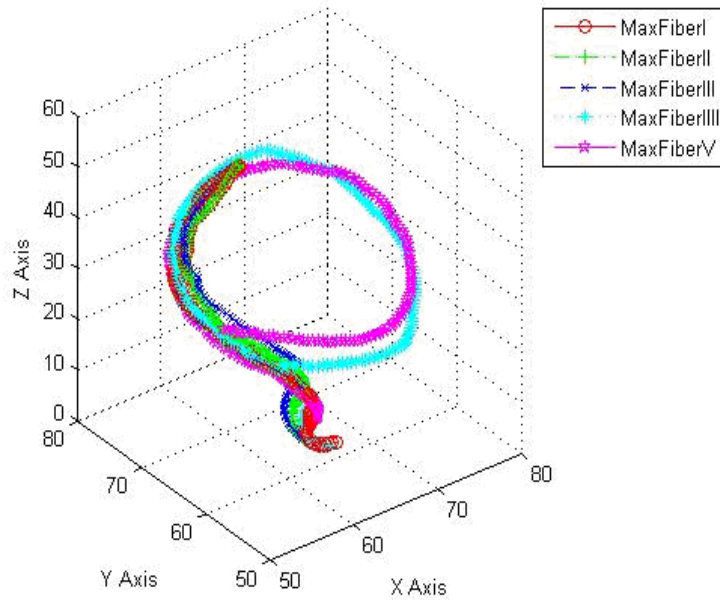
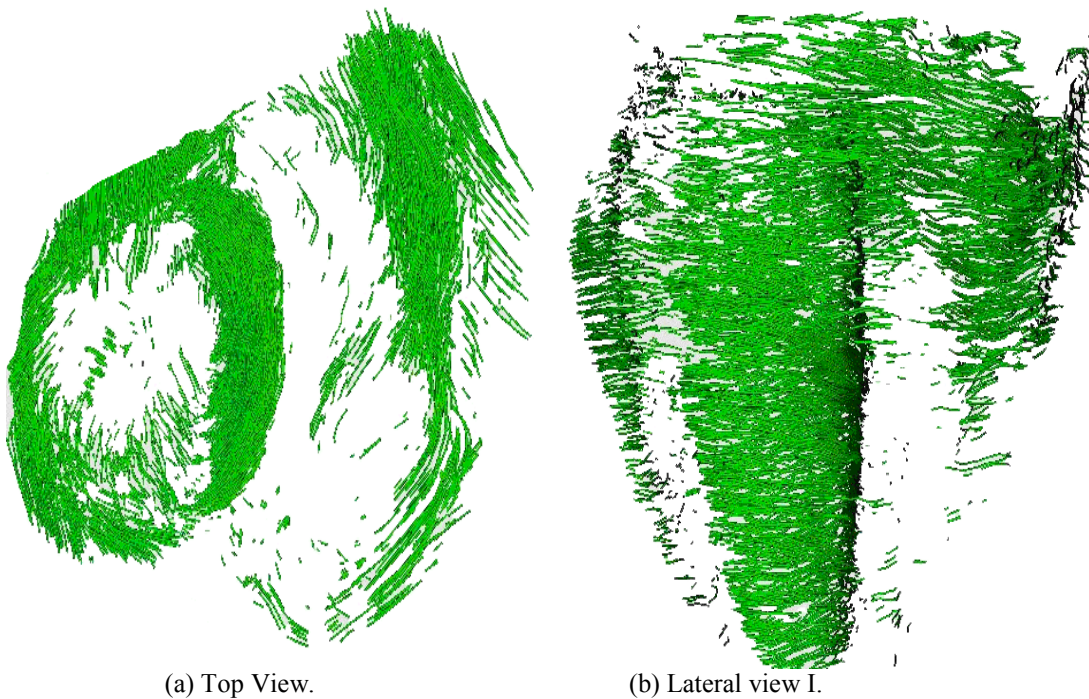
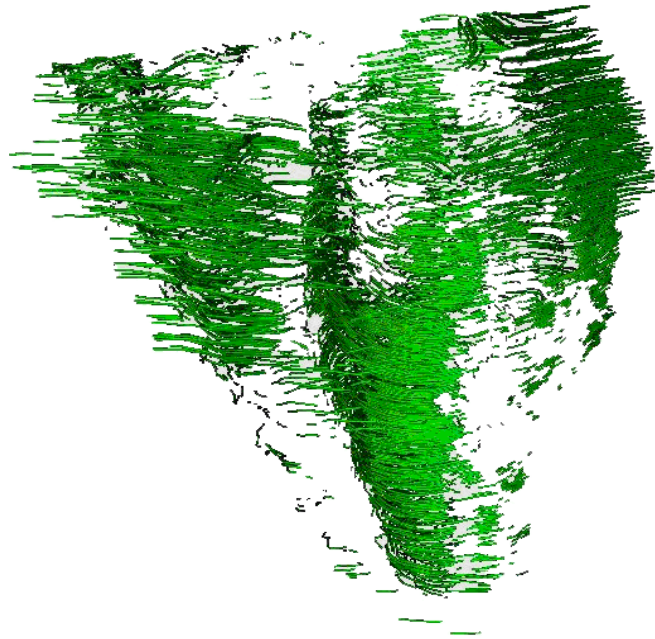


Fig.4-22 Five longest fibers of the heart.





(c) Lateral view II.

Fig.4-23 Fiber structures of helix angles between -22.50 and 22.50

The myocardial fiber orientation was defined by transforming the primary eigenvector from the Cartesian coordinates to the local cylindrical myocardial coordinates. The epicardial tangent planes are tangent to the epicardial circle and parallel to the LV apex-base axis. Fiber helix angle is defined as the angle between the projection of the primary eigenvector onto the tangent plane and the transverse plane. In order to compare the circumferential fibers and the longitudinal fibers in the myocardial structure, we use the helix angle threshold as a threshold to categorize the fiber distribution. For circumferential fibers, the angle threshold is defined as $-22.50 \sim 22.50$. For longitudinal parts, the angle threshold is defined as $67.50 \sim 900$ and $-67.50 \sim -900$. Fig.4-23 gives the circumferential fibers of the whole heart in three dimensional views. The longitudinal parts of the whole heart in three dimensional views are shown in Fig.4-24. For longitudinal fibers, the fiber color is mapped by the helix angle value; the color of circumferential fibers is green. That allows us to clearly visualize the fiber distribution of different parts. These results offer an interesting indication of the correlation with the myocardial mechanical characters of the heart, such as the circumferential strain, the longitudinal strain, the contraction, the consumption of the cardiac wall, etc.

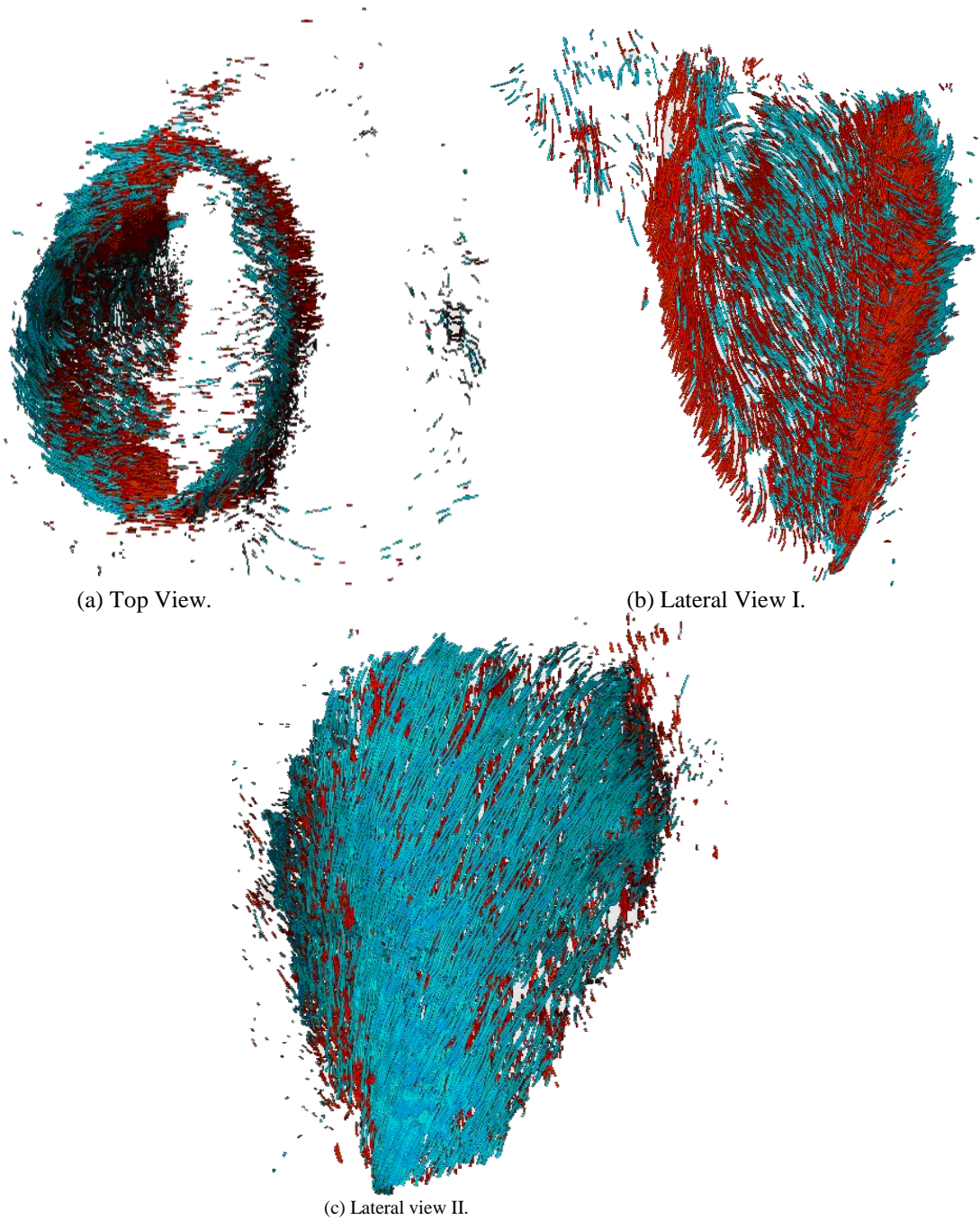


Fig.4-24 Fiber structures of helix angles between 67.5° and 90° , and between -67.5° and -90° .

4.5. Reference value of myocardial tracking algorithms to the underwater robot path tracking methods

The human heart tracking application of the DT-MRI images in this chapter is to highlight the advantages of underwater robots in the choice of the return path tracking algorithm in the chapter 5.

The main reason and the reference value are summarized as the following parts:

1. In the human myocardium tracking process, because of magnetic resonance image acquisition is in fact the records of water molecules movement in the human myocardial fibers. In relatively ideal conditions, the movement of water molecules is known to regularly follow the path of myocardial movement, and cardiac path can be perfectly acquired through the movement of water molecules that have been collected to complete

the tracking process. However, due to the limitations of magnetic resonance imaging apparatus such as the capacity of magnetic induction strength level, the uncertainty of circumstances etc., makes the water molecule movement hardly along the initial the ideal path movement and there are many unreliable factors.

In the choice of the underwater robots return path, it can found that because underwater robots in advance reach the destination, through a combination of multiple image sensors such as sonar means, they can already build the direction of movement field in a particular space with the grid technology (The grid technology will be described in detail in Chapter V). This kind of movement is similar with the human cardiac path tracking ideas as the magnetic resonance apparatus can record the initial direction of the water molecules.

However, because sonar image sensor used in devices consists of inevitable limitations of the spatial distribution of underwater objects. Due to the instability and external interference etc., the direction distribution recorded in advance of the underwater robot exploration process is obviously unreliable. However, there are also many reliable directions in the previous direction field. Therefore, in the return path tracking process, how we cannot waste of information of the known initial direction field and also take into account the path of instability in the underwater space field. There is a tradeoff to solve this problem for the final tracking algorithm.

The cardiac path tracking is a comprehensive scene of instability field for describing the underwater robots return path tracking process. In the low reliability cardiac images, it is necessary to calculate the path of the maximum probability distribution. Compared to the underwater environment of underwater robot, in the stable environment for the underwater exploration, only the streamline algorithm need to be considered for the tracking process described in the previous chapter. However, in complex multi-interference of water, sea, etc., the instability is increased by these factors. Therefore, the myocardial image tracking is equivalent to return path movement of the underwater robots. We must take into account the instability caused by the interference or limitations of devices etc.

Therefore, we need to investigate the circumstances of this complex path tracking algorithm. Myocardial tracking image will be exactly satisfied with the simulation in this area, it is the equivalent of an underwater robot of the return path field in a comprehensive 'real environment'², which is a good reflection of the simulation environment. The aim of this chapter is to introduce the knowledge of the return movements of the underwater robot and verify the importance and feasibility of this algorithm.

2. For the movement of underwater robots, the number of the reconstruction paths is relatively smaller and it is difficult to describe the differences with the interference or without the interference. Therefore, this information should be gathered and compared for the better descriptions of the differences in the use of the myocardial fiber path field. Thus, in a similar high degree of non-stability of the actual working environment, combined with the direction information field, a reasonable underwater robots return path tracking theory is similarly constructed and the proof is given to confirm the advantages of the myocardial tracking algorithm. The following chapter in detail introduce a variety of theories of the underwater robots return path algorithm and gives a more powerful and impressive experimental basis.

² The significance of "real environment" described here includes two parts. One is that DT-MRI combined with true micro-environment of water molecules appears random Brownian motion of the true probability of the experimental environment; the other is that in macro view, the possible random movements of the underwater robots in the space can be reflected in this relatively real environment. Therefore, that this cardiac experimental fiber track is a good example of the application that can be used as the reference for an underwater robot movement simulation in this 'real environment'.

4.6. Summary

This chapter not only discusses the processing steps of DT-MRI image data, but also describes how to create a tensor field and give the definition of micro-data structure of the tensor field and the concept of anisotropy, etc. Combination of a number of path tracking algorithms, the cardiac tracking application is considered. The qualitative and quantitative comparisons of the new algorithm and traditional algorithm are to find the difference. The experimental results prove that the improvements of the new algorithm.

Finally, the reference value and the significance from the application of this chapter are proposed for the underwater robot return routing algorithm. These make a reasonable basis for the theories of path tracking of underwater robot.

PARTIE III

CONCLUSION

Chapter 5 CONCLUSION AND FUTURE WORK

Summary

5.1. Review of the contribution of this research	103
5.2. Future work.....	104
5.3. Publication of the author	105

5.1. Review of the contribution of this research

(1) Super-mini underwater robot system design

To overcome the shortcomings in practical applications of previous underwater robots, we propose a new platform consists of a real time, powerful, multi-sensor feedback control software, hardware and many valuable improvement of the mechanical design. Through the experiments, the results verify the effectiveness of this new platform. It also provides a good foundation for the future work.

(2) Super-mini robot motion controller design

Due to the deficiencies existed in the previous control ideas of sliding mode controller, a new adaptive neural sliding mode controller with the balanced controller (ANNSMB) theory is proposed. We also propose to apply an adaptive fuzzy sliding mode controller (AFSMC) theory to control the motion work of underwater robot. Based on the simulation and practical experiment from the PID controller, sliding mode controller, simple fuzzy sliding mode controller, AFSMC controller and ANNSCB controller, the results are analyzed and compared. The new proposed controller ANNSMB and AFSMC can get better results. ANNSMB shows the best performance and efficiency that can reduce the chattering phenomena in the traditional sliding mode controller and decrease the unexpected views of the high static error, overshoot etc.

(3) Underwater 3D obstacle reconstruction technology research

Due to the low visibility and the non-intuitive underwater environment, the operator is very difficult to intuitively grasp the movement status of underwater robots and the distribution of space objects etc. only by the cameras. To solve these problems, we propose a new method of three-dimensional underwater environment reconstruction technique. We analyze and propose the data acquisition theory and some processing methods. The key points of data collections methods etc. have been pointed out. DT-MRI image processing algorithms and three-dimensional object reconstruction theory are proposed to be combined to realize the reconstruction of underwater objects etc.

(4) 3D path planning and its reconstruction

For the complexity of the high dimensional paths exploration, we propose a new random path tracking algorithm based on Bayesian theory. Through three-dimensional simulation of the path tracking experiments, the results demonstrate that the new algorithm is a simple, easy

implementation algorithm, and in case of unexpected obstacles, it can show strong robustness and adaptability.

The underwater robot in the choice of the return path is similar to path choice of DT-MRI images. From the comparison and analysis of the results, they are relative and can be learned from each other. We propose a method called the maximum energy path tracking algorithm theory as an active tracking algorithm. From DT-MRI experiments, it has been demonstrated the effectiveness, performance and robustness. The results of DT-MRI cardiac fiber tracking are of great importance and reference values to the tracking application of underwater robot path tracking. Based on the streamline algorithm, the maximum energy tracking algorithm, combining with the reference of cardiac fiber tracking, we propose to apply these efficient methods to solve the problems of underwater robot return path tracking.

(5) DT-MRI works

For the human cardiac DT-MRI application, we propose a new maximum energy fiber tracking algorithm to construct the fiber structure of heart. We compare this new algorithm with previous algorithms and propose several criteria to verify the effectiveness, feasibility, and performance of the new proposed method. We investigate the uncertainties existed in DT-MRI images and compare and discuss the characters of anisotropy parameters and their affects to the fiber tracking results. We propose to compare and view the fibers according to different helix angles. Finally, the inner characters of fibers' different structures and distribution demonstrate the characters of the heart mechanics.

5.2. Future work

(1) Improve the super-mini underwater robot intelligent control system to enhance its work ability in a complex environment. Using the accumulation of ROV experience, we would like to develop AUV.

(2) Underwater robot motion controller is to be carried out and improved by adding the prediction compensation function.

(3) Studying the blind spots of the image sonar. The error sources that are conducted by the deficiency of the equipment or the outside interference should be more discussed in detail.

(4) Improve the theory of underwater robot path exploration algorithm. The algorithm proposed in this paper has some shortcomings in the global optimization.

In the next step, the variation integration path algorithm and dynamic optimization idea will be proposed to make up these limitations. Improve the streamline, the maximum energy tracking method for the motion of underwater robots. Improved algorithms will be considered to adapt a wide range of possible mutation of the non-stability of interference, and enhance the reliability of algorithm. Based on the improved multi-sensor platform, we will do the experiment to test the practical ability of the path algorithm.

5.3. Publication of the author

Journal paper

- [Song 2011]Song, X., Zou Z. J.
Modeling, design and experiment of improved super-mini underwater robot[J], International Journal of Innovative computing, Information and Control, 2011, 7(3):1109-1120.
- [Song 2011]Song, X., Zou Z. J.
A design of adaptive track controller for underwater vehicle[J], ICIC Express Letters, 2011, 5(3):661-666.
- [Song 2011]Song, X., Zou Z. J.
Nonlinear underwater vehicle's controller design with adaptive disturbance prediction and smoother[J], International Journal of Control, Automation, and Systems.(Accepted, To be published)
- [Song 2007]Song, X., Ye, J. W.
Application of Sliding Mode Fuzzy Control for Submersible Vehicle[J], Shipbuilding of China, 2007, 49(1):84-89.
- [Song 2007]Song, X., Ye, J. W. and Chen, Y. M.
A new digital communication network system based on marine wireless radio[J], Ship Engineering, 2007, 29(6):18-31.
- [Song 2007]Song, X., Ye, J. W. and Wu, L. M.
Application of the integral sliding mode controller with fuzzy logic to submersible vehicle[J], International Journal of Innovative computing, Information and Control, 2007, 3(4):897-906.
- [Song 2007]Song, X., Ye J. W., Liang F. L. and Chen Y. M.
Improved Design of the Super-Mini Underwater Robot and Intelligent Control System[J], Robotics, 29(6):596-600.
- [Song 2006]Song, X., Ye J. W.
Real-time Multi-channel Signal Press Sensor Data Acquisition System Based on the EPP Model[J], Modern Electronics Technique[J], 2006, 28(22):77-79.
- [Chen 2007]Chen Y. M., Ye J. W., Song X.
Design and modeling of a wave motion compensation stable platform system, Machine Tool & Hydraulics[J], 2007, 35(10):115-117.
- [Chen 2007]Chen Y. M., Ye J. W., Song X.
Simulation experiment of the hydraulic mechanism of a wave motion compensation stable platform system[J], Ship & Ocean Engineering, 2007, 36(6): 103-106.
- [Ye 2006] Ye J. W., Chen Y. M., Wang D. J., Song X., Liu Y. Q., Huang Y. T.
Wave Motion compensation scheme and its model tests for the salvage of an ancient sunken boat[J], China Ocean Engineering, 2006, 20(4):635-643.

Conference Paper

- [Song 2010]Song X., Zhu Y. M., Yang F. and Luo J. H.
Quantitative study of fiber tracking results in human cardiac DTI[C], 10th IEEE International Conference on Signal Processing, 2010, pp. 724-727.
- [Song 2010]Song X., Zhu Y. M., Yang F. and Luo J. H.
Analysis of myocardial fiber structure using DTI[C], Second International Conference on Future Computer and Communication, 2010, pp.109-112.
- [Song 2010]Song X., Zou Z.J.
A fuzzy sliding mode controller with adaptive disturbance approximation for underwater robot[C], Proceedings of International Asia Conference on Informatics in Control, Automation and Robotics 2010: 50-53.
- [Song 2010]Song X., Zou Z. J.
A robust and adaptive underwater obstacles' recognition based on fuzzy clustering algorithm[C], 20th International offshore (ocean) and Polar Engineering Conference 2010.
- [Song 2010]Song X., Zou Z. J.
Underwater sonar images processing and its real-time application of super-mini ROV[C], Proceedings of the ASME 2010, 29th International Conference on Ocean, Offshore and Arctic Engineering, 2010.
- [Song 2006]Song X., Ye J. W., Wu L. M.,
Integral sliding mode controller based on fuzzy logic for the heading control of the submersible vehicle[C], Proc. Of the international conference on computing, information, control, 2006:183-186.
- [Feng 2010]Feng Y., Zhu Y. M., Song X., Luo J. H., and Clarysse P.
Interpolation of human cardiac DT-MRI data using polar coordinates[C], 10th IEEE International Conference on Signal Processing, 2010, pp. 678-681.
- [Feng 2009]Feng Y., Song X., Zhu Y. M. et. al.
Noise-reduced TPS interpolation of primary vector fields for fiber tracking in human cardiac DT-MRI[C], Lecture Notes in Computer Science, Functional Imaging and Modeling of the Heart, 2009, 5528:78-86.
- [Feng 2009]Feng Y., Zhu Y.M., Song X., et. al.
Interpolation et débruitage du champ devecteurs 3-D en IRM cardiaque du tenseur de diffusion[C], XXXIIe Colloque Gretsi Traitement du signal et des images univervté de Bourgogne, 2009.
- [Gao 2009]Gao Y.Z., Ye J. W., Song X., et. al.
A Reinforcement Learning Algorithm Based Neural Network Used for Course Angle Control of Remotely Operated Vehicle[C], Second International Conference on Intelligent Computation Technology and Automation, 2009:31-34,

Submitted paper:

Song X., Zhu Y. M., Yang F., et. al.

Maximum energy tracking approach to reconstruction human cardiac fibers from diffusion tensor magnetic resonance images[J], IEEE Transactions on Medical Imaging.

Bibliographies

- [Amato 1998] Amato, N., O. Bayazit, L. Dale, et al. OBPRM : An obstacle-based PRM for 3D workspaces[J], *Robotics: The algorithmic perspective* 1998: 155~168.
- [An 2001] An XinWei, Zhang Xiaobing. The research of three dimension medical image reconstruction [J], *Journal of electron devices*, 2001, 19(5): 948-950.
- [Arimoto 1984] Arimoto, S., F. Miyazaki. Stability and robustness of PID feedback control for robot manipulators of sensor capability[J], *Robot research*, 1984: 783-799.
- [Arsigny 2005] Arsigny, V., P. Fillard, X. Pennec, et al. Fast and simple calculus on tensors in the Log-Euclidean framework[C], *Proceedings of Medical Image Computing and Computer-assisted Intervention, Lecture Notes in Computer Science* 2005: 115-122.
- [Besag 1986] Besag, J. On the statistical analysis of dirty pictures[J], *Journal of the royal statistical society*, 1986, 48(3): 259~302.
- [Basser 1994] Basser, P., J. Mattiello, D. LeBihan. MR diffusion tensor spectroscopy and imaging[J], *Biophysical Journal*, 1994, 66: 259-267.
- [Basser 1996] Basser, P. J., P. Carlo. Microstructural and physiological features of tissues elucidated by quantitative diffusion tensor mri[J], *Journal of magnetic resonance* 1996: 209~219.
- [Basser 2000] Basser, P. J., S. S. Pajevic, C. Pierpaoli, J. Duda and A. Aldroubi. In Vivo Fiber Tractography Using DT-MRI Data[J], *Magn. Reson. Med.*, 2000, 44: 625~632.
- [Batchelon 2001] Batchelon, P. G., D. L. G. Hill, F. Calamante, et al. Study of connectivity in the brain using the full diffusion tensor from MRI [J], *Springer-Verlag*, 2001: 121-133.
- [Batlle 1998] Batlle, J., E. Mouaddib, J. Salvi. Recent progress in coded structured light as a technique to solve the correspondence problem: survey[J], *Pattern Recognition*, 1998, 31(7).
- [Behrens 2003] Behrens, T., M. Woolrich, M. Jenkinson, H. Johansen-Berg, R. Nunes, S. Clare, P. Matthews, J. Brady, and S. Smith. Characterization and propagation of uncertainty in diffusion-weighted MR imaging[J], *Magn. Reson. Med.*, 2003, 50, no.5: 524-532.
- [Björnemo 2002] Björnemo, M., A. Brun, R. Kikinis, and C.-F. Westin. Regularized stochastic white matter tractography using diffusion tensor MRI[C], *5th Int. Conf. Med. Image Computing Computer Assist. Intervention Tokyo, Japan*, 2002: 25~28.
- [Bezdek 1981] Bezdek, JC (1981). "Pattern recognition with fuzzy objective function algorithm," Plenum, New York.
- [Canny 1985] Canny, J. F. A voronoi method for the piano movers problem[C], *IEEE International conference on robotics and automation*, 1985: 530~535.
- [Carano 2003] Carano, A., B. N. Van, C. A. de. MRI measurement of cerebral water diffusion and its application to experimental research[J], *Biomedical imaging in experimental neuroscience* 2003: 21-54.

-
- [Castellani 2005] Castellani, U., A.Fusiello, V.Murino, et al. A complete system for on-line 3D modelling from acoustic images[J], *Signal Processing Image Communication* 2005, 20: 832-382.
- [Chance 2003] Chance, T. S. AUV Surveys: Extending our Reach 20000Km later[C], *Proceedings of the 13th International symposium on unmanned unthered submersible technology New Hampshire, 2003*: 24-27.
- [Chen 1997] Chen, D., Z. R. Szczerba, J., J. Uhran, J. A framed-quadtree approach for determining Euclidean shortest paths in a 2-D environment[J], *IEEE International conference on robotics and automation, 1997*, 13(5): 668~681.
- [Choi 2004] Choi, S. k.,J. Yuh. Experimental study on a learning control system with bound estimation for underwater vehicles[J], *Autonomous Robots*, 2004, 3: 187-194.
- [Choset A 1995] Choset, H.,B. J. Sensor based planning. I. The generalized voronoi graph[J], *IEEE International conference on robotics and automation, 1995*, 2: 1643~1648.
- [Choset B 1995] Choset, H.,J. Burdick. Sensor based planning. II Incremental construction of the generalized Voronoi graph[J], *IEEE International conference on robotics and automation, 1995*, 2: 1649~1655.
- [Conte 1996] Conte, G.,A. Serrani. Modeling and simulation of underwater vehicle[C], *Proceedings on IEEE international Symposium on Computer Aided Control System Design, Dearborn, 1996*: 15-18.
- [DeBitetto 1994] DeBitetto, P. A. Fuzzy logic for depth control of unmanned undersea vehicles[C], 1994: 233-241.
- [Denis 2001] Denis, L. B. Diffusion Tensor Imaging: concepts and applications[J], *J Magn.Reson.Imaging*, 2001, 13: 534-546.
- [Dugelay 1996] Dugelay, S., J. M. Augustin, C. CGraffigne. Segmentation of multibeam acoustic imagery in the exploration of the deep sea bottm[C], *13th international conference on pattern recongintion Vienna 1996*: 437-445.
- [Edwards 1998] Edwards, C., S. Spurgeon. Sliding mode control : theory and applications [M]. London:Taylor and Francis, 1998.
- [Fan 1988] Fan shangyong. Ship maneuverability[M]:National defense industry press, 1988.
- [Fan 2004] Fan Xiao-ping, Luo Xiong, et.al. Path planning for robots based on ant colony optimization algorithm under complex environment[J], *Control and Decision*, 2004, 19(2): 166-170.
- [Filler 1991] Filler, A., H. Winn, Howe FA, et al. Axonal transport of super paramagnetic metal oxide particles : potential for magnetic resonance assessments of axoplasmic flow in clinical neuroscience[C], *Proceedings Society of Magnetic Resonance in Medicine,10th Annual Meeting, San Francisco, 1991*: 985.
- [Fillard 2007] Fillard, P., Xavier Pennec, Vincent Arsigny, Nicholas Ayache. Clinical DT-MRI Estimation, Smoothing, and Fiber Tracking With Log-Euclidean Metrics[J], *IEEE Trans. Med. Imaging*, 2007, 26(11): 1472-1482.

-
- [Fillard 2003] Fillard, P., J. Gilmore, W. Lin, et al. Quantitative analysis of white matter fiber properties along geodesic path[C], Proceedings of medical image-computing and computer-assisted intervention, Saint-Malo, 2003: 16-23.
- [Fletcher 2004] Fletcher, S., Joshi. Principal geodesic analysis on symmetric spaces : statistics of diffusion tensors[J], Proceedings of ECCV 2004 workshop on computer vision approaches to medical image analysis, 2004, 3117: 87-98.
- [Fossen 1991] Fossen, T. I., Sagatun, S. I. Adaptive control of nonlinear underwater robotic systems [C], IEEE Int. Conf. on robotics and automation ICRA'91, Sacramento, CA, USA, 1991.
- [Fossen 1994] Fossen, T. I. Guidance and Control of Ocean Vehicles[M]: John Wiley & Sons, 1994.
- [Fossen 1995] Fossen, T. I., T. I. Fjellstad. Robust adaptive control of underwater vehicles: a comparative study.[C], Proceedings of the third IFAC workshop on control applications in marine systems, 1995.
- [Fossen 2000] Fossen, T. I., M. Blanks. Nonlinear output feedback control of underwater vehicle propellers using feedback from estimated axial flow[J], IEEE Journal of Oceanic Engineering, 2000, 25(2): 241-255.
- [Friman 2005] Friman, O., Carl-Fredrik Westin. Uncertainty in White Matter Fiber Tractography[J], med image Comput Comput Assist Interv. MICCAI 2005, 2005: 107-114.
- [Friman 2006] Friman, O., Gunnar Farneback, Carl-Fredrik Westin. A Bayesian approach for stochastic white matter tractography[J], IEEE Transactions on Medical Imaging, 2006, 25: 965-978.
- [Gilbert 2007] Gilbert, S. H., A. P. Benson, P. Li, and A. V. Holden. Visualization of Dog Myocardial Structure from Diffusion Tensor Magnetic Resonance Imaging: The Paradox of Uniformity and Variability[C], Proceedings of the 4th International Conference on Functional Imaging and Modeling of the Heart (FIMH'07), 2007: 403-412.
- [Goheen 1990] Goheen, K. R., E. R. Jefferys. Multivariable self-turning autopilots for autonomous underwater vehicles[J], IEEE Journal of Oceanic Engineering, 1990, 15(3): 144-151.
- [Gorban 2007] Gorban A, Kegl B, Wunsch D and Zinovyev A. "Principal manifolds for data visualization and dimension reduction," Springer, Berlin-Heidelberg-New York.
- [Gössl 2002] Gössl, C., L. Fahrmeir, B. Pütz, L. M. Auer, and D. P. Auer. Fiber Tracking from DTI Using Linear State Space Models: Detectability of the Pyramidal Tract[J], NeuroImage, 2002: 378-388.
- [Ha 2001] Ha, Q. P., Q. H. Nguyen, D. C. Rye, et al. Fuzzy sliding mode controllers with applications[J], IEEE Transactions on Industrial Electronics, 2001, 48(1): 38-46.
- [Hartley 2000] Hartley, R., A. Zisserman. Multiple View Geometry in Computer Vision[M]: Cambridge University Press, 2000.
- [Healey 1993] Healey A, J., D. Leonard. Multivariable sliding mode control for autonomous diving and steering of unmanned underwater vehicles[J], IEEE Journal of Oceanic Engineering, 1993, 18(3): 327-339.

-
- [Helm 2005] Helm, P. A., M. F. Beg, M. I. Miller, and R. L. Winslow. Measuring and Mapping Cardiac Fiber and Laminar Architecture Using Diffusion Tensor MR Imaging[J], *Annals of the New-York Academy of Science*, 2005, 1047: 296-307.
- [Hong 2004] Hong qi, Zhang shusheng, Wang Jing. Volume Rendering Techniques [J], *Application research of computers*, 2004, 23(1): 16-18.
- [Hsu 1998] Hsu, E., Muzikant AL, Matulevicius SA, Penland RC, Henriquez CS. Magnetic resonance myocardial fiber-orientation mapping with direct histological correlation[J], *Am J physiol.*, 1998: 1627-1634.
- [Hsu 1999] Hsu, D., L. J, R.Motwani. Path planning in expansive configuration spaces[J], *international Journal of Computational Geometry and Applications*, 1999, 9(4): 495~512.
- [Hsu 2005] Hsu, D., J. Latombe, H. Kurniawati. On the probabilistic Foundations of probabilistic roadmap planning [C], *12th Int. symp. on Robotics Research*, 2005.
- [Huyn 1980] Huyn, N., R. Dechter, J. Pearl. Probabilistic Analysis of the complexity of A*[J], *Artificial intelligence*, 1980, 15(3): 241-254.
- [Hu 2003] Hu Yue-Min. Theory and application of variable structure controller[M]. BeiJing: Science press, 2003.
- [Ishii 1998] Ishii, K., T. Fujii, T. Ura. Neural network system for online controller adaptation and its application to underwater robot[C], 1998: 755-761.
- [Janglova 2004] Janglova, D. Neural network in mobile robot motion[J], *International journal of advanced robotic systems*, 2004, 1(1): 15~22.
- [Jianping 2003] Jianping, T.,S. YANG, X. Genetic algorithm based path planning for a mobile robot[J], *IEEE International conference on robotics and automation*, 2003, 1: 1221-1226.
- [Jolliffe 2002] Jolliffe IT , "Principal component analysis," Springer, 2nd ed., NY, 2002.
- [Jones 2005] Jones, D., C. Pierpaoli. Confidence mapping in diffusion tensor magnetic resonance imaging tractography using a bootstrap approach[J], *Magn. Reson. Med.*, 2005, 53: 1143-1149.
- [Juidette 2000] Juidette, H.,H. Youlal. Fuzzy dynamic path planning using genetic algorithms[J], *Electronics letters*, 2000, 36(4): 374-376.
- [Kambhampati 1986] Kambhampati, S., K. L. Davis, S., Multi-resolution path planning for mobile robots[J], *IEEE journal of Robotics and Automation*, 1986, 2: 135~145.
- [Kamgar-Parsi 1998] Kamgar-Parsi, B., L. J. Rosenblum, E. O. Belcher. Underwater imaging with a moving acoustic lens[J], *IEEE Trans. Image Process*, 1998, 7(1): 91-99.
- [Kassim 1992] Kassim A A,K. B. V. K. V. A neural network architecture for path planning[J], *International Joint conference on neural networks*, 1992, 2: 782~792.
- [Kato 1993] Kato, N., Y. Ito, J. Kojima, et al. Guidance and control of autonomous underwater vehicle AQUA EXPLORER 1000 for inspection of underwater cables.[C], In *8th int'l Sympon unmanned untethered submersible technology*, 1993: 195~211.

-
- [Kavraki 1994] Kavraki, L.,J. Latombe. Randomized preprocessing of configuration space for fast path planning [J], IEEE International conference on robotics and automation, 1994: 2138~2139.
- [Keppel 1975] Keppel, E. Approximating complex surfaces by triangulation of contour lines[J], IBM journal of research development, 1975: 2-11.
- [Khatib 1986] Khatib, O. Real-time obstacle avoidance for manipulators and mobile robots[J], Int. Journal of Robotics Research, 1986, 5: 90-98.
- [Koyama 2006] Koyama, T., K. Tamai, K. Togashi. Current status of body MR imaging: fast MR imaging and diffusion-weighted imaging[J], Int J clin Oncol, 2006, 11: 278-285.
- [Lazar 2005] Lazar, M., A. Alexander. Bootstrap white matter tractography (BOOT-TRACT)[J], NeuroImage, 2005, 24: 524-532.
- [Lu 2006] Lu, Y., Aldroubi A, Gore JC, Anderson A, and Ding Z. Improved fiber tractography with Bayesian tensor regularization[J], NeuroImage, 2006, 31: 1061-1074.
- [Lacroule 1994] Lacroule, P.,M. Levoy. Fast volume rendering using a shear-warp factorization of the viewing transformation[C], Proc.SIGGRAPH, 1994: 451-458.
- [Latombe 1991] Latombe, J. C. Robot Motion Planning[M], 1991.
- [Lavalle 1998] LaValle, S. M., Rapidly-exploring random trees: a new tool for path planning [R], Iowa state university 1998.
- [Lavalle 2000] Lavalle, S. M.,J. Kuffner. Rapidly-exploring random trees: Progress and prospects[J], In Proc. Int workshop on algorithm foundations of robotics(WAFR), 2000: 293~308.
- [Lazar 2003] Lazar, M., D.M.Weinstein, J.S.Tsuruda, et al. White matter tractography using diffusion tensor deflection [J], Hum.Brain Mapp., 2003: 306-321.
- [Lenoid 2003] Lenoid, Z., Alan H.Barr Heart-Muscle Fiber Reconstruction from Diffusion Tensor MRI[C], Proceedings of the 14th IEEE Visualization 2003(VIS'03), 2003: 79.
- [Levoy 1988] Levoy, M. Display of surfaces from volume data[J], 1988, 8(5): 29-37.
- [Liang 2003] Liang, C.-Y.,J.-P. Su. A new approach to the design of a fuzzy sliding mode controller[J], Fuzzy Sets and Systems, 2003, 139: 111-124.
- [Linnett 1994] Linnett, L. M., S. J. Clarke, D. R. Carmichael. The analysis of sidescan sonar images for seabed types and objects[C], Proceedings of second conference on underwater acoustics, 1994.
- [Liu 1994] Liu, Y. H.,S. Arimoto. Computation of the tangent graph of polygonal obstacles by moving-line processing[J], IEEE International conference on robotics and automation, 1994, 10(6): 823-830.
- [Liu 2001] Liu chengliang, Zhang kai, Fu zhuang et. al. Application research of artificial neural network in robot trajectory planning [J], Robot, 2001, 23(7): 605~607.
- [Lorensen 1987] Lorensen, W. E., H. E. Cline. Marching Cubes: A high resolution 3D surface construction algorithm[J], Computer Graphics, 1987, 21(4): 163-169.

-
- [Lu 2002] Lu, Y., O. Masaki. On the 3-D Reconstruction of Seabed Using Multiple Sidescan Sonar Images[C], MVA, 2002.
- [Lu 2006] Lu, Y., A. Aldroubi, J.C. Gore, A. Anderson and Z. Ding. Improved fiber tractography with Bayesian tensor regularization[J], *NeuroImage*, 2006, 31:1061-1074.
- [Minati 2006] L.Minati, D.Aquino. Probing neural connectivity through diffusion Tensor imaging(DTI)[J], *Cybernetics and systems*, 2006: 263-268.
- [Mori 1999] Mori, S., P. Barker. Diffusion magnetic resonance imaging : its principle and applications[J], *A Nat Rec B New Anat*, 1999, 257: 102-109.
- [Mori 1999] Mori, S., Crain, B.J., Chacho, V.P., van Zijl, P.C.M. Three dimensional tracking of axonal projections in the brain by magnetic resonance imaging[J], *Ann.Neurol.*, 1999: 265-269.
- [Morrison 1993] Morrison, A. T., D. R. Yoerger. Determination of the hydrodynamic parameters of an underwater vehicle during small scale, nonuniform, 1-dimensional translation[C], *Proc. IEEE/MTS OCEAN'93*, 1993: 277-282.
- [Nakamura 1992] Nakamura, Y., S. Savant. Nonlinear tracking control of autonomous underwater vehicles[C], *Proceedings of IEEE Int.Conf. on Robotics and Automation*, 1992: A4-A9.
- [Nearchou 1998] Nearchou, A. C. Path planning of a mobile robot using genetic heuristics[J], *ROBOTICA*, 1998, 16: 575-588.
- [Newman 1977] Newman, J. N. *Marine Hydrodynamics[M]*: The MIT Press, 1977.
- [Nguyen 2007] Nguyen, Q., K. Edwin. Adaptive PD-controller for positioning of a remotely operated vehicle close to an underwater structure: Theory and experiments[J], *Control Engineering Practice*, 2007, 15: 411-419.
- [Nilsson 1969] Nilsson, N. J. *A Mobile Automation: An Application of Artificial Intelligence Techniques[C]*, *Proc. 1st Int Joint Conf. on Artificial Intelligence*, Washington D.C., 1969: 509-520.
- [Parsons 1990] Parsons, D., J. F. Canny. A motion planner for multiple mobile robots[J], *IEEE International conference on robotics and automation*, 1990: 8-13.
- [Parker 2001] Parker, G. J. M., C. A. M. Wheeler-Kingshott, and G. J. Barker. Distributed Anatomical brain connectivity derived from diffusion tensor imaging[J], *Springer-Verlag Berlin Heidelberg*, 2001: 106-120.
- [Parker 2003] Parker, G. J. M., Haroon, H.A., Wheeler-Kingshott, C. A. M. A framework for a streamline-based probabilistic index of connectivity (PICo) using a structural interpretation of MRI diffusion measurements[J], *J. Magn. Reson. Imaging*, 2003: 242-254.
- [Pennec 1999] Pennec, X. Probabilities and statistics on Riemannian manifolds: basic tools for geometric measurements[C], *Proceedings of the IEEE Workshop on Nonlinear Signal and Image Processing*, Antalya, Turkey, 1999.
- [Pennec 2006] Pennec, X., P. Fillard, N. Ayache. A Riemannian framework for tensor computing[J], *Int. J. Comp. Vis*, 2006, 66: 41-66.
- [Peng 1995] Peng Liang, Lu Yingchun, Wan lei, et al. Neural network control for intelligent underwater vehicle motion [J], *The ocean engineering*, 1995, 13(2): 38-46.

-
- [Pepijn 2006] Pepijn, W.J. Van de Ven, Johansen, et al. Neural network augmented identification of underwater vehicle models[J], Control Engineering Practice, 2006.
- [Peter I 2006] Peter, B. K. Introduction to diffusion tensor imaging mathematics: Part I. Tensors, rotations, and eigenvectors[J], Concepts in Magnetic Resonance, 2006, 28A: 101-122.
- [Peter II 2006] Peter, B. K. Introduction to diffusion tensor imaging mathematics: Part II. Anisotropy, diffusion-weighting factors, and gradient encoding schemes[J], Concepts in Magnetic Resonance, 2006, 28A: 123~154.
- [Peter III 2006] Peter, B. K. Introduction to diffusion tensor imaging mathematics: Part III. Tensor calculation, noise, simulations, and optimization[J], Concepts in Magnetic Resonance, 2006, 28A: 155~179.
- [Pierpaoli 1996] Pierpaoli, C., P. Jezzard, P. J. Basser, et al. Diffusion tensor MR imaging of the human brain[J], Radiology, 1996: 637-648.
- [Pierpaoli 1996] Pierpaoli, C., Jezzard, P., Basser, P.J., Barnett, A., and Dichiro, G. . Diffusion tensor MR imaging of the human brain[J], Radiology, 1996: 637-648.
- [Poupon 2000] Poupon, C., C.A.Clark, V.Frouin, et al. Mangin regularization of diffusion-based direction maps for the tracking of brain white matter fascicles [J], Neuroimage, 2000, 12: 184-195.
- [Qin 2001] Qin XuJia, Ou ZongYing, Ji FengXin et.al.Relativity treating in surface reconstruction of 3d medical images with MT algorithm and model simplification[J], Chinese Journal of Biomedical Engineering, 2001, 21(5): 398-403.
- [Qin 2004] Qin Yuan-qing, Sun De-bao, et al. Path Planning for Mobile Robot Based on Particle Swarm Optimization [J], Robot, 2004, 26(3): 22-225.
- [Richards 1992] Richards, T., A. Heide, J. Tsuruda, et al. Vector analysis of diffusion images in experimental allergic encephalomyelitis[C], Society for Magnetic Resonance in Medicine, Berlin 1992: 412.
- [Rusinkiewicz 2002] Rusinkiewicz, S., O. Hall-Holt, M. Levoy. Real-time 3d model acquisition[C], Proceedings of the Siggraph(SIGGRAPH 2002), 2002: 438-446.
- [Shi 1995] Shi dasheng. Underwater vehicle maneuverability [M]: National defense industry press, 1995.
- [Smallwood 2004] Smallwood, D. A., L. W. Louis. Model-Based dynamic positioning of underwater robotic vehicles: Theory and Experiment[J], IEEE Journal of oceanic engineering, 2004, 29: 169- 186.
- [Smith 1994] Smith, S. M., G. J. S. Rae, D. T. Anderson, et al. Fuzzy logic control of an autonomous underwater vehicle[J], Control Engineering Practice 1994, 2(2): 321-331.
- [Song 2004] Song BaoWei. Design theory and technology of underwater vehicle [M]. Xi an: Northwestern polytechnical university press, 2004.
- [Song 2007] Song Xin, Ye Jia-wei. et.al. Improved design of super-mini underwater robot and its intelligent control system[J], Robot, 2007, 29: 596~600.

-
- [Song 2007] Song, X., J. Ye, L.-m. Wu. Application of the integral sliding mode controller with fuzzy logic to submersible vehicle[J], International Journal of Innovative computing, information & control, 2007, 3: 897~906.
- [Song 2008] Song Xin, Ye Jia-Wei. Application of sliding mode fuzzy controller in submersible vehicle[J], Shipbuilding of China, 2008, 49: 84~89.
- [Stentz 1994] Stentz, A., The D* Algorithm for real2time planning of optimal traverses [R], CMU 1994.
- [Sun 2000] Sun shudong, Lin mao.Path planning of multi mobile robots using genetic algorithms. [J], Acta automatica sinica, 2000, 26(5): 673~676.
- [Sun 2005] Sun Bo, Chen wei-dong, Xi yu-geng. Particle Swarm Optimization Based Global Path Planning for Mobile Robots [J], Control and decision, 2005, 20(9): 1052-1060.
- [Tabaii 1944] Tabaii, S. S., F. El-Hawary, M. El-Hawary. Hybrid adaptive control of autonomous underwater vehicle[C], 1994: 275-282.
- [Tan 1999] Tan, K. K., Q.-G. Wang, C. Hang. Advances in PID Control[M]: UK : Springer-Verlag, 1999.
- [Tian 2003] Tian Jie, Bao shanglian, Zhou mingquan. Medical image process and analysis [M]. BeiJing: Publishing house of electronics industry, 2003.
- [Tuch 1999] Tuch, D. S., Weisskoff, R.M., Belliveau, J.W., and Wedeen, V.J., High angular resolution diffusion imaging of the human brain[A], in VIIth ISMRM Philadelphia, 1999.
- [Utkin 1992] Utkin, V. L. Sliding modes in control and optimization[M]: Springer-verlag, 1992.
- [Van 2003] Van, D., V. J. Loop Tuning Fundamentals[J], Control Engineering, 2003.
- [Wai 2003] Wai, R. J. Tracking control based on neural network strategy for robot manipulator[J], Neurocomputing, 2003.
- [Westin 1997] Westin, C.-F., S. E. Maier, B. Khidir, et al. Geometical diffusion measures of MRI from Tensor Basis Analysis [C], Proc. of the international society for magnetic resonance medicine(ISMRM), Vancouver Canada, 1997.
- [Westin 2002] Westin, C.-F., S.E.Maier, H.Mamata, et al. Processing and visualization for diffusion tensor MRI[J], Medical image analysis, 2002, 6(2): 93-108.
- [Westin 2002] Westin, C.-F., S.E. Maier, H. Mamata, A. Nabavi, F.A. Jolesz, R. Kikinis R. Processing and Visualization for Diffusion Tensor MRI[J], Medical Image Analysis, 2002, 6: 93-108.
- [Westover 1990] Westover, L. Footprint evaluation for volume rendering [J], Computer Graphics, 1990, 24(4): 367~376.
- [William 1987] William, E. L., E. C. Harvey. Marching cubes: A high resolution 3D surface construction algorithm.[J], SIGGRAPH, 1987.
- [Wilmarth A 1999] Wilmarth, S., N. Amato, P. Stiller. MAPRM: A probabilistic roadmap planner with sampling on the medial axis of the free space[C], IEEE International Conference on Robotics and Automation, 1999: 1024~1031.

-
- [Wilmarth B 1999] Wilmarth, S., N. Amato, P. Stiller. MAPRM: A probabilistic roadmap planner with sampling on the medial axis of the free space [J], Technical report 1999:
- [Wong 2001] Wong, L. K., F. H. F. Leung, Tam.P.K.S. A fuzzy sliding controller for nonlinear systems[J], IEEE Transactions on Industrial Electronics, 2001, 48(1): 32-37.
- [Xie 1991] Xie XL and Beni G (1991). "A validity measure for fuzzy clustering," IEEE Trans. Pattern Anal. Machine Intell., Vol 13, No 8, pp 841-847.
- [Yang 2001] YANG, S., X.M. MAX. Neural network approaches to dynamic collision-free trajectory generation[J], IEEE Trans On Systems, Man, and Cybernetics, Part B, 2001, 31(3): 302-318.
- [Yang 2002] Yang Yupeng, Li Shaoyuan. Fuzzy optimization algorithm and its application to visual robot path planning [J], Control and decision, 2002, 12: 723-726.
- [Yoerger 1985] Yoerger, D. N.,J.-J. E. Slotine. Robust trajectory control of underwater vehicles[J], IEEE Journal of oceanic engineering, 1985, 10(4): 462-470.
- [Yoerger 1986] Yoerger, D. N., J. B. Newman, J.-J. E. Slotine. Supervisory control system for the JASON ROV[J], IEEE Journal of oceanic engineering, 1986, 11(3): 392-399.
- [Yu 2001] Yu jianli, V. Kroumov, Sun zeng-qi et.al. Fast algorithm for path planning based on neural network [J], Robot, 2001, 23(3): 201~205.
- [Yuh 1990] Yuh, J. A neural net controller underwater robotic vehicles[J], IEEE Journal of Oceanic Engineering, 1990, 15(3): 161-166.
- [Yuh 1995] Yuh, J. Underwater robotic vehicles: Design and Control[M]: TSI Press, 1995.
- [Yuh 1996] Yuh, J. An adaptive and learning control system for underwater robots[C], 13th world congress International Federation of Automatic Control, San Francisco, CA., 1996: 145-150.
- [Zhang 2002] Zhang YouSai, Chen fuming. Volume Rendering of 3-D Medical Volumetric Data [J], Computer engineering and application, 2002, 8: 18-19.
- [Zhang 2004] Zhang YanJun, Ye BoSheng. An Improved Algorithm for Three-Dimensional Surface Reconstruction Based on Contour Data of Medical Images [J], Computer engineering and application, 2004, 40 (13): 215-218.
- [Zhu 1992] Zhu JiFan. Underwater vehicle design [M]. ShangHai: Shanghai JiaoTong university press, 1992.
- [Zhu 2005] Zhu baoqing. Ants Predictive Algorithm for Path Planning of Robot in a Complex Dynamic Environment[J], Chinese journal of computers, 2005, 28(11): 1898-1906.

FOLIO ADMINISTRATIF

THESE SOUTENUE DEVANT L'INSTITUT NATIONAL DES SCIENCES
APPLIQUEES DE LYON

NOM : SONG

DATE de SOUTENANCE : 13 juillet 2011

Prénoms : Xin

TITRE : Path reconstruction in diffusion tensor magnetic resonance imaging

NATURE : Doctorat

Numéro d'ordre : 2011-ISAL-

Ecole doctorale : Ecole Doctorale Electronique, Electrotechnique, Automatique

Spécialité : Image et System

Cote B.I.U. - Lyon :

CLASSE :

Résumé : The present thesis aims to investigate the similarities between the heart fiber tracking algorithm and the underwater robot path tracking algorithm, and propose some new ideas and methods to solve the problem of choosing the coming back paths of underwater robot and construct the fiber structure of the human heart. Nowadays super-mini underwater cable robots are playing more and more important parts in the application of oceans, rivers, lakes and shallow water. However, the complicated underwater environment and the poor underwater vision make super-mini underwater cable robot hardly to be controlled. Traditionally, the manual control method by operators is adopted by this kind of robots. Unfortunately, the robots can hardly work normally in these practical circumstances. Therefore, to overcome these shortcomings and improve the abilities of these underwater cable robots, this thesis proposes several improvements, including the system design, the motion controller design, three dimensional obstacle recognition and three dimensional path reconstruction techniques, etc.

The following details are given: (1) Super-mini underwater robot system design by developing a much more powerful and intelligent control platform for underwater robot; (2) Super-mini robot motion controller design by proposing a new adaptive neural network sliding mode controller with balanced parameter controller (ANNSMB); (3) Research of three dimensional underwater environment reconstruction by investigating the theory of data collection and several new adaptive online processing techniques, and in particular by adopting diffusion tensor magnetic resonance imaging (DT-MRI) algorithm and the theory of three dimensional obstacle reconstruction for the application of the underwater robot; (4) Three dimensional path planning and its reconstruction by proposing a new random three dimensional path tracking algorithm based on Bayesian theory; (5) Algorithms and application of DT-MRI by proposing a new maximum energy fiber tracking algorithm to construct the fiber structure of the heart.

MOTS-CLES: three dimensional reconstructions; motion control; path planning; energy algorithm; Bayesian random algorithm; sliding mode; adaptive algorithm

Laboratoire (s) de recherche :

CREATIS, CNRS UMR 5220, INSERME U1044

Directeur de thèse: Yue-Min Zhu

Président de jury :

Composition du jury : Carlos Canudas de Wit, Guo-Liang Huang, Isabelle Magnin, Jean-Claude Vivalda, Cheng-Zhong Xu, Jia-Wei Ye, Yue-Min Zhu, Zao-Jian Zou